공학박사 학위논문

Development of Heat Transfer Model for Horizontal U-Shaped Heat Exchanger Submerged in Pool

수조 내 수평 U자형 열교환기에 대한
열전달 모델 개발

2015 년 8 월

서울대학교 대학원
에너지시스템공학부
전 성 수

Development of Heat Transfer Model for Horizontal U-Shaped Heat Exchanger Submerged in Pool

수조 내 수평 U자형 열교환기에 대한 열전달 모델 개발

지도교수 박 군 철

이 논문을 공학박사 학위논문으로 제출함
2015 년 4 월

서울대학교 대학원
에너지시스템공학부
전 성 수

전성수의 박사 학위논문을 인준함
2015 년 6 월

위 원 장 서 균 렬 (인)

부위원장 박 군 철 (인)

위 원 조 형 규 (인)

위 원 김 응 수 (인)

위 원 송 철 화 (인)

Abstract

Development of Heat Transfer Model for Horizontal U-Shaped Heat Exchanger Submerged in Pool

Seong-Su Jeon

Department of Energy System Engineering

The Graduate School

Seoul National University

A horizontal U-shaped heat exchanger submerged in a large pool has been developed as a key equipment of passive safety systems such as PAFS, PCCS, and ECS. The reliable prediction of the heat exchanger heat transfer performance has been an important issue for the optimum design of the heat exchanger and the safety analysis of the nuclear power plants installed with these passive safety systems. In order to obtain a reliable prediction of the local heat transfer coefficients at the inside/outside tube wall and the heat removal performance of the heat exchanger in the PAFS, this study performed the heat transfer analysis using MARS-KS 1.2 and developed the heat transfer model package for the horizontal U-shaped heat exchanger submerged in a pool.

The heat transfer model package consisted of the horizontal in-tube

condensation model and the natural convective nucleate boiling model on the horizontal U-shaped heat exchanger submerged in a pool. For the horizontal in-tube condensation model, this study assessed the predictive capability of the previous horizontal in-tube condensation heat transfer models for annular and stratified flows using various horizontal in-tube steam condensation experimental data. From the assessments of nineteen annular flow- and eleven stratified flow condensation models, it was found that the annular flow condensation model by Dobson and Chato (1998) and the stratified flow condensation model by Cavallini et al. (2006) were the most applicable models to the heat exchanger of the passive safety system. By replacing the models by Shah (1979) and Chato (1962) in the original MARS code with the models by Dobson-Chato (1998) and Cavallini et al. (2006), this study improved the predictive capability of MARS for the horizontal in-tube condensation heat transfer in the heat exchanger of the passive safety system.

For the natural convective nucleate boiling model, this study first investigated the predictive capability of the previous nucleate boiling models for the horizontal U-shaped HX submerged in a pool using the PASCAL data. From the assessments of seven nucleate pool boiling and eight forced convective boiling models, it was found that, among previous nucleate boiling models, there was no model applicable to the horizontal U-shaped heat exchanger submerged in a pool. Thus, this study investigated the nucleate boiling heat transfer mechanism on the horizontal U-shaped heat exchanger submerged in a pool, taking into account the PASCAL experimental data, MARS simulations and literature survey comprehensively. Furthermore, this study developed the nucleate boiling heat transfer model on the horizontal U-shaped heat exchanger submerged in a pool.

From the validation results of the proposed nucleate boiling model against the PASCAL and ATLAS-PAFS data, it was found that the proposed nucleate boiling model predicted the experimental heat transfer coefficients well on the upper and lower parts of the U-shaped tube within a deviation of ±19 %. For the natural convection model, this study proposed the natural convection heat transfer model on the horizontal U-shaped HX submerged in a pool based on the PASCAL data. The proposed natural convection model satisfactorily predicted the heat transfer coefficients of the PASCAL within a deviation of ±33 %. Finally, this study developed the natural convective nucleate boiling model on the horizontal U-shaped heat exchanger submerged in a pool by combining the proposed nucleate boiling model and the natural convection model.

The proposed heat transfer model package on the horizontal U-shaped heat exchanger submerged in a pool was validated with the PASCAL, ATLAS-PAFS, and NOKO experimental data. The validation results revealed that the proposed model package could provide the improved prediction of the local heat transfer coefficients at the inside/outside tube wall and the heat removal performance of the heat exchanger in the passive safety systems, especially PAFS, compared to the default models in MARS-KS 1.2.

It is expected that the proposed heat transfer model package on the horizontal U-shaped heat exchanger submerged in a pool is applied to the best-estimate thermal-hydraulic analysis codes and thus contributes to the reliable design and the safety analysis of the passive safety system with this type of heat exchanger.

Keywords

Horizontal U-shaped heat exchanger, Passive safety system, PAFS, Condensation model, Natural convective nucleate boiling model, MARS code, PASCAL

Student Number: 2010-30259

List of Contents

List of Tables

List of Figures

Chapter 1

Introduction

1.1 Background and Motivation

1.1.1 Passive Safety System with Horizontal U-shaped Heat Exchanger Submerged in Pool

In the field of nuclear engineering, there have been many efforts to develop the passive safety systems in order to simplify the nuclear power plant (NPP) design and increase the reliability of the performance of essential safety functions, and eliminate the costs of the installation, maintenance, and operation of active systems (IAEA, 2009). Especially, recent researches have focused on the development of a horizontal U-shaped heat exchanger (HX) submerged in a pool (see Fig. 1.1) as a key equipment of a passive heat removal system because it has some advantages over the vertical one from the economical and structural standpoints (Arai et al., 2000).

As representative passive safety systems with this type of HX, there are the passive auxiliary feed-water system (PAFS), the passive containment cooling system (PCCS), and the emergency condenser system (ECS). During an accident

condition of the NPP, these passive safety systems mitigate accidents by cooling the nuclear system effectively via the heat transfer through the steam condensation inside the U-shaped tubes and the water boiling outside the U-shaped tube (see Fig. 1.1). By the transfer of the core decay heat to the cold water in the pool as a final heat sink passively, the integrity of the NPP can be ensured. The detail technical descriptions of PAFS, PCCS, and ECS are as follows.

A. Passive Auxiliary Feedwater System (PAFS)

In South Korea, as one of the advanced safety features, PAFS is being developed to be adopted in the advanced power reactor plus (APR+). The PAFS can completely replace the conventional active auxiliary feedwater system (MKE, 2011). A schematic diagram of the PAFS for the APR+ is shown in Fig. 1.2. It is composed of a steam-supply line, a U-shaped passive condensation heat exchanger (PCHX), a return-water line, and a passive condensate cooling tank (PCCT). When the water level in the steam generator (SG) becomes lower than 25 % of the wide range of the water level transmitter during an accident, the actuation valve at the return-water line opens and then the natural circulation flow of the PAFS is formed. The PAFS cools the SG secondary-side down and eventually removes the decay heat from the reactor core by condensing the steam in horizontal U-shaped tubes submerged in the PCCT where the natural convection flow accompanying boiling heat transfer occurs at the outside wall of the PCHX (Kang et al., 2012).

Figure 1.3 shows a design of a PCHX bundle in PAFS (Kang et al., 2012). One bundle of the PCHX has 60 tubes in three rows, and the average length of the tubes is about 8.4 m. The PCCT contains 4 bundles (240 tubes in total), where the

bundles are placed in two rows on the bottom of the PCCT. The normal water level in the PCCT is 8.9 m, so that it can remove the decay heat from the reactor core during 8 hours of hot shutdown by the evaporative heat transfer until the HX tubes are exposed into the atmosphere.

B. Passive Containment Cooling System (PCCS)

A PCCS is a safety equipment to prevent the containment break due to over-pressurization during the NPP accident such as loss of coolant accident (LOCA). It has been developed to be applied to the advanced BWR such as the economic simplified boiling water reactor (ESBWR). A schematic view of the PCCS is shown in Fig. 1.4. The PCCS has horizontal U-tube HXs placed in a pool of water outside of the containment. It directly connects drywell (DW) to wetwell (WW). There is no return line to DW. The steam generated in DW flows into the PCCS HX with non-condensable (NC) gases driven by the pressure difference between DW and WW. Then, the steam becomes condensate by the heat exchange with the cold water in the PCCS pool. The condensate and NC gas are drained into WW suppression pool by gravity and pressure difference, respectively. By the transfer of the core decay heat to the atmosphere outside passively, the integrity of containment can be ensured.

C. Emergency Condenser System (ECS)

The siede wasser rekctor-1000 (SWR-1000) is a new innovative boiling water reactor being developed by Siemens AG. It adopts the ECS as one of the passive safety features to increase the safety margins and the grace period for operator actions during accidents (Schaffrath and Prasser, 1998). A schematic diagram of

the ECS for the SWR-1000 is shown in Fig. 1.5. The emergency condensers are heat exchangers, which consist of a parallel arrangement of horizontal U-tubes and a condenser pool filled with cold water. At normal reactor water level, the emergency condensers are flooded with cold water but during any accident where reactor water level drops, the heat-exchanging surfaces inside the tubes are gradually uncovered, and the incoming steam condenses on the cold surfaces. The condensate is returned to the reactor vessel then the decay heat from the reactor core is removed.

1.1.2 Prediction Capability of Best-Estimate Thermal-Hydraulic Analysis Code on HX Heat Removal Performance

During the NPP accidents, the passive safety systems can cool the nuclear system effectively by the transfer of the core decay heat to the cold water in the pool. However, the accident progression could be changed significantly by the heat removal performance of the HX. For this reason, the accurate prediction of the heat removal performance, or capacity, of the HX has been an important issue in the reliable design of HX and the safety analysis of NPP installed with these passive safety system.

At present, the design and the safety analysis of the passive safety systems are performed mainly using the best-estimate thermal-hydraulic analysis codes (BE codes) such as RELAP5, MARS, and etc. Among these, MARS, used in this study, has the following features.

MARS (multi-dimensional analysis of reactor safety) has been developed by Korea atomic energy research institute (KAERI) with the objective of producing a

state-of-the-art realistic thermal hydraulic systems analysis code with multi-dimensional analysis capability (Jeong et al., 1999; Lee et al., 2002). The main structures of MARS are based on the consolidated version of RELAP5/MOD3.2 (USNRC, 1988) and COBRA-TF codes (Thurgood et al., 1983), which are adopted as one-dimensional and three-dimensional thermal-hydraulic (TH) modules, respectively. For a 3D simulation, MARS incorporates a multi-dimensional component named MULTID. MARS adopts a non-homogeneous, non-equilibrium two-fluid model for a two-phase flow and it has been used in many key areas of the nuclear industry, including PWR safety analysis and advanced reactor design.

For the prediction of horizontal in-tube condensation heat transfer, the MARS code employs Shah (1979) and Chato (1962) models for the annular and stratified flow regimes, respectively. Colburn-Hougen (1934) method is used to predict condensation degradation by the presence of NC gas. For the prediction of natural convection and nucleate boiling heat transfer, MARS employs the models by Churchill and Chu (1975) and Chen (1966), respectively (KAERI, 2009). In conclusion, MARS has the prediction capability for the heat removal performance of the horizontal U-shaped HX submerged in a pool basically.

However, present BE codes under-predict the heat removal performance of the HX significantly (Kim et al., 2013; Cho et al., 2013) because the present BE codes do not have the suitable models for both the condensation heat transfer in the horizontal tube and the natural convective and nucleate boiling heat transfer on the horizontal tube, both of which ultimately determining the heat transfer performance of the HX (see Fig. 1.1). This is because, in the TH field of previous nuclear engineering, most researches predicting condensation and boiling heat

transfer have focused on vertical tubes. There are few models developed for the horizontal U-shaped HX in the passive safety systems. Furthermore, there are few validation-researches on the applicability of previous models proposed from different engineering fields to the horizontal U-shaped HX of the passive safety systems. Therefore, for the accurate prediction of the heat transfer performance of the HX with the BE codes, it is required to develop and secure suitable models for both the condensation heat transfer in the horizontal tube and the natural convective and nucleate boiling heat transfer on the horizontal tube.

1.2 Objectives and Scope

The target passive safety system of this study is the PAFS. It has the U-shaped HX deeply submerged in a pool of water. To obtain a reliable prediction of the local heat transfer coefficient (HTC) at the inside/outside tube wall and the heat removal performance of the horizontal U-shaped HX in the PAFS using the BE code, it is required to develop the HX heat transfer model package suitable to BE codes.

The HX heat transfer model package for the horizontal U-shaped HX submerged in a pool consists of the condensation heat transfer model in horizontal tube and the natural convective nucleate boiling heat transfer model on horizontal tubes (see Fig. 1.1). To develop the HX heat transfer model package applicable to the PAFS, this study performed the heat transfer analysis using MARS-KS 1.2 with the aims of improving the horizontal in-tube condensation heat transfer model in BE codes and developing the natural convective nucleate boiling heat

transfer model for the horizontal U-shaped HX submerged in a pool. The outline of this study is described in Fig. 1.6. The research scopes are summarized as follows:

Improvement of horizontal in-tube condensation model: In the horizontal condenser tube of the passive safety system, the main flow regimes are annular flow and stratified flow patterns. In order to improve the horizontal in-tube condensation model in BE codes, this study investigates the predictive capability of the previous horizontal in-tube condensation heat transfer models for annular and stratified flow, respectively, within various conditions encountered in the passive safety system using the MARS code and selects the condensation models applicable to the HX of the passive safety system. Specifically, followings are performed. 1) Various horizontal in-tube condensation heat transfer models for each flow regime are collected from the published literature: 19 condensation models for annular flow and 11 condensation models for stratified flow. 2) All condensation models are incorporated into the MARS code. 3) The heat transfer data is collected from four condensation experiments: Purdue-PCCS (Wu, 2005), JAEA-PCCS (Kondo et al., 2006), PASCAL (MKE, 2011; Kang et al., 2012), and NOKO (Schaffrath and Prasser, 1998). Those experiments were conducted to test the performance of horizontal type HX in the passive safety systems such as PCCS, PAFS, and ECS. 4) The collected experimental data is classified into two categories according to the flow pattern (ranging from annular flow to stratified flow). 5) Using the classified experimental data, MARS simulations are performed to assess the condensation models for each flow regime. 6)

Those experimental data are compared with the predictions from the MARS code modified with each condensation model. 7) Finally, this study selects the condensation models applicable to HX of the passive safety system based on the evaluation for the predictive capability of each model. Then, the horizontal in-tube condensation model in MARS is improved by replacing the default condensation models in MARS with the selected condensation models for each flow regime.

Development of natural convective nucleate boiling heat transfer model on horizontal U-shaped tube submerged in pool: In order to improve the prediction capability of BE codes for the natural convective and nucleate boiling heat transfer on the horizontal U-shaped tube, followings are performed. 1) From a literature survey, various nucleate boiling heat transfer correlations ranging from 7 pool boiling correlations to 8 forced convective boiling correlations on the horizontal tubes are reviewed. Then, all boiling correlations are incorporated into the MARS code. 2) The water boiling data are collected from PASCAL (Kang et al., 2012; Kim et al., 2013; Bae et al., 2013) and ATLAS-PAFS (Kang et al., 2012; Bae et al., 2014) experiments. Those experiments were conducted by KAERI to evaluate the performance of the horizontal U-shaped HX in the PAFS. They provided the detailed heat transfer data. 3) For the PASCAL experiment, MARS simulations are performed to assess the prediction capability of the previous nucleate boiling correlations. MARS predictions by each correlation are compared with the experimental data. Then, the prediction capability of each correlation is evaluated. 4) The main mechanisms for the boiling heat transfer on the

horizontal U-shaped HX submerged in a pool are investigated, taking into account the PASCAL experimental data, MARS simulations and literature survey comprehensively. Then, the prediction method is proposed. 5) Based on the prediction method, a new boiling model for the horizontal U-shaped HX submerged in a pool is developed with MARS. Then, the proposed model is validated with the experimental data at low subcooling conditions (up to ~30 K) from the PASCAL and ATLAS-PAFS. 6) Additionally, the natural convection heat transfer model on the horizontal U-shaped HX submerged in a pool is developed based on the PASCAL data. This is because the water temperature in the HX pool is low at the initial phase of the NPP accident and thus the heat transfer outside the HX tube surface is governed by the natural convection. 7) Finally, this study develops the natural convective nucleate boiling model on the horizontal U-shaped heat exchanger submerged in a pool by combining the proposed nucleate boiling model and the natural convection model.

Validation of HX heat transfer model: The HX heat transfer model package for the horizontal U-shaped HX submerged in a pool is developed by combining the proposed condensation model and the developed natural convective nucleate boiling model. This heat transfer model package is implemented to the MARS code. The HX heat transfer model package is validated with three passive safety system-related experimental data of PASCAL, ATLAS-PAFS, and NOKO.

Chapter 2 presents the improvement of the horizontal in-tube condensation

heat transfer model based on the assessments of the previous annular and stratified flow condensation models. In Chapter 3, the development of the natural convective nucleate boiling heat transfer model for the horizontal U-shaped tube submerged in a pool is described. The validation results of the HX heat transfer model package are covered in Chapter 4.

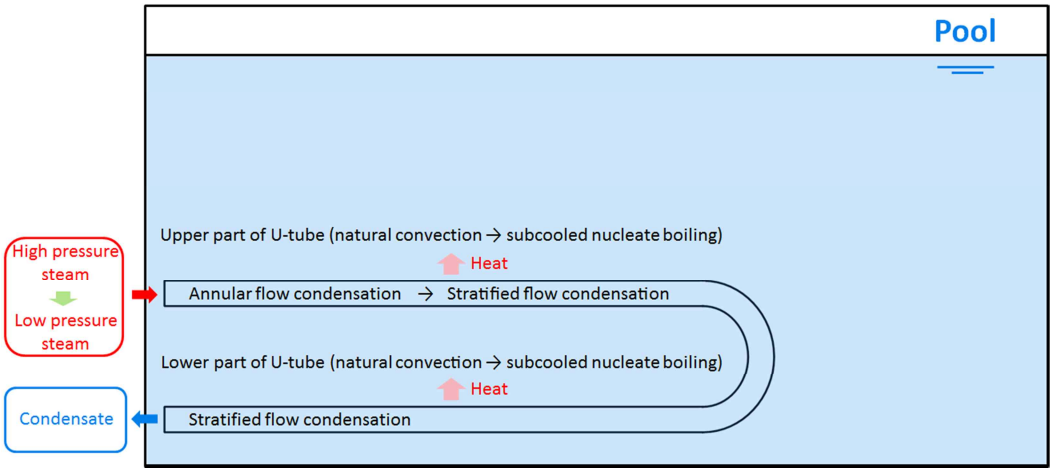

Figure 1.1 Heat transfer modes in horizontal U-shaped HX submerged in pool

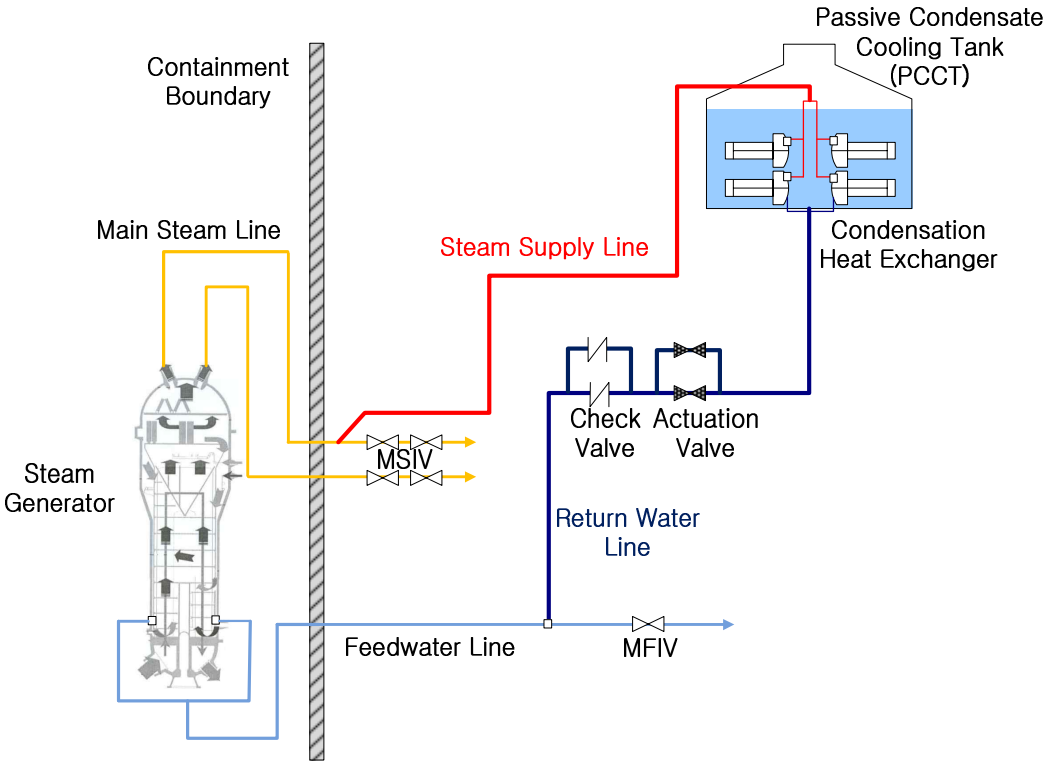

Figure 1.2 Schematic diagram of APR+ PAFS (MKE, 2011)

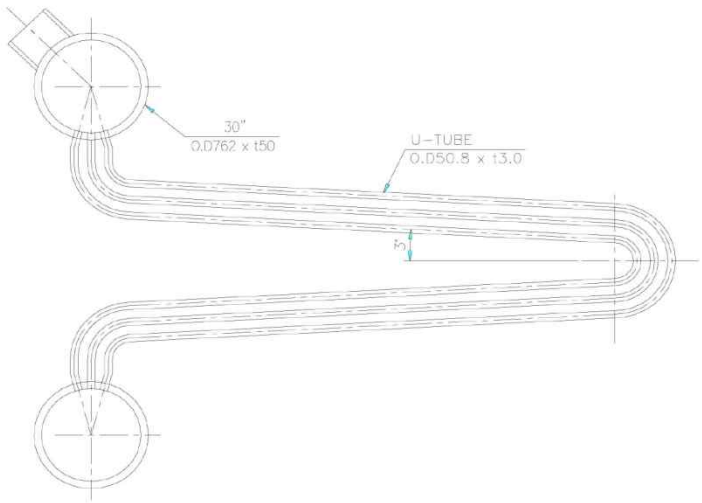

Figure 1.3 PCHX bundle of APR+ PAFS (Kang et al., 2012)

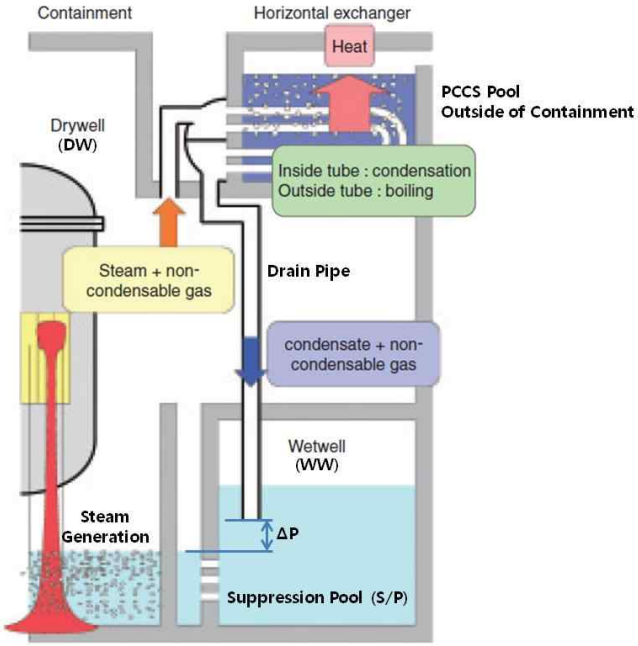

Figure 1.4 Schematic diagram of PCCS (Kondo et al., 2006)

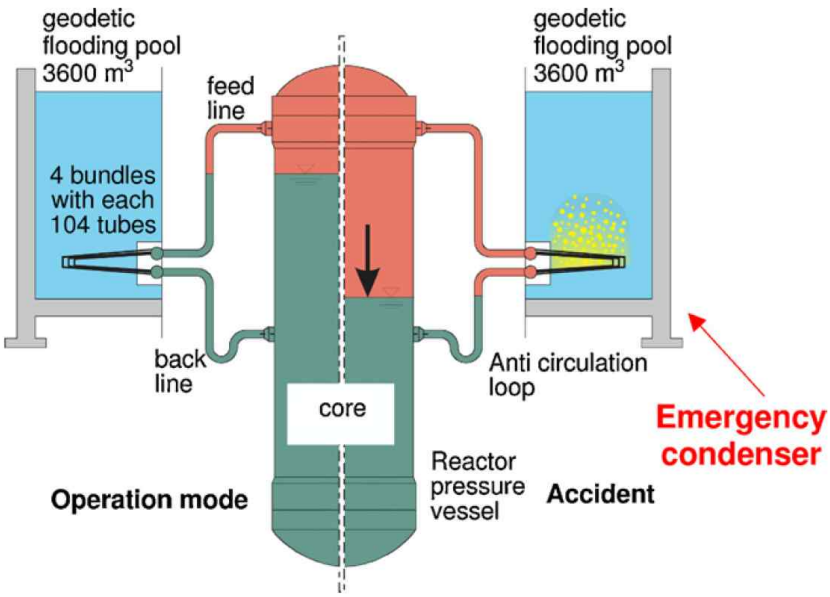

Figure 1.5 Emergency condenser of SWR-1000 (Krepper and Beyer, 2010)

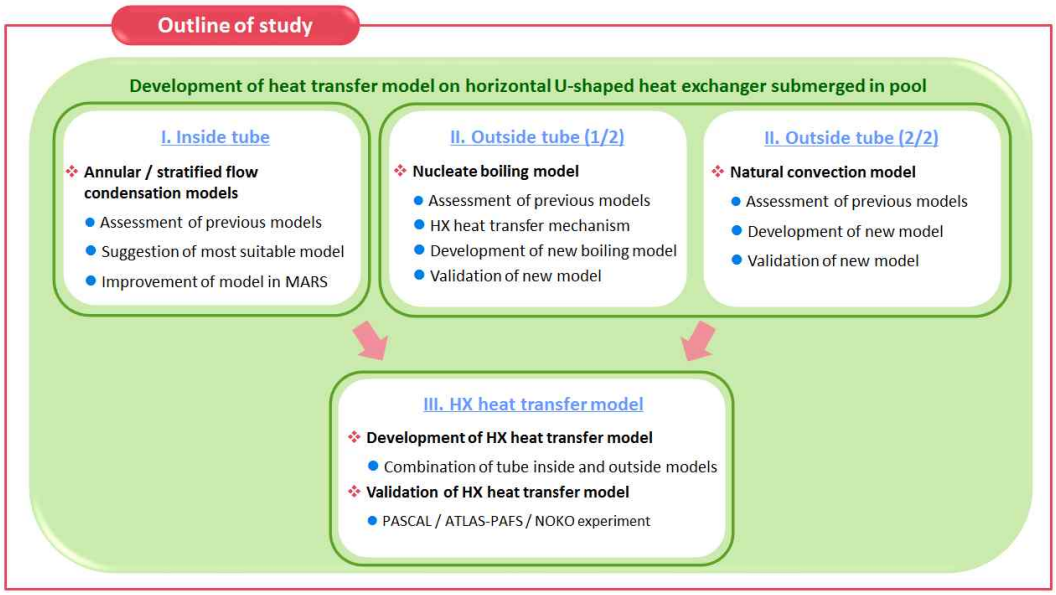

Figure 1.6 Research outline

Chapter 2

Improvement of MARS on Horizontal In-Tube Condensation Heat Transfer Model

2.1 State-of-the-Art

Horizontal in-tube condensation is a frequent and important phenomenon encountered in many industrial applications such as refrigeration and air-conditioning systems, chemical process industries, power engineering and other thermal processing plants. In advanced NPP designs, this phenomenon is proposed as an important heat transfer process in the horizontal type heat exchanger of the passive safety system because this mode of heat transfer has a high heat removal capability.

Over the past few decades, in various engineering fields, there have been many experimental and analytical researches using working fluids such as refrigerants and organic fluids, and numerous models have been proposed to understand and predict the horizontal in-tube condensation heat transfer. All models tend to predict the heat transfer most accurately in the flow regime for which they were derived. However, they, based on the use of limited database, show a considerable deviation for the experimental data from different authors for

different fluids and flow conditions. Moreover, there is not a single correlation that can be universally applied to all flow regimes because the heat and mass transfer process is strongly influenced by the local flow regimes.

In the field of nuclear engineering, many researches have focused on the condensation heat transfer models in vertical tube. Recently, the mechanistic condensation model for the nearly-horizontal heat exchanger tube under the steam flowing conditions was developed by Ahn et al. (2014) and the validation researches of the model implemented to BE codes have been performed; however, there are still few condensation models developed for HX of the passive safety system. Furthermore, there are few validation researches on the applicability of previous models to the HX of the passive safety systems. Therefore, for the optimum design and safety analysis of the passive safety systems, it is necessary to assess the predictive capability of the previous condensation models for each flow regime of the steam-water two phase flows using various experimental data first.

2.2 Review of Previous Condensation Models

2.2.1 Determination of Main Flow Regime

Before the assessments of the previous condensation models for each flow regime, it is essential to determine the main flow regimes encountered in the HX tube of the passive safety systems. Through many researches on the horizontal in-tube condensation, it is confirmed that the flow regime is dominated by the

balance between vapor shear force and gravity force. When the vapor shear force predominates, annular-mist or annular flow pattern appears, and when the gravity force is dominant, wavy, stratified, and slug flow patterns appear. Among those flow patterns, this study focused on the annular and stratified flow patterns (see Fig. 1.1) because they are the main flow regimes encountered in a horizontal condenser.

For the annular-mist flow, with the appearance of a thin annular film with a mixture of vapor and mist in the core flow, it might appear in the tube inlet region where the gas flow rate is very high but the region is very short; for this reason, this study considers the annular-mist flow as a part of the annular flow. For the wavy flow, with the appearance of waves on the interface between the liquid pool and the vapor, it might appear as transition flow between annular and stratified flow but it is not easy to distinguish the stratified flow from wavy flow; for this reason, this study considers the wavy flow as a part of the stratified flow. For the slug flow, it might appear in the tube outlet region where the vapor flow rate is still high and the quality is low, but this pattern might cause the mechanical problem like the water hammer due to the flow instability. Generally, heat exchangers are designed to ensure that slug flow pattern does not appear in the condenser tube. For this reason, this study does not consider the slug flow condensation.

2.2.2 Stratified Flow Condensation Models

Numerous horizontal in-tube condensation models are available in the literature, and most of these models can be categorized as gravity dominated

stratified flow or shear dominated annular flow models. In this section, stratified flow condensation models to be assessed are presented. The correlations and main parameters for each model are shown in Table 2.1.

Akers and Rosson (1960) developed the condensation heat transfer models for the refrigerants and organic fluids with an introduction of Reynolds number, which cover both annular and stratified flow regimes. The Akers and Rosson (1960) model is very old but is still recommended as fundamental design tools for horizontal tube condensers. Chato (1962) studied the stratified flow with lower vapor velocity. He developed a modified version of the classic Nusselt (1916) theory for the falling film condensation. In analytical model by Chato (1962), the heat transfer through the thick condensate layer at the bottom portion of the tube is considered negligible compared to the heat transfer through the thin film on the upper portion of the tube wall.

Rosson and Meyers (1965) studied the stratified flow with higher vapor velocity using acetone and methanol as a working fluids. They obtained the HTC at different angles around the periphery of the condenser tube and proposed different heat transfer correlations for top and bottom of the tube. For top of the tube, they modified the classic Nusselt model by introducing the effect of vapor shear. For the bottom of the tube, the von Karman analogy was used to predict the HTCs. The beta is a parameter for perimeter fraction to get the circumferentially averaged HTCs. Jaster and Kosky (1976) modified the Chato (1962) model by introducing the vapor void fraction to consider the liquid pool depth variation in the stratified flow. He also assumed that the heat transfer through the thick liquid layer at the bottom portion of the tube is negligible. This assumption is reasonable for very low vapor velocities, but the heat transfer in the liquid pool might not be

negligible in high vapor velocity situations where wavy or stratified flow could prevail with substantial convective heat transfer in the bottom part of the tube (Dobson and Chato, 1998).

Tandon et al. (1995) presented a modified model from that of Akers and Rosson using their experimental data based on refrigerants such as R12 and R22. They modeled the heat transfer in both the shear-controlled-flows (annular and semi-annular flow) and gravity-controlled flows (wavy flow). Fujii (1995) developed two condensation models for shear-controlled and gravity-controlled regimes using his experimental data based on the refrigerants such as R22 and R134a. Dobson and Chato (1998), based on their condensation tests using zeotropic refrigerants, developed flow regime map based two-phase flow condensation heat transfer models for both annular and stratified-wavy flow regimes. For the stratified-wavy flow regime, they significantly improved the Chato (1962) model. Their model considered both the film condensation at the top of the tube and forced convective condensation at the bottom of the tube. Sweeney and Chato (1996) made a simple modification on the Dobson and Chato (1998) model by considering the effect of mass flux to predict the HTC of zeotropic mixtures based on R-407C. They modeled the heat transfer in both wavy-stratified and annular flow regimes.

Cavallini et al. (2002) developed a flow regime map based condensation model for the annular flow and stratified flow regimes and validated it with over 2000 data points consisting of 9 different refrigerants obtained by independent research workers. Their stratified flow condensation model includes both film and convective condensation heat transfer. Thome et al. (2003) developed a flow pattern based condensation heat transfer model for the mist, annular, stratified

wavy, and fully stratified flow regimes. Their model considers both film and convective condensation effects in the stratified wavy and fully stratified flow regimes. Thome et al. (2003) compared their model with a large condensation database of 15 different fluids that includes 1850 refrigerant data points and 2771 hydrocarbon data points. Cavallini et al. (2006) presented a new condensation model to predict HTCs of fluid flowing inside horizontal smooth tubes based on their extensive analysis of 425 experimental heat transfer data points. Their model gives two sets of formulas: one for higher flow rates (annular flow regime) and one for lower flow rates (wavy stratified flow regime). The model has been verified with a total number of 5478 data points relative to HCFCs, HFCs, HCs, carbon dioxide, ammonia, and water from several independent laboratories.

2.2.3 Annular Flow Condensation Models

Numerous horizontal in-tube condensation models for the annular flow are available in the literature. In this section, the annular flow condensation models to be assessed are presented. They can be divided into three major categories: two-phase multiplier based, shear based, and boundary layer based models. The correlations and main parameters for each model are shown in Table 2.2.

The first category is the two-phase multiplier-based model as the most common approach. Analogous to the assumption made by Lockhart and Martinelli (1947) for the prediction of two-phase frictional pressure drop, this model assumes that the heat transfer process in annular two-phase flow can be calculated from that in single-phase flow of the liquid by introducing a suitable two-phase multiplier. In this model, the single-phase HTCs are typically predicted by the

Dittus and Boelter (1930) correlation, and the two-phase multiplier is usually given as a function of some of the following parameters: vapor quality, viscosity and density ratios, reduced pressure, liquid Froude number, Martinelli parameter and etc. These type models are as follows.

Akers et al. (1959), based on a database for several refrigerants and organic fluids, developed a two-phase multiplier-based model that became known as the equivalent Reynolds number model in the literature. This model defines the all-liquid mass flow rate that provides the same HTC and wall shear stress as an annular condensing flow. The equivalent Reynolds number is determined from an equivalent mass velocity, which in turn is obtained by applying a multiplying factor to the total mass velocity. Akers and Rosson (1960) developed the condensation heat transfer models for the refrigerants and organic fluids by introducing Reynolds number, which cover both annular and stratified flow regimes. It is a modified version of the Dittus-Boelter (1930) single-phase forced convective heat transfer correlation. Their model is applicable to turbulent annular flow. Though the models by Akers et al. (1959) and Akers and Rosson (1960) are very old but are still recommended as fundamental design tools for horizontal tube condensers.

Boyko and Kruzhilin (1967) proposed the two-phase multiplier type condensation model based on the analogy between hydraulic resistance and heat transfer in accordance. It was reported that the model presented an approximate prediction of heat transfer during steam condensation inside a tube. Cavallini and Zecchin (1974), based upon a theoretical analysis for heat and momentum similarity in annular flow regime, developed a simple dimensionless semi-empirical model for the condensation of various organic refrigerants. This model

is shown to be of the two-phase multiplier type. Shah (1979) developed a two-phase multiplier type condensation heat transfer model. It has been compared with a wide variety of experimental data for turbulent condensation conditions, especially in vertical tubes, for years. It has been widely used in the annular flow regime as one of the most comparative condensation model. It was incorporated as a turbulent flow condensation model in BE codes such as RELAP5 (USNRC, 2006) or MARS (KAERI, 2009).

Bivens and Yokozeki (1994) made a modification on the Shah (1979) model with an introduction of the empirical term that contains mass flux. This was introduced in order to fit their experimental data with a wide range of mass flows, where various types of flow patterns occur. Tandon et al. (1995) presented a modified model from that of Akers and Rosson using their experimental data based on refrigerants such as R12 and R22. They modeled the heat transfer in both the shear-controlled-flows (annular and semi-annular flow) and gravity-controlled flows (wavy flow). Fujii (1995) developed two condensation models for shear-controlled (annular flow) and gravity-controlled regimes (wavy-stratified flow) using his experimental data based on the refrigerants such as R22 and R134a. Tang (1997), based on his condensation measurements for R-22, R-134a and R410A, proposed a modified version of Shah (1979) model. This model is valid in the annular flow only.

Dobson and Chato (1998), based on their condensation tests using zeotropic refrigerants, developed flow regime map based two-phase flow condensation heat transfer models for both annular and stratified-wavy flow regimes. They significantly improved the Chato (1962) model that includes both the stratified-wavy flow and annular flow model. For the annular flow regime, they used a two-

phase multiplier approach to develop the condensation model. Sweeney and Chato (1996) made a simple modification on the Dobson and Chato (1998) model by considering the effect of mass flux to predict the HTC of their experiment based on R-407C. They modeled the heat transfer in both the wavy-stratified and annular flow regimes.

Cavallini et al. (2006) presented a new condensation model to predict HTCs of fluid flowing inside horizontal smooth tubes based on their extensive analysis of 425 experimental heat transfer data points. Their model gives two sets of formulas: one for higher flow rates (annular flow regime) and one for lower flow rates (wavy stratified flow regime). The model has been verified with a total number of 5478 data points relative to HCFCs, HFCs, HCs, carbon dioxide, ammonia, and water from several independent laboratories. Shah (2009) presented an improved version of the previous published model (Shah 1979), extended to a wider range of parameters. The new model has been shown to be in good agreement with experimental data for highly turbulent flows.

The second category is the shear stress-based model. It was originally developed by Carpenter and Colburn (1951), which was subsequently modified by Soliman et al. (1968) and then was modified by Chen et al. (1987). This model assumes that the major force acting on the condensate film was the vapor shear rather than the gravity, and the dominant thermal resistance to heat transfer in turbulent liquid flow occurs in the laminar sub-layer of the liquid film. This model includes the shear stress term which is affected by three factors: gravity, momentum and friction.

The third category is the boundary layer-based (analytical) model. It is similar to the shear-based model, except that the thermal resistance is considered

throughout the entire liquid film thickness, not just in the laminar sub-layer. There are many boundary layer-based models available, including those of Kosky and Staub (1971), Traviss et al. (1973), Moser et al. (1998), and Cavallini et al. (2002). They developed theoretical analyses based on the analogy between momentum and heat transfer. For these models, the HTC is a function of the interfacial vapor-liquid shear stress and the liquid film thickness.

Kosky and Staub (1971) developed the boundary layer-based model to be applied for the annular flow condensation. They assumed uniform film thickness along the circumference. In this model, the HTCs are determined as a function of the dimensionless temperature, dimensionless condensate layer (or film) thickness and the steam velocity at the vapor-liquid interface. Traviss et al. (1973) investigated the flow regime maps for condensation inside tubes. They analytically derived a condensation model for the annular flow regime by the introduction of some dimensionless parameters with a use of momentum and heat transfer similarity. It is the most widely quoted model in this class. Moser et al. (1998) developed a semi-analytical model for condensation in the annular flow regime, accounting for an effect of tube wall curvature. They devised correction factors to fulfill the shortcomings of Akers et al. (1959) model. Cavallini et al. (2002) developed a flow regime map based condensation model for the annular flow and stratified flow regimes and validated it with over 2000 data points consisting of 9 different refrigerants obtained by independent research workers. Their annular flow condensation model is based on an interfacial shear, which is similar to that developed by Kosky and Staub (1971).

Thome et al. (2003) developed the flow pattern based condensation heat transfer model which covers the mist, annular, stratified wavy, and fully stratified

flow regimes. Other than above three approaches (two-phase multiplier based, shear based, and boundary layer based models), this model is based on film flow, rather than the liquid turbulent flow. Their model includes the effects of liquid vapor interfacial roughness, or wave, for the annular flow. Thome et al. (2003) compared their model with a large condensation database of 15 different fluids that includes 1850 refrigerant data points and 2771 hydrocarbon data points.

2.3 Analysis Approach

2.3.1 Description of Collected Experiments

This study collected the heat transfer data from 4 horizontal in-tube condensation experiments by Wu (2005), Kondo et al. (2006), Kang et al. (2012), and Schaffrath and Prasser (1998). Those experiments were conducted to investigate the TH behavior in the condenser tube locally and to confirm the heat transfer performance of the passive safety systems such as PCCS, PAFS, and ECS. The experimental information for the test section geometry, test conditions, main flow regime in condenser tube, and secondary side cooling type are summarized in Table 2.3. The detailed descriptions of collected experiments are as follows.

A. Purdue-PCCS Experiment

In Purdue University, the steam condensation experiments with a presence of NC gas in a horizontal heat exchanger were performed to support the horizontal PCCS design (Wu, 2005). Figure 2.1 shows the schematic diagram of the

experimental facility, which consists of the SG, the NC gas supply line, the coolant water supply, the test section, the condensate collection system, the associated piping and water storage tanks, the instrumentation and the data acquisition system. The test section is a double pipe, concentric-tube heat exchanger. The inner tube is the condenser tube and the outer tube is the annular cooling jacket. The steam and NC gas mixture is injected into the condenser tube and the cooling water is injected into the cooling jacket in a countercurrent pattern.

Geometrical data of the test section is shown in Table 2.3. The condenser tube is a 4.5 m long SS304 tube of 27.5 mm ID and 2.1 mm wall thickness with a heat transfer length of 3.0 m. The outer diameter of cooling jacket is 63.5 mm.

In the experiment, the centerline, tube inner/outer wall and coolant temperatures were measured at 14 cross-sections along the test section (see Fig. 2.2). From the measured temperatures, the local HTCs at the top and bottom of the tube were separately obtained as follows.

1) The local heat fluxes at the top and bottom of the tube are separately calculated as

$$q''_{wall,in,*}(z) = \frac{k_w \left(T_{wi,*}(z) - T_{wo,*}(z) \right)}{r_{w,in} ln \left(\frac{r_{wo}}{r_{wi}} \right)} \tag{2.1}$$

2) The local HTCs at the top and bottom of the tube are respectively derived as

$$h_*(z) = \frac{q''_{wall,in,*}(z)}{T_{cl}(z) - T_{wall,in,*}(z)} \tag{2.2}$$

In Eqs. (2.1) and (2.2), z is defined as the length from the start of the heat transfer region, T_{cl} is the centerline temperature, and the subscript '*' indicates the

“top” or “bottom” of tube.

Purdue-PCCS experiment, which was the only one to provide the overall and local heat transfer data for the steam-water stratified flow regime from the inlet region of the condenser tube. The test conditions of this experiment were briefly listed in Tables 2.3 and 2.4. The steam flow rate ranged from 6.0~23.0 g/s. The test section inlet total pressure was 1~4 bar. The coolant inlet temperature and flow rate were fixed at 318.15 K and 1.48 kg/s, respectively. In the experiment, the inlet air mass fraction of 1~20 % were used but this study used the experimental data for the test conditions of case 6, 3, 20, 101, 24, and 27 with low inlet air mass fraction, 1~2 %.

For the prediction of the horizontal in-tube condensation heat transfer, the NC gas effect should be considered importantly because it affects the condensation degradation. However, the present system codes have many uncertainties in the NC gas model as well as the condensation model. This study first focused on the assessment of the condensation heat transfer model. In order to exclude the NC gas effect on the condensation heat transfer as much as possible, the pure steam or low NC gas concentration data were used. The assessment of NC gas model might be appropriate after good condensation model is selected.

B. JAEA-PCCS Experiment

In Japan atomic energy agency (JAEA), a single U-tube condensation heat removal experiment was performed to investigate the TH behavior in the U-tube locally and to confirm the heat transfer performance of the PCCS (Nakamura et al., 2000; Kondo et al., 2006). Figure 2.3 shows a schematic of the single U-tube test facility, which consists of the steam generation tank, NC gas supply line, coolant

water supply, test section, wetwell simulation tank, etc. The test section is composed of the U-type condenser tube and four annular cooling circuits. The mixture of steam and NC gas is injected into the condenser tube and the cooling water is injected into four cooling circuit inlet in a co-current pattern.

Geometrical data of the test section is shown in Table 2.3. The U-tube is composed of two 4 m straight parts and a U-bend whose radius is 0.3 m. The tube, made from SUS304, is 29 mm in the inner diameter and 1.4 mm in the thickness. The straight parts are composed by 16 cells whose length is 0.25 to 1 m in the flow direction. Each cell has a concentric water jacket to measure local heat removal rate. The diameter of the water jacket for the secondary coolant is 43 mm.

In the experiment, the centerline, tube wall and coolant temperatures were measured at 16 cells along the test section (see Fig. 2.3). From the measured temperatures, the local HTCs at the top and bottom of the tube were separately obtained as follows.

1) The local heat removal rate is calculated from the enthalpy difference of the secondary coolant between the blanket inlet and outlet, and the mass flow rate.

$$\dot{q}(z) = \left(H_{outlet}(z) - H_{inlet}(z) \right) W \tag{2.3}$$

2) The primary local HTCs at the top and bottom of the tube are derived from the centerline temperatures and the wall surface temperature, respectively.

$$h_{*}(z) = \frac{\dot{q}(z) / A}{T_{cl}(z) - T_{wall,in,*}(z)} \tag{2.4}$$

In Eqs. (2.3) and (2.4), z is defined as the length from the start of the heat transfer region, T_{cl} is the centerline temperature, and the subscript '*' indicates the "top" or "bottom" of tube.

The representative test condition obtained from the open literature for JAEA-

PCCS experiment is as follows (see Table 2.3). The steam and NC gas mixture velocity at the tube inlet was 20 m/s. The test section inlet pressure was 7 bar. The NC gas concentration was 1 % (volume) at the tube inlet. The secondary coolant, pressurized at 3 bar, was forced-circulated at the mass flow rate of 0.2 kg/s.

C. PASCAL Experiment

To validate the cooling and operational performance of the PAFS and to investigate the local TH behavior in the PCHX and the characteristics of the natural convection with pool boiling in the PCCT, KAERI performed the separate effect test using the PASCAL (PAFS Condensing Heat Removal Assessment Loop). Figure 2.4 shows the schematic diagram of the PASCAL (Kim et al., 2013). The main components of the PASCAL are a SG, steam-supply line, single U-shaped tube called as PCHX, return-water line, and PCCT. The steam injected into the PCHX is condensed by the heat exchange with the cold water in the PCCT.

Geometrical data of the test section is as follows (see Table 2.3). The PCHX is 8.4 m long tube with the inner diameter of 44.8 mm and the wall thickness of 3 mm. The U-tube is composed of two 3.22 m straight parts and a U-bend whose radius is 0.2667 m. The inclination is 3.0° in both upper and lower straight parts. The PCCT is the main heat sink of the SG. The dimensions of the PCCT are: length 6.7 m, width 0.112 m, height ~11.5 m.

In the experiment, the tube inner/outer wall temperatures were measured at 11 different axial locations along the tube length and the fluid temperature profile inside the tube was obtained in a radial direction (see Fig. 2.5). In addition, the local water temperatures were measured at 133 positions in the PCCT. From the measured temperatures, the local HTCs at the top and bottom of the tube were

determined separately by the same way as those of Purdue-PCCS experiment (see Eqs. (2.1) and (2.2)).

In the experiment, three quasi-steady state cases were performed with three given SG thermal power conditions, 300 kW, 540 kW, and 750 kW. The quasi-steady state data was obtained when the heat removal rate of the PCHX tube was nearly equivalent to the SG thermal power supplied for simulating the decay heat. For the assessments of the horizontal in-tube condensation models, the test conditions at quasi-steady state were briefly listed in Table 2.5. The steam flow rate ranged from 0.15~0.43 kg/s. The test section inlet pressure was 13~67 bar.

D. NOKO Experiment

The NOKO is a multipurpose TH test facility to experimentally investigate the emergency condenser effectiveness of the SWR-1000. A schematic diagram of the NOKO test facility is shown in Fig. 2.6. The main components of the facility are the pressure vessel (height 12.6 m, diameter 0.448 m), the laterally connected emergency condenser bundle and the condenser pool representing the core flooding pool of the SWR1000, which is the main heat sink of the reactor. The steam generated from pressure vessel is injected into the emergency condenser bundle. Then, the steam becomes condensate by the heat exchange with the cold water in condenser pool.

Geometrical data of the HX test section is as follows (see Table 2.3). The emergency condenser test bundle is composed of four U-tubes. The average tube length is ~9.8 m, the inner diameter is 38.7 mm, and the wall thickness is 2.9 mm. The inclination is 1.6° in the upper straight part and 3.2° in the lower straight part. The main dimensions of this pool are: length 6 m, diameter 2 m, volume 20 m^3.

In the NOKO tests, steady state cases were simulated to validate the cooling and operational performance of the emergency condenser. The steady state conditions such as the natural circulation flow rate and operating pressure obtained from the experiments were listed in Table 2.6.

2.3.2 Data Classification according to Flow Regime

In order to assess the condensation models for each flow regime, it is required to classify the collected experimental data into two categories according to the flow regimes ranging from annular flow to stratified flow. This study classified the experimental data for each flow regime considering synthetically the information from the experimental document and the flow pattern predicted from the horizontal flow regime map in the MARS code. For JAEA-PCCS (Kondo et al., 2006), PASCAL (Kang et al., 2012), and NOKO (Schaffrath and Prasser, 1998) experiments, the local flow regimes were identified by the visual observation, local temperature measurement, and analysis of the improved version of ATHLET code, respectively. For most test conditions of these 3 experiments, the main flow regime were identified as annular flow at the inlet region of the upper straight part of the condenser tube and stratified flow beyond the annular flow region. For this reason, the heat transfer data from these 3 experiments were used to assess both annular and stratified flow condensation models. On the other hand, for Purdue-PCCS (Wu, 2005) experiment, the local flow regime was identified by the analysis using the Mandhane flow regime map (Mandhane et al., 1974) and the Jaster and Kosky flow regime identification criteria (Jaster and Kosky, 1976). For most of the test conditions, the major flow regimes in the horizontal condenser

tubes were identified as wavy and stratified flow (Wu, 2005; Wu and Vierow, 2006). For this reason, this study selected the heat transfer data from Purdue-PCCS experiment as a stratified flow condensation data.

The local condensation heat transfer accumulated from the inlet region affects the change of the flow regime, which affects again the local condensation heat transfer. This means that, for the case that the annular flow appears at the inlet region, if the condensation heat transfer in the annular flow region is not predicted well, consequently, the condensation heat transfer in the stratified flow cannot be predicted well. In general, the flow regime is changed from the annular flow to the stratified flow as the condensation progresses along the condenser tube. In such cases, the heat transfer data in the stratified flow region beyond the annular flow region cannot be used to assess the stratified flow condensation models before the appropriate annular flow condensation model is selected. Therefore, this study first assesses the stratified flow condensation models using Purdue-PCCS experiment. Next this study assesses the annular flow condensation models using JAEA-PCCS, PASCAL and NOKO experiments. Finally, the additional validation of the stratified flow condensation model selected as good one is discussed by combining the stratified flow condensation model with the annular flow condensation model.

2.3.3 MARS Modeling of Collected Experiments

A. MARS Nodalization for Purdue-PCCS Experiment

Figure 2.7 shows the MARS nodalization scheme for the simulation of the Purdue-PCCS experiment. The time-dependent volume, TDV-100, was used to

provide the inlet boundary condition for steam/NC gas mixture. In this volume, the NC gas concentration was determined by adjusting the bulk inlet temperature because the partial pressure of a NC gas was determined by subtracting the saturated pressure of steam corresponding to the bulk inlet temperature from the total inlet pressure. The inlet flow rate of the steam/NC gas mixture was controlled by the time-dependent junction, TDJ-125. The mixture flow rate was simply determined by the summation of the steam flow rate and NC gas flow rate. The pipe component, C200, was used to model the condenser tube. Steam and NC gas mixture is injected into this component from the TDV-100. The time-dependent volume, TDV-298 and TDV-300, were used to provide the boundary conditions for the pressure outlet. The condensate water is drained into the TDV-300 and the remaining steam and NC gas mixture is vented to the TDV-298. The heat structure, HS-200, was used to calculate the heat transferred from the steam/NC gas mixture to the coolant through the condenser tube wall.

In order to examine the condensation heat transfer of the inside of the condenser tube, other parts such as conduction in the tube wall or convective heat transfer in the cooling jacket must be accurately modeled (Bang et al., 2009). In this nodalization scheme, the secondary side was not modeled and the measured outer wall temperatures were used directly in the heat structure as a boundary condition to remove the undesirable effects, or uncertainties, due to the secondary-side heat transfer model as much as possible.

B. MARS Nodalization for JAEA-PCCS Experiment

Figure 2.8 shows the MARS nodalization scheme for the simulation of the JAEA-PCCS experiment. The time-dependent volume, TDV-100, was used to

provide the inlet boundary condition for steam/NC gas mixture. In this volume, the NC gas concentration was determined by adjusting the bulk inlet temperature because the partial pressure of the NC gas was determined by subtracting the saturated pressure of steam corresponding to the bulk inlet temperature from the total inlet pressure. The inlet flow rate of the steam/NC gas mixture was controlled by the time-dependent junction, TDJ-125. The mixture flow rate was simply determined by the summation of the steam flow rate and NC gas flow rate. The pipe component, C200, was used to model the condenser tube. Steam and NC gas mixture is injected into this component from the TDV-100. The time-dependent volumes, TDV-298 and TDV-300, were used to provide the outlet boundary conditions for the pressure outlet. The condensate water is drained into the TDV-300 and the remaining steam and NC gas mixture is vented to the TDV-298. The heat structure, HS-200, was used to calculate the heat transferred from the steam/NC gas mixture to the coolant through the condenser tube wall.

Unlike the Purdue-PCCS nodalization (see Fig. 2.7), in the JAEA-PCCS nodalization, the secondary-side cooling jacket was modeled to consider the effects of coolant injected into four cooling circuit inlet. Pipe components, C510, C540, C570, and C600, are used to model the four cooling circuit. TDV-500, 520, 530, 550, 560, 580, 590, 610 are used to provide the same inlet boundary condition for coolant. Thus the effect of uncertainty due to the conduction in the tube wall and secondary-side heat transfer model may exist in JAEA-PCCS simulations.

C. MARS Nodalization for PASCAL Experiment

Figure 2.9 shows the MARS nodalization scheme for the simulation of the

PASCAL experiment. The time-dependent volume, TDV-100, was used to provide the inlet boundary condition for pure saturated steam. The inlet flow rate of the steam was controlled by the time-dependent junction, TDJ-125. The pipe component, C200, was used to model the PCHX. Steam is injected into this tube from the TDV-100. The time-dependent volumes, TDV-298 and TDV-300, were used to provide the outlet boundary conditions. The condensate water is drained into the TDV-300 and the remaining steam is vented to the TDV-298. The heat structure, HS-200, was used to calculate the heat transferred from the steam to the cold water in the PCCT through the condenser tube wall.

In order to examine the condensation heat transfer of the inside of the condenser tube, other parts such as conduction in the tube wall or convective heat transfer with pool boiling in the condenser pool must be accurately modeled (Bang et al., 2009). Like the Purdue-PCCS nodalization (see Fig. 2.7), the secondary side was not modeled in the PASCAL nodalization, and the measured outer wall temperatures were used directly in the heat structure as a boundary condition to remove the undesirable effects, or uncertainties, due to the secondary-side heat transfer model such as the natural convection and pool boiling as much as possible.

D. MARS Nodalization for NOKO Experiment

Figure 2.10 shows the MARS nodalization scheme for the simulation of the NOKO experiment. The time-dependent volume, TDV-100, was used to provide the inlet boundary condition for pure saturated steam. The inlet flow rate of the steam was controlled by the time-dependent junction, TDJ-125. The pipe component, C200, was used to model the bundle of four condensing tubes. Steam

is injected into this tube bundle from the TDV-100. The time-dependent volumes, TDV-298 and TDV-300, were used to provide the outlet boundary conditions. The condensate water is drained into the TDV-300 and the remaining steam is vented to the TDV-298. The heat structure, HS-200, was used to represent the heat transferred from the steam to the cold water in the condenser pool through the condenser tube wall.

Unlike the Purdue-PCCS nodalization of Fig. 2.7, in these NOKO simulations, the condenser pool was modeled because the local wall temperatures were not provided in the NOKO experiment. Pipe components, C090 and C092, are used to model the condenser pool. They are connected by the multiple junction, MJ-091, to simulate the natural convection in the pool. TDV-094 is coupled to the pool for pressure control. Thus, the effect of uncertainty due to the secondary-side heat transfer model such as the natural convection and pool boiling may exist in NOKO simulations.

2.4 Results and Discussion

In order to assess the condensation model for annular and stratified flows, total 19 annular and 11 stratified flow models presented in Tables 2.1 and 2.2 were incorporated into the MARS code. Using this modified MARS code, simulations for Purdue-PCCS, JAEA-PCCS, PASCAL and NOKO experiments were performed. The models were assessed through 3 items: 1) overall heat transfer rate, 2) local heat flux, and 3) local HTC. The overall heat transfer rate is the most important parameter in the performance and safety analysis of the HX and the

local heat transfer rate is the critical parameter considered to be in the optimum design of the HX. The models which predict both overall and local heat transfer rate well can be evaluated as good models.

2.4.1 Simulation of Purdue-PCCS Experiment

A. Overall Heat Transfer Rate

Table 2.7 shows the comparison of the experimental data against the calculation results from MARS with different models for overall heat transfer rate through the condenser tube. The original MARS code, based on the combination of models by Shah (1979) and Chato (1962), predicted the data significantly well within a mean deviation of 3 %. Models by Akers and Rosson (1960), Rosson and Meyers (1965), Jaster and Kosky (1976), Dobson and Chato (1998), Sweeney and Chato (1996), Cavallini et al. (2002), Thome et al. (2003) and Cavallini et al. (2006) predicted the data reasonably well within a mean deviation of 4 %. On the other hand, models by Chato (1962), Tandon et al. (1995), Fujii (1995) predicted the data generally well with a mean deviation of 4.22, 5.56, and 3.97 % respectively but, for the cases of 24 or 27, they under-predicted the data with a deviation of more than 10 %. However, considering the complexity of the horizontal in-tube condensation phenomenon, about 15 % deviation in estimating the condensation heat transfer might not be a bad result. Therefore, it is concluded that all previous models can be used to predict the overall heat transfer rate in Purdue-PCCS experiment for the steam-water stratified flow condition even though they were developed mainly based on refrigerants, not steam.

B. Local Heat Flux

Figure 2.11 shows the comparison of the experimental data against the calculation results from MARS with different models for local heat flux. In the experiment, the local heat fluxes were obtained separately from the top and bottom of the condenser tube wall whereas, in the MARS code, it was provided as volume averaged value. In general, the local heat flux continuously decreased from the top of the tube to the bottom of the tube. Thus, this author decided that good models were the ones which could provide the nearest results to the average values of top and bottom heat fluxes.

On the other hand, low NC gas concentration data was used in these simulations but the NC gas effect might be important because the NC gas concentration increases along the tube. This study divided the heat transfer region into two sub-sections (section 1 indicates the high heat transfer region near the inlet, and section 2 indicates the low heat transfer region near the outlet) and focused on the prediction of the heat transfer in the section 1 where NC gas concentration is low. By this, the NC gas effect on the condensation heat transfer could be excluded as much as possible. Furthermore, given that the horizontal in-tube condensation heat transfer is significantly influenced by the local flow regime, which is determined by the heat transfer accumulated from the inlet, to focus on the high heat transfer region may be a valid method for the assessment of condensation model.

Generally, models by Akers and Rosson (1960), Chato (1962), Tandon et al. (1995), Sweeney and Chato (1996), and Cavallini et al. (2002) under-predicted the data in section 1 and similarly- or over- predicted the data in section 2. On the contrary to this, models by Rosson and Meyers (1965), Jaster and Kosky (1976),

Fujii (1995), Dobson and Chato (1998), Thome et al. (2003), Cavallini et al. (2006) similarly- or over-predicted the data in section 1, and similarly- or under-predicted the data in section 2. There were no models to predict well the data in both sections for all conditions. However, it should be noted that Cavallini et al. (2006) model is very good at predicting the data in section 1 for all cases though it under-predicted the data in section 2. Considering that the main condensation heat transfer region is section 1, it is worthy of recommendation as a good model for steam-water stratified flow conditions in Purdue-PCCS experiment.

On the other hand, from these figures, it is notable that the graph shapes for the local heat flux were very different according to the models even though all models provided good predictions for overall heat transfer rate. This means that all models which predict the overall heat transfer rate well are not good models. For example, although Chato (1962) model under-predicted significantly the data in section 1, it could predict the overall heat transfer rate well with a mean deviation of 4.22 % because it over-predicted the data in section 2. In this case, if the heat exchanger length is optimally designed to be short, the model may fail to predict the overall heat transfer rate. In other words, if this model is used to design the condenser tube, the tube length might conservatively become longer for the complete condensation. This is undesirable from the viewpoint of system maintenance and initial cost. In this respect, it is found that the analysis of the local heat flux as well as the overall heat transfer is essential to assess the condensation models.

C. Local HTC

In order to assess the condensation model, this study compared the local HTCs

obtained from the experiment with those calculated from the MARS code. For the analysis of the local HTCs, the followings were taken into consideration. In the experiment, the local HTCs were determined using the centerline temperature, as shown in Eq. (2.2), which is almost constant in the inlet region but suddenly decreases beyond some point, as shown in Fig. 2.12. This means that, near the inlet region, the local steam saturation temperature corresponding to the steam partial pressures of the mixture is measured at the centerline but if the centerline is flooded with the condensate water as the condensation progresses along the tube, the subcooled water temperature is measured at the centerline. According to this, the local HTC which is defined as a function of the temperature difference between the steam and the tube inner wall is changed as a function of the temperature difference between the subcooled water and the tube inner wall. However, in 1D code such as MARS or RELAP5, there is no concept for the centerline and it could not know whether the centerline is flooded with the condensate water or not. For this reason, it is very difficult to compare the data with the MARS predictions for the local HTCs throughout the condenser tube. Therefore, in this study, the local HTCs were compared within the "steam region", ~1.4 m, where the centerline temperature is the steam temperature. Given that the "steam region" is significantly overlapped with the section 1 (see Fig. 2.11) which is the main condensation heat transfer region, this may be a valid method to assess the condensation model.

Figure 2.13 shows the comparison between the experimental data and MARS calculation results for local HTCs under different stratified flow conditions. It was found that the original MARS code generally underestimated the experimental local HTCs. This means that Shah (1979) model as well as Chato (1962) model

does not predict the experimental data well and it is required to modify the condensation model in the MARS code.

For the stratified flow condensation models, the comparison results are divided into two groups according to the inlet mass flow rate. For cases 6, 20 and 24 with relatively low mass flow rate per each pressure, all predicted HTCs were between the top and bottom values of experimental HTCs (see Figs. 2.13(a), (c), and (e)). Many models with the exception of the Akers and Rosson (1960), Chato (1962), Rosson and Meyers (1965), Tandon et al. (1995), Sweeny and Chato (1996) and Cavallini et al. (2002) models showed good agreement with the experimental data. However, for cases 3, 101 and 27 with relatively high mass flow rate per each pressure, the models by Akers and Rosson (1960), Chato (1962), Tandon et al. (1995), Sweeny and Chato (1996) and Cavallini et al. (2002) significantly under-predicted the local HTCs; and Rosson and Meyers (1965), Jaster and Kosky (1976), Fujii (1995), Dobson and Chato (1998), and Thome et al. (2003) models overestimated the HTCs locally (see Figs. 2.13(b), (d), and (f)).

For all cases, the Cavallini et al. (2006) model shows good agreement with experimental data. In other words, Cavallini et al. (2006) model provides the nearest results to the average value of top and bottom HTCs. Though Cavallini et al. (2006) model over-predicts the local HTCs for the condition of case 3 a little, given that lower HTCs were obtained from the top of tube wall than those of case 6 despite the increase of mass flux, those results can be acceptable. Therefore, from this assessment, it is concluded that Cavallini et al. (2006) model appears to be the most accurate one to predict the condensation heat transfer for steam-water stratified flow conditions in Purdue-PCCS experiment.

2.4.2 Simulation of JAEA-PCCS Experiment

A. Local HTC

In order to assess the annular flow condensation model, this study compared the local HTCs obtained from the JAEA-PCCS experiment with those calculated from the MARS code as shown in Fig. 2.14. According to the assessment described in Chapter 2.4.1, the local HTCs were compared within the "steam region", from inlet to 3 m distance, where the centerline temperature was the steam temperature and the flow regime was identified as the annular flow (see Fig. 2.15 (Kondo et al., 2006)).

Including the original MARS code, based on the combination of models by Shah (1979) and Chato (1962), the models by Akers et al. (1959), Akers and Rosson (1960), Boyko and Kruzhilin (1967), Tandon et al. (1995), Fujii (1995), Tang (1997), Sweeny and Chato (1996), Cavallini et al. (2002, 2006), Shah (2009), Chen et al. (1987), and Thome et al. (2003) under-predicted the local HTCs throughout the annular flow region of the condenser tube significantly. The Bivens and Yokozeki (1994) model over-predicted the local HTCs considerably except the inlet region (~0.5 m). On the contrary to this, the models by Cavallini and Zecchin (1974), Dobson and Chato (1998), Kosky and Staub (1971), Traviss et al. (1973), and Moser et al. (1998) showed qualitatively good agreements with the experimental data. Especially, for the inlet region (~0.5 m), Kosky and Staub (1971) model predicted the data well and, beyond the inlet region, Dobson and Chato (1998) model presented the nearest results to the experimental data overall. Therefore, it could be concluded that the models by Cavallini and Zecchin (1974), Dobson and Chato (1998), Kosky and Staub (1971), Traviss et al. (1973), and

Moser et al. (1998) are appropriate to use for the prediction of the annular flow condensation heat transfer in JAEA-PCCS experiment.

B. Local Heat Flux

The local HTC is the most important variable for the assessment of the condensation models. However, as described in Chapter 2.4.1, the comparison of the local HTCs throughout the condenser tube between the code and experiment is difficult if the water temperature is measured at the centerline of the tube as the condensation progresses along the test section. For JAEA-PCCS experiment, the water temperature was measured at the centerline of the lower straight part of the U-tube. In order to assess the predictive capability of the condensation models for whole region of the condenser tube, this study analyzed the local heat flux which is easy to compare.

Figure 2.16 shows the comparison between the experimental data and MARS calculation results for the local heat fluxes. The heat transfer region is roughly divided into two sub-sections: section 1 indicates the annular flow region (0 - 4 m) in the upper straight part of the U-tube, and section 2 indicates the wavy and stratified flow region (4 - 8 m) in the lower straight part of the U-tube. This study assessed the condensation models according to each flow regime.

For the annular flow region, the predictive capabilities of models by Akers et al. (1959), Shah (1979), Dobson and Chato (1998), and Kosky and Staub (1971) were assessed. Both Akers et al. (1959) model, which showed the lowest HTCs (see Fig. 2.14), and Shah (1979) model, which is the annular flow condensation model in MARS, under-predicted the local heat fluxes significantly. Dobson and Chato (1998) and Kosky and Staub (1971) models, which presented good results

for the local HTCs (see Fig. 2.14), predicted the data better than the models by Akers et al. (1959) or Shah (1979) but still under-estimated the local heat fluxes. No condensation models predict the local heat fluxes in JAEA-PCCS experiment well. This might be because the uncertainty of secondary-side heat transfer model is included in this MARS nodalization scheme. However, considering that the heat resistance (1/hA) at the secondary side is larger than the primary side, the gaps between the results may be considered acceptable. Furthermore, it could be concluded that the models by Dobson and Chato (1998) and Kosky and Staub (1971) are appropriate to use for the prediction of the annular flow condensation heat transfer in JAEA-PCCS experiment.

For the wavy and stratified flow region, the predictive capabilities of 11 stratified flow condensation models, presented in Table 2.1, were assessed. In order to assess the stratified flow condensation models, it is essential to set the flow condition at the starting point of wavy and stratified flow, 4 m point from the inlet, similarly with the experimental flow condition at that point. The local condensation heat transfer is affected by the local flow structure, or condition, which is determined by the removal heat accumulated from the inlet; for this reason, this study artificially made the heat transfer in the annular flow region similar to that of the experiment by adjusting the fouling factor in the MARS code input. By this adjustment, each stratified flow condensation model could be assessed with the similar flow condition at 4 m point.

The experimental local heat fluxes decreased rapidly in the main condensation heat transfer region (4 – 6 m) but there were no models to predict this trend well. The models by Akers and Rosson (1960), Chato (1962), Tandon et al. (1995), and Cavallini et al. (2002) under-predicted the data in the main condensation heat

transfer region and similarly- or over-predicted the data beyond that region. On the contrary to this, models by Rosson and Meyers (1965), Jaster and Kosky (1976), Fujii (1995), Sweeney and Chato (1996), Dobson and Chato (1998), Thome et al. (2003), and Cavallini et al. (2006) similarly- or over-predicted the data in the main condensation heat transfer region, and predicted the data beyond that region well. However, it is notable that Cavallini et al. (2006) model, which showed good predictive capability for the stratified flow condensation heat transfer in the Purdue-PCCS experiment, predicted the heat transfer at the starting point of the wavy and stratified flow. Considering that the predictions by Cavallini et al. (2006) model were connected smoothly with the local heat fluxes in the annular flow region and were qualitatively similar to the experimental data, it was concluded that Cavallini et al. (2006) model was appropriate to use for the prediction of the stratified flow condensation heat transfer in JAEA-PCCS experiment.

C. Overall Heat Transfer Rate

Table 2.8 shows the comparison of the experimental data against the calculation results from MARS with different models for overall heat transfer rate, or capacity, through the condenser tube. The original MARS code, based on the combination of models by Shah (1979) and Chato (1962), under-predicted the data with a deviation of 9.16 %. On the contrary to this, when the model by Dobson and Chato (1998) or Kosky and Staub (1971) was used as the annular flow condensation model instead of Shah (1979) model, the gaps between the results decreased by 6.19 %. Furthermore, when the model by Cavallini et al. (2006) was used as the stratified flow condensation model instead of Chato (1962)

model, the gaps between the results decreased more by 6.07 %. Consequently, it is found that the models by Dobson and Chato (1998), Kosky and Staub (1971) are more appropriate to use for the prediction of the annular flow condensation heat transfer in JAEA-PCCS experiment than Shah (1979) model.

2.4.3 Simulation of PASCAL Experiment

A. Local HTC

In order to assess the annular flow condensation model, this study compared the local HTCs obtained from the experiment with those calculated from MARS. The local HTCs were compared within the steam region. Since the steam temperatures were measured at the centerline to the end (~ 8.4 m) of the condenser tube in PASCAL experiments, this study could compare the local HTCs with the experimental data throughout the condenser tube. On the other hand, in PASCAL experiments, the local flow regime could be identified by the distribution of the fluid temperature inside the PCHX tube as shown in Fig. 2.17. It was found that the annular flow appeared along the inlet region, ~ 2 m, in the upper straight part of the PCHX tube and, beyond this region, the stratified flow appeared. Therefore, this study assessed the annular flow condensation models in the near-inlet region of the PCHX tube.

Figure 2.18 shows the comparison between the experimental data and MARS calculation results for local HTCs under different annular flow conditions. For all cases, Shah (1979) model generally underestimated the experimental local HTCs. The models by Akers et al. (1959), Sweeny and Chato (1996), Cavallini et al. (2002, 2006), Chen et al. (1987) and Shah (2009) predicted the local HTCs lower

than Shah (1979) model generally. This means that these models significantly under-predicted the local HTCs throughout the annular flow region of the condenser tube. On the contrary to this, models by Akers and Rosson (1960), Boyko and Kruzhilin (1967), Cavallini and Zecchin (1974), Bivens and Yokozeki (1994), Tandon et al. (1995), Fujii (1996), Tang (1997), Dobson and Chato (1998), Kosky and Staub (1971), Traviss et al. (1973), Moser et al. (1998), and Thome et al. (2003) presented the local HTCs higher than Shah (1979) model generally. The predictions by these models were between the top and bottom HTCs obtained from the experiment. Especially, it is worthy of notice that the models by Dobson and Chato (1998), Cavallini and Zecchin (1974), Kosky and Staub (1971), Traviss et al. (1973), and Moser et al. (1998), which showed good predictive capability for the annular flow condensation heat transfer in the JAEA-PCCS experiment, predicted the data well in PASCAL experiments. It is found that these models are appropriate to use for the prediction of the annular flow condensation heat transfer in the PASCAL experiment.

In order to investigate the capability of the annular flow condensation model combined with the stratified flow condensation model, this study modified the MARS code using Dobson and Chato (1998) model for an annular flow condensation model, which was the more recently developed model among above five annular flow models, and Cavallini et al. (2006) model for a stratified flow condensation model. Figure 2.19 shows the predictions from the combination of models by Dobson and Chato (1998) and Cavallini et al. (2006) compared with the calculations from the original MARS code with the combination of models by Shah (1979) and Chato (1962). For all cases, the combination of models by Dobson and Chato (1998) and Cavallini et al. (2006) predicted the experimental

local HTCs better than the original MARS code. Furthermore, it was found that the combination of models by Dobson and Chato (1998) and Cavallini et al. (2006) showed qualitatively better trend in the stratified flow region than the combination of Dobson and Chato (1998) and Chato (1962). Therefore, it was concluded that the stratified flow condensation model by Cavallini et al. (2006) was appropriate to use for the prediction of the stratified flow condensation heat transfer in the PASCAL experiment.

B. Overall Heat Transfer Rate

In addition to the comparison of local HTCs, the comparison of overall heat transfer rate was also carried out to assess the predictive capability of the condensation models. To achieve this, each annular flow condensation model was combined with the stratified flow condensation model by Cavallini et al. (2006). Table 2.9 shows the comparison of the experimental data against the calculation results from MARS for the capacity and average deviations of each model. The original MARS code, based on the combination of models by Shah (1979) and Chato (1962), under-predicted the capacity with an average deviation of 7.12 %. As the SG thermal power was lowered from 750 kW to 300 kW, the deviation was gradually increased from 4.38 % to 10.0 %.

On the contrary to this, the MARS code modified with the different annular and stratified flow condensation models instead of the combination of Shah (1979) and Chato (1962) models predicted the capacity for all cases within the average deviation of 2.51 %. Compared with the original MARS code, the average deviation decreased up to about 4.6 %. Especially, for the case of SS-300-P1, the deviation significantly decreases from 10.0 % to ~1.3 %. This decrease of the

deviation is mainly due to the change of the stratified flow condensation model from Chato (1962) to Cavallini et al. (2006). Without the combination with the annular flow condensation model, Cavallini et al. (2006) model alone predicted the capacity with an average deviation of 2.51 % while the model by Chato (1962) predicted the capacity with an average deviation of 16.36 %.

From Table 2.9, it is found that the models by Cavallini and Zecchin (1974), Dobson and Chato (1998), Kosky and Staub (1971), Traviss et al. (1973), and Moser et al. (1998), which showed good predictive capability for the annular flow condensation heat transfer in the JAEA-PCCS experiment, predicted the data in PASCAL experiments well. Especially, the models by Cavallini and Zecchin (1974), Dobson and Chato (1998), and Traviss et al. (1973) predicted the capacity within an average deviation of 2 % well. Therefore, it is concluded that these models are appropriate to use for the prediction of the condensation heat transfer for the steam-water annular flow.

2.4.4 Simulation of NOKO Experiment

In NOKO experiment, local HTCs were not reported by the authors (Schaffrath and Prasser, 1998). This study assessed the predictive capability of the condensation models by the analysis of the emergency condenser power, called as capacity. According to the horizontal flow regime map in MARS, the local flow regimes were identified as the annular and stratified flows in the condenser tube bundle. This means that the emergency condenser power is determined as the summation of the local heat transfer rate in both the annular and stratified flow regions. Therefore, for the analysis of the emergency condenser power, it is

required to use the MARS code with the combination of the annular and stratified flow condensation models. This study used both the original MARS code with the combination of models by Shah (1979) and Chato (1962) and the modified MARS code with the combination of models by Dobson and Chato (1998) and Cavallini et al. (2006). By comparing these two codes, the predictive capabilities of the combined condensation models were assessed.

Figure 2.20 and Table 2.10 show the comparison of the experimental data against the calculation results from the MARS code for the capacity. The original MARS code under-predicted the capacity with 7.71 % of average deviation whereas, the modified MARS code under-estimated the capacity with 2.70 % of average deviation. For all cases, the modified MARS code presented better results than the original MARS code. Therefore, it is concluded that the proposed combination of the Dobson and Chato (1998) and Cavallini et al. (2006) is applicable to use for the prediction of the steam condensation heat transfer.

2.5 Improvement of MARS on Horizontal In-Tube Condensation Heat Transfer Model

2.5.1 Selection of Annular Flow Condensation Model

From the assessments of nineteen annular flow condensation models, following conclusions are drawn.

(1) A default annular flow condensation model in MARS is the model by Shah (1979) based on the two-phase multiplier (see Table 2.2). Shah (1979) model has

been compared with a wide variety of experimental data for turbulent condensation conditions, especially in vertical tubes, for years. It has been widely used in the annular flow regime as one of the most comparative condensation model. However, the MARS code, based on the Shah (1979) model, generally under-estimated the annular flow condensation heat transfer in the horizontal condenser tube of the passive safety system.

(2) The models by Cavallini and Zecchin (1974), Dobson and Chato (1998), Kosky and Staub (1971), Traviss et al. (1973), Moser et al. (1998) showed good predictive capability of the condensation heat transfer for the steam-water annular flow. Especially, as the latest annular flow condensation model, the model by Dobson and Chato (1998) gave the most reasonable results under the operating condition of the passive safety system generally. Since Dobson and Chato (1998) used a two-phase multiplier approach to develop the condensation model, the correlation form is similar to the MARS default correlation (see Table 2.2) by Shah (1979); however, the correlation by Dobson and Chato (1998) was developed only based on more recent data obtained from the horizontal in-tube condensation experiments. As a result, it showed better results than the model by Shah (1979).

For the optimum design of the passive safety systems and safety analysis of the NPP using the BE code, it is required to improve the annular flow condensation model. Based on the assessment results, this author determined the annular flow condensation model by Dobson and Chato (1998) as the most applicable model to the HX of the passive safety system.

2.5.2 Selection of Stratified Flow Condensation Model

From the assessments of eleven stratified flow condensation models, following conclusions are drawn.

(1) A default stratified flow condensation model in MARS is the model by Chato (1962) for the stratified flow condensation with the lower vapor velocity. It assumes that the heat transfer through the thick condensate layer at the bottom portion of the tube is considered negligible compared to the heat transfer through the thin film on the upper portion of the tube wall. This assumption is reasonable for very low vapor velocities, but the heat transfer in the liquid pool might not be negligible in high vapor velocity situations where wavy or stratified flow could prevail with substantial convective heat transfer in the bottom part of the tube (Dobson and Chato, 1998). Since the vapor velocity in the condenser tube of the passive safety system is not very low to ignore, Chato (1962) model is not physically valid to be applied to the prediction of the stratified flow condensation heat transfer in the horizontal condenser tube of the passive safety system. As a result, the MARS code, based on the Chato (1962) model, generally under-estimated the experimental data for the stratified flow condensation.

(2) From the assessments of eleven stratified flow condensation models with the Purdue-PCCS data, the model by Cavallini et al. (2006) showed good predictive capability of the stratified flow condensation heat transfer for all test conditions. Furthermore, from the analysis of the JAEA-PCCS and PASCAL experiments, it was found that the stratified flow condensation model by Cavallini et al. (2006) was also applicable to the prediction of the condensation heat transfer for various steam-water stratified flow conditions. Unlike the model by Chato

(1962), the model by Cavallini et al. (2006) considered both the film condensation at the top of the tube and forced convective condensation heat transfer at the bottom of the tube (see Table 2.1). It has been verified with a total number of 5478 data points relative to HCFCs, HFCs, HCs, carbon dioxide, ammonia, and water from several independent laboratories. Therefore, it showed better results than the model by Chato (1962).

For the optimum design of the passive safety systems and safety analysis of the NPP using the BE code, it is essential to improve the stratified flow condensation model. Based on the assessment results, this author determined the stratified flow condensation model by Cavallini et al. (2006) as the most applicable model to the HX of the passive safety system.

2.5.3 Improvement of Horizontal In-Tube Condensation Model

For the prediction of horizontal in-tube condensation heat transfer, the original MARS code employs Shah (1979) and Chato (1962) models for the annular and stratified flow regimes, respectively. MARS determines the condensation HTC from the maximum of the values predicted by Shah (1979) and Chato (1962) models (see Eq. (2.5)) because the use of the maximum value ensures a smooth transition between models.

$$h = max\left(h_{annu},\, h_{strat}\right) \tag{2.5}$$

The original MARS code under-estimated the local HTCs and the heat removal performance of the HX in the passive safety system. To improve the horizontal in-tube condensation model in MARS, this study replaced the models by Shah (1979) and Chato (1962) with the annular flow condensation model by

Dobson and Chato (1998) and the stratified flow condensation model by Cavallini et al. (2006), respectively. For the smooth transition between models depending on the flow regime, this study applied the Eq. (2.5). The additional validation results of the proposed condensation model are described later in Chapter 4.

Table 2.1 Stratified flow condensation models (1/4)

1	Akers and Rosson (1960)
	$h = 13.8 Re_v^{0.2} Pr_l^{1/3} Ja_l^{-1/6} \left(\frac{k_l}{D} \right)$
2	Chato (1962)
	$h = 0.296 \left[\frac{\rho_l (\rho_l - \rho_v) h_{fg} g D^3}{k_l \mu_l (T_{sat} - T_w)} \right]^{1/4} \left(\frac{k_l}{D} \right)$
3	Rosson and Meyers (1965)
	$h = \left(\beta Nu_{top} + (1-\beta) Nu_{bot} \right) \left(\frac{k_l}{D} \right)$
	$Nu_{top} = 0.31 Re_g^{0.12} \left[\frac{\rho_l (\rho_l - \rho_v) h_{fg} g D^3}{k_l \mu_l (T_{sat} - T_w)} \right]^{1/4}$ $Nu_{bot} = \frac{\phi \sqrt{8 Re_l}}{5 + \frac{5}{Pr} ln(5Pr + 1)}$ $\beta = 0.27 Re_g^{0.1}$ for $\frac{Re_g^{0.6} Re_l^{0.5}}{Ga} < 6.4 \times 10^5$ $\beta = \frac{1.74 \times 10^{-5} Ga}{\sqrt{Re_g Re_l}}$ for $\frac{Re_g^{0.6} Re_l^{0.5}}{Ga} > 6.4 \times 10^5$
4	Jaster and Kosky (1976)
	$h = 0.725 \left[\frac{\rho_l (\rho_l - \rho_v) h_{fg} g D^3 \alpha_{Zivi}^3}{k_l \mu_l (T_{sat} - T_w)} \right]^{1/4} \left(\frac{k_l}{D} \right)$
5	Tandon et al. (1995)
	$h = 23.1 Re_v^{1/8} Pr_l^{1/3} Ja_l^{-1/6} \left(\frac{k_l}{D} \right)$

Table 2.1 Stratified flow condensation models (2/4)

6	Fujii (1995)
	$h = 0.725\left(\frac{GaPr_l}{Ja_l}\right)^{0.25}\left[\frac{\left(1+0.003\sqrt{Pr_l}a^{(3.1-0.5/Pr_l)}\right)^{0.3}}{(1+bc)^{0.25}}\right]\left(\frac{k_l}{D}\right)$
	$a = 0.47\sqrt{\frac{\rho_l}{\rho_v}}\left(\frac{Ja_l}{Pr_l}\right)^{1/12}\left(Re_l\frac{x}{1-x}\right)^{0.9}\left(\frac{GaPr_l}{Ja_l}\right)^{-0.275}$ $b = 1.55\sqrt{\frac{\rho_v}{\rho_l}}\left[1+1.6\times10^{11}\left(\frac{Ja_l}{Pr_l}\right)^5\right]^{0.25}\left[\left(\frac{GaPr_l}{Ja_l}\right)^{0.25}\left(Re_l\frac{x}{1-x}\right)^{-1}\right]^{1.8}$ $c = 40exp\left(\frac{-2.6\times10^{-4}Re_l}{1-x}\right)$
7	Dobson and Chato (1998)
	$h = \left[\begin{array}{l}\frac{0.23Re_{go}^{0.12}}{1+1.1X_{tt}^{0.58}}\left[\frac{GaPr_l}{Ja_l}\right]^{0.25} \\ +\left(1-\frac{\theta_{strat}}{\pi}\right)\left[0.0195Re_l^{0.8}Pr_l^{0.4}\sqrt{1.376+\frac{c_1}{X_{tt}^{C_2}}}\right]\end{array}\right]\left(\frac{k_l}{D}\right)$
	$1-\frac{\theta_{strat}}{\pi} = \frac{arccos(2\alpha_{Zivi}-1)}{\pi}$ $Fr_{lo} > 0.7:\ c_1 = 7.242,\ c_2 = 1.655$ $Fr_{lo} \le 0.7:\ c_1 = 4.172+5.48Fr_{lo}-1.564Fr_{lo}^2,\ c_2 = 1.773-0.169Fr_{lo}$
8	Sweeny and Chato (1996)
	$h = h_{Dobson}\left(\frac{G}{300}\right)^{0.3}$
9	Cavallini et al. (2002)
	$h = 0.725\left[\frac{k_l^3\rho_l(\rho_l-\rho_v)h_{fg}g}{\mu_l D(T_{sat}-T_w)}\right]^{1/4}\left[1+0.82\left(\frac{1-x}{x}\right)^{0.268}\right]^{-1}+h_{lo}(1-x)^{0.8}\left(1-\frac{\theta_{strat}}{\pi}\right)$
	$1-\frac{\theta_{strat}}{\pi} = \frac{arccos(2\alpha_{Zivi}-1)}{\pi},\ h_{lo} = 0.023Re_{lo}^{0.8}Pr_l^{0.4}\left(\frac{k_l}{D}\right)$

Table 2.1 Stratified flow condensation models (3/4)

10	Thome et al. (2003)
	$h = \dfrac{h_f r\theta + h_c (2\pi - \theta) r}{2\pi r}$
	$h_c = 0.003 Re_{lf}^{0.74} \, \mathrm{Pr}_l^{0.5} \dfrac{k_l}{\delta} f_i$ $h_f = 0.728 \left[\dfrac{\rho_l (\rho_l - \rho_v) g h_{fg} k_l^3}{\mu_l D (T_{sat} - T_w)} \right]^{1/4}$ $f_i = 1 + \left(\dfrac{u_v}{u_l} \right)^{1/2} \left(\dfrac{(\rho_l - \rho_v) g \delta^2}{\sigma} \right)^{1/4} \left(\dfrac{G}{G_{strat}} \right)$ $\theta = \theta_{strat} \left[\dfrac{G_{wavy} - G}{G_{wavy} - G_{strat}} \right]^{0.5}$ $\theta_{strat} = 2\pi - 2 \left[\begin{array}{l} \pi(1-\alpha) + \left(\dfrac{3\pi}{2} \right)^{1/3} \left[1 - 2(1-\alpha) + (1-\alpha)^{1/3} - \alpha^{1/3} \right] \\ -\dfrac{1}{200} (1-\alpha)\alpha \left[1 - 2(1-\alpha) \right] \left[1 + 4\left((1-\alpha)^2 + \alpha^2 \right) \right] \end{array} \right]$ $G_{wavy} = \left[\dfrac{16 A_{vd}^3 g D \rho_l \rho_v}{x^2 \pi^2 (1 - (2h_{ld} - 1)^2)^{0.5}} \left[\dfrac{\pi^2}{25 h_{ld}^2} \left(\dfrac{We}{Fr} \right)_l^{-1.023} + 1 \right] \right]^{0.5} + 50 - 75 e^{-(x^2 - 0.97)^2 / x(1-x)}$ $\left(\dfrac{We}{Fr} \right)_l = \dfrac{g D^2 \rho_l}{\sigma}$ $G_{strat} = \left[\dfrac{(226.3)^2 A_{ld} A_{vd}^2 \rho_v (\rho_l - \rho_v) \mu_l g}{x^2 (1-x) \pi^3} \right]^{1/3} + 20x$ $A_{vd} = \dfrac{A_v}{D^2} = \dfrac{\alpha A}{D^2}$, $h_{ld} = 0.5 \left(1 - cos \left(\dfrac{2\pi - \theta_{strat}}{2} \right) \right)$ $A_{ld} = \dfrac{A_l}{D^2} = \dfrac{(1-\alpha) A}{D^2}$ $\quad A_l = (1-\alpha) A$ $\quad A_l = \dfrac{(2\pi - \theta)}{8} [D^2 - (D - 2\delta)^2]$

Table 2.1 Stratified flow condensation models (4/4)

11	Cavallini et al. (2006)
	$h = \left[h_{annular} \left(\frac{J_g^T}{J_g} \right)^{0.8} - h_{strat} \right] \left(\frac{J_g}{J_g^T} \right) + h_{strat}$
	$h_{annu} = h_{lo} \left[1 + 1.128 x^{0.8170} \left(\frac{\rho_l}{\rho_v} \right)^{0.3685} \left(\frac{\mu_l}{\mu_v} \right)^{0.2363} \left(1 - \frac{\mu_v}{\mu_l} \right)^{2.144} Pr_l^{-0.1} \right]$ $h_{strat} = 0.725 \left[1 + 0.741 \left(\frac{1-x}{x} \right)^{0.3321} \right]^{-1} \left[\frac{k_l^3 \rho_l (\rho_l - \rho_v) h_{fg} g}{\mu_l D (T_{sat} - T_w)} \right]^{1/4} + (1 - x^{0.087}) h_{lo}$

Table 2.2 Annular flow condensation models (1/5)

	Two phase multiplier based models
1	Akers et al. (1959)
	$h = 0.0265 Re_{eq}^{0.8} Pr_l^{1/3} \frac{k_l}{D}$ for $Re_{eq} > 50,000$ $h = 5.03 Re_{eq}^{1/3} Pr_l^{1/3} \frac{k_l}{D}$ for $Re_{eq} < 50,000$
2	Akers and Rosson (1960)
	$h = 0.1 Re_v^{2/3} Pr_l^{1/3} Ja_l^{-1/6} \left(\frac{k_l}{D} \right)$
3	Boyko and Kruzhilin (1967)
	$h = 0.024 Re_{lo}^{0.8} Pr_l^{0.43} \left[1 + x \left(\frac{\rho_l}{\rho_v} - 1 \right) \right]^{0.5} \left(\frac{k_l}{D} \right)$
4	Cavallini and Zecchin (1974)
	$h = 0.05 Re_{eq}^{0.8} Pr_l^{1/3} \left(\frac{k_l}{D} \right)$
5	Shah (1979)
	$h = 0.023 Re_l^{0.8} Pr_l^{0.4} \left[1 + \frac{3.8}{P_r^{0.38}} \left(\frac{x}{1-x} \right)^{0.76} \right] \left(\frac{k_l}{D} \right)$
6	Bivens and Yokozeki (1994)
	$h = h_{Shah} \left(0.78738 + \frac{6187.89}{G^2} \right)$
7	Tandon et al. (1995)
	$h = 0.084 Re_v^{0.67} Pr_l^{1/3} Ja_l^{-1/6} \left(\frac{k_l}{D} \right)$
8	Fujii (1995)
	$h = 0.0125 Re_l^{0.9} Pr_l^{0.63} \left(\frac{\rho_l}{\rho_v} \right)^{0.45} \left(\frac{x}{1-x} \right)^{0.1x+0.8} \left(\frac{k_l}{D} \right)$

Table 2.2 Annular flow condensation models (2/5)

9	Tang (1997)
	$h = 0.023 Re_l^{0.8} Pr_l^{0.4} \left[1 + 4.863 \left(\frac{-x \ln p_r}{1-x} \right)^{0.836} \right] \left(\frac{k_l}{D} \right)$
10	Dobson and Chato (1998)
	$h = 0.023 Re_l^{0.8} Pr_l^{0.4} \left[1 + \frac{2.22}{X_{tt}^{0.89}} \right] \left(\frac{k_l}{D} \right)$
11	Sweeny and Chato (1996)
	$h = h_{Dobson} \left[0.7 \left(\frac{G}{300} \right)^{0.3} \right]$
12	Cavallini et al. (2006)
	$h = 0.023 Re_{lo}^{0.8} Pr_l^{0.4} \left(\frac{k_l}{D} \right) \left[1 + 1.128 x^{0.8170} \left(\frac{\rho_l}{\rho_v} \right)^{0.3685} \left(\frac{\mu_l}{\mu_v} \right)^{0.2363} \left(1 - \frac{\mu_v}{\mu_l} \right)^{2.144} Pr_l^{-0.1} \right]$
13	Shah (2009)
	$h = h_{Shah} \left(\frac{\mu_l}{14 \mu_v} \right)^{0.0058 + 0.557 P_r}$
	Interfacial shear based models
14	Chen et al. (1987)
	$h = k_l g^{1/3} \left(\frac{\mu_l}{\rho_l} \right)^{-2/3} \left[0.036 Pr_l^{0.65} A_D^{0.5} \left(Re_{lo} - Re_l \right)^{0.7} Re_l^{0.2} \right]$ $A_D = \frac{0.252 \mu_l^{1.177} \mu_v^{0.156}}{D^2 g^{2/3} \rho_l^{0.553} \rho_v^{0.78}}$

Table 2.2 Annular flow condensation models (3/5)

	Boundary layer based models
15	Kosky and Staub (1971)
	$h = \dfrac{\rho_l C_{p,l}}{T^+}\left(\dfrac{\tau}{\rho_l}\right)^{0.5}$
	$T^+ = \delta^+ Pr_l$ for $\delta^+ \le 5$ $T^+ = 5\left[Pr_l + \ln\left[1 + Pr_l\left(\dfrac{\delta^+}{5} - 1\right)\right]\right]$ for $5 < \delta^+ < 30$ $T^+ = 5\left[Pr_l + \ln\left(1 + 5Pr_l\right) + 0.495\ln\left(\dfrac{\delta^+}{30}\right)\right]$ for $30 \le \delta^+$ $\delta^+ = \left(\dfrac{Re_l}{2}\right)^{0.5}$ for $Re_l \le 1{,}145$ $\delta^+ = 0.0504 Re_l^{7/8}$ for $Re_l > 1{,}145$ $\tau = \left(\dfrac{dP}{dz}\right)_f \dfrac{D}{4}$ $\left(\dfrac{dP}{dz}\right)_f = \dfrac{2\phi_{lo}^2 f_{lo} G^2}{D\rho_l}$ $\phi_{lo} = \left[1 + x\left(\dfrac{\rho_l}{\rho_v} - 1\right)\right]^{0.5}$ $f_{lo} = 0.079\left(\dfrac{GD}{\mu_l}\right)^{-0.25}$
16	Traviss et al. (1973)
	$h = Re_l^{0.9} Pr_l \dfrac{F_1}{F_2}\left(\dfrac{k_l}{D}\right)$ for $F_1 < 2$ $h = Re_l Pr_l \dfrac{F_1^{1.15}}{F_2}\left(\dfrac{k_l}{D}\right)$ for $F_1 > 2$
	$F_1 = 0.15\left[\dfrac{1}{X_{tt}} + \dfrac{2.85}{X_{tt}^{0.476}}\right]$ $F_2 = 5Pr_l + 5\ln\left(1 + 5Pr_l\right) + 2.5\ln\left(0.00313 Re_l^{0.812}\right)$

Table 2.2 Annular flow condensation models (4/5)

17	Moser et al. (1998)
	$h = h_{lo} F$
	$h_{lo} = \frac{k_l Nu}{D} = \frac{k_l}{D} St\, Re_e Pr_l$ $F = 1.31(0.0994 Re_e^{7/8})^{0.126 Pr_L^{-0.448}} Re_l^{-0.113 Pr_l^{-0.563}} Pr_l^{-0.185}$ $St = \frac{0.5 f}{1.07 + 12.7(0.5 f)^{0.5}(Pr_l^{2/3} - 1)}$ $f = 0.079 Re_e^{-0.25}$ $Re_e = Re_{lo} \phi_{lo}^{8/7}$ $\phi_{lo} = \left[A + 3.24 x^{0.78} (1-x)^{0.24} \left(\frac{\rho_l}{\rho_v}\right)^{0.91} \left(\frac{\mu_v}{\mu_l}\right)^{0.19} \left(1 - \frac{\mu_v}{\mu_l}\right)^{0.7} Fr^{-0.0454} We^{-0.035} \right]^{0.5}$ $A = (1-x)^2 + x^2 \rho_l f_{go} (\rho_v f_{lo})^{-1}$ $Fr = \frac{G^2}{gD\rho_h^2}$ $We = \frac{G^2 D}{\rho_h \sigma}$ $\rho_h = \left(\frac{x}{\rho_v} + \frac{1-x}{\rho_l}\right)^{-1}$ $f_{go} = 0.25 \left[0.86859 \ln \left(\frac{Re_{go}}{1.964 \ln Re_{go} - 3.8215} \right) \right]^{-2}$ $f_{lo} = 0.25 \left[0.86859 \ln \left(\frac{Re_{lo}}{1.964 \ln Re_{lo} - 3.8215} \right) \right]^{-2}$

Table 2.2 Annular flow condensation models (5/5)

18	Cavallini et al. (2002)
	$h = \dfrac{\rho_l C_{p,l}}{T^+}\left(\dfrac{\tau}{\rho_l}\right)^{0.5}$
	$\phi_{lo}^2 = E + \dfrac{1.262FH}{We^{0.1458}}$ $\qquad We = \dfrac{G^2 D}{\rho_v \sigma}$ $E = (1-x)^2 + \dfrac{x^2 \rho_l f_{go}}{\rho_v f_{lo}}$ $\qquad F = x^{0.6978}$ $H = \left(\dfrac{\rho_l}{\rho_v}\right)^{0.3278}\left(\dfrac{\mu_v}{\mu_l}\right)^{-1.181}\left(1-\dfrac{\mu_v}{\mu_l}\right)^{3.477}$ $f_{lo} = 0.046\left(\dfrac{GD}{\mu_l}\right)^{-0.2}$, $\quad f_{go} = 0.046\left(\dfrac{GD}{\mu_v}\right)^{-0.2}$ for $Re_{go} > 2{,}000$ $f_{lo} = 16\left(\dfrac{GD}{\mu_l}\right)^{-1}$, $\quad f_{go} = 16\left(\dfrac{GD}{\mu_v}\right)^{-1}$ for $Re_{go} \le 2{,}000$
	Etc.
19	Thome et al. (2003)
	$h = 0.003 Re_{lf}^{0.74}\,\mathrm{Pr}_l^{0.5}\,\dfrac{k_l}{\delta} f_i$ $Re_{lf} = \dfrac{4G(1-x)\delta}{(1-\alpha)\mu_l}$ $\qquad f_i = 1 + \left(\dfrac{u_v}{u_l}\right)^{1/2}\left(\dfrac{(\rho_l - \rho_v) g \delta^2}{\sigma}\right)^{1/4}$ $u_l = \dfrac{G(1-x)}{\rho_l(1-\alpha)}$ $\qquad u_v = \dfrac{Gx}{\rho_v \alpha}$

Table 2.3 Horizontal in-tube steam condensation experiments

	Purdue-PCCS (Wu, 2005)	**JAEA-PCCS (Kondo et al., 2006)**	**PASCAL (Kang et al., 2012)**	**NOKO (Schaffrath, 1998)**
No. of Tube	1	1	1	4
Tube Length [m]	3	~9	8.4	9.8
Tube ID [mm]	27.5	29	44.8	38.7
Tube Thickness [mm]	2.1	1.4	3	2.9
Inclination of Straight Part	0°	0°	3°	1.6° (upper) / 3.2° (lower)
Inlet Steam Flow Rate [kg/s]	0.006-0.023	~0.046	0.15-0.43	0.10-0.52 (per tube)
NC gas Concentration [%]	1-2	1	-	-
Pressure [bar]	1, 2, 4	7	~13, ~32, ~67	~10, ~30, ~70
Main Flow Regime	Wavy/Stratified	Annular/Stratified		
Secondary-Side Cooling	Forced convection		Natural convective nucleate boiling	

Table 2.4 Test conditions of Purdue-PCCS experiment

Case No.	Inlet P [bar]	Inlet Steam Mass Flow [g/s]	Inlet Air Mass Fraction [%]	Secondary-side Coolant	
				Temperature [K]	Mass Flow Rate [kg/s]
6	100	6.0	2	318.15	1.48
3		11.50	1		
20	200	6.0	1		
101		11.50	1		
24	400	11.50	1		
27		23.00	1		

Table 2.5 Test conditions of PASCAL experiment

ID	SS-300-P1	SS-540-P1	SS-750-P1
SG power [kW]	299.8	540	750.2
Pressure [bar]	13.42	32.2	67.36
Mass flow rate [kg/s]	~ 0.15	~ 0.2955	~ 0.43

Table 2.6 Steady-state test conditions of NOKO experiment

No	Test	Primary Conditions		Secondary Conditions		
		Pressure [bar]	Mass Flow Rate [kg/s]	Pressure [bar]	Temperature [K]	Water Level [m]
1	EU1-3	10.0	0.42	1.1	339.25	1.33
2	EU1-4		0.50	1.1	361.15	1.33
3	EU3-2	30.1	0.69	1.1	336.35	1.40
4	EU3-3		1.01	1.1	374.85	1.43
5	EU3-4		1.17	1.4	384.15	1.37
6	EU4-1		0.65	1.2	378.25	1.41
7	EU5-2	70.7	0.78	1.1	317.75	1.37
8	EU5-4		1.60	1.4	384.15	1.39
9	EU5-6		2.08	1.7	390.15	1.34
10	EU6-2		1.19	1.5	386.65	1.38

Table 2.7 Predicted overall heat transfer rate for Purdue-PCCS experiment (1/2)

No	Test	6		3		20	
		Q [kW]	**δ [%]**	**Q [kW]**	**δ [%]**	**Q [kW]**	**δ [%]**
	Experiment	14.10	-	25.09	-	14.07	-
0	MARS	14.31	1.49	26.38	5.14	14.49	2.99
1	Akers-Rosson	14.32	1.56	26.44	5.38	14.34	1.92
2	Chato	14.31	1.49	24.94	-0.60	14.49	2.99
3	Rosson-Meyers	14.45	2.48	26.94	7.37	14.51	3.13
4	Jaster-Kosky	14.42	2.27	26.58	5.94	14.75	4.83
5	Tandon et al.	14.31	1.49	25.59	1.99	14.41	2.42
6	Fujii	14.19	0.64	26.54	5.78	13.66	-2.91
7	Dobson-Chato	14.45	2.48	26.89	7.17	14.51	3.13
8	Sweeney-Chato	14.23	0.92	25.63	2.15	13.92	-1.07
9	Cavallini (2002)	14.32	1.56	26.44	5.38	14.44	2.63
10	Thome et al.	14.49	2.77	27.02	7.69	14.53	3.27
11	Cavallini (2006)	14.48	2.70	26.81	6.86	14.56	3.48

Table 2.7 Predicted overall heat transfer rate for Purdue-PCCS experiment (2/2)

No	Test	101		24		27		Mean
		Q [kW]	**δ [%]**	**Q [kW]**	**δ [%]**	**Q [kW]**	**δ [%]**	**δ [%]**
	Experiment	27.90	-	28.25	-	50.45	-	-
0	MARS	27.16	-2.65	27.47	-2.76	51.25	1.59	2.77
1	Akers-Rosson	26.16	-6.24	26.46	-6.34	49.54	-1.80	3.87
2	Chato	27.13	-2.76	27.52	-2.58	42.92	-14.93	4.22
3	Rosson-Meyers	27.08	-2.94	27.61	-2.27	52.12	3.31	3.58
4	Jaster-Kosky	26.76	-4.09	26.68	-5.56	50.77	0.63	3.89
5	Tandon et al.	26.33	-5.63	26.70	-5.49	42.20	-16.35	5.56
6	Fujii	26.87	-3.69	25.30	-10.44	50.62	0.34	3.97
7	Dobson-Chato	27.09	-2.90	27.89	-1.27	51.85	2.78	3.29
8	Sweeney-Chato	26.03	-6.70	26.11	-7.58	49.83	-1.23	3.27
9	Cavallini (2002)	26.74	-4.16	27.16	-3.86	49.80	-1.29	3.15
10	Thome et al.	27.28	-2.22	27.45	-2.83	51.62	2.32	3.52
11	Cavallini (2006)	27.34	-2.01	27.25	-3.54	51.57	2.22	3.47

Table 2.8 Predicted overall heat transfer rate for JAEA-PCCS experiment

No	**Experiment**		***Q* [kW]**	**δ [%]**
			~110	**-**
	Annular Flow Model	Stratified Flow Model		
1	Shah (1979)	Chato (1962)	99.927	-9.16
2	Dobson and Chato (1998)	Chato (1962)	103.19	-6.19
3	Kosky and Staub (1971)	Chato (1962)	102.88	-6.47
4	Shah (1979)	Cavallini et al. (2006)	100.73	-8.43
5	Dobson and Chato (1998)	Cavallini et al. (2006)	103.32	-6.07
6	Kosky and Staub (1971)	Cavallini et al. (2006)	103.27	-6.12

Table 2.9 Predicted capacities for PASCAL experiment (1/3)

No	Case		SS-300-P1	
			Q [kW]	δ [%]
	Experiment		300	-
	Annular flow	Stratified flow		
1	Shah (1979)	Chato (1962)	270	-10.0
2	Cavallini and Zecchin (1974)	Cavallini et al. (2006)	297.12	-0.96
3	Dobson and Chato (1998)		296.67	-1.11
4	Akers and Rosson (1960)		296.54	-1.15
5	Traviss et al. (1973)		296.12	-1.29
6	Fujii (1995)		296.11	-1.30
7	Tang (1997)		296.11	-1.30
8	Thome et al. (2003)		296.12	-1.29
9	Tandon et al. (1995)		296.11	-1.30
10	Kosky and Staub (1971)		296.59	-1.14
11	Moser et al. (1998)		296.16	-1.28
12	Cavallini et al. (2002)		296.62	-1.13
13	Shah (1979)		296.11	-1.30
14	Sweeny and Chato (1996)		296.11	-1.30
15	Boyko and Kruzhilin (1967)		296.11	-1.30
16	Akers et al. (1959)		296.37	-1.21
17	Bivens and Yokozeki (1994)		296.19	-1.27
18	Chen et al. (1987)		296.11	-1.30
19	Shah (2009)		296.11	-1.30
20	Cavallini et al. (2006)		296.11	-1.30
21	-		296.11	-1.30
22	-	Chato (1962)	259.03	-13.66

Table 2.9 Predicted capacities for PASCAL experiment (2/3)

No	Case		SS-540-P1	
			Q [kW]	δ [%]
	Experiment		530	-
	Annular flow	Stratified flow		
1	Shah (1979)	Chato (1962)	493	-6.98
2	Cavallini and Zecchin (1974)	Cavallini et al. (2006)	531.12	0.21
3	Dobson and Chato (1998)		529.58	-0.08
4	Akers and Rosson (1960)		527.23	-0.52
5	Traviss et al. (1973)		524.96	-0.95
6	Fujii (1995)		523.79	-1.17
7	Tang (1997)		524.11	-1.11
8	Thome et al. (2003)		523.39	-1.25
9	Tandon et al. (1995)		523.67	-1.20
10	Kosky and Staub (1971)		522.73	-1.37
11	Moser et al. (1998)		522.23	-1.47
12	Cavallini et al. (2002)		521.60	-1.58
13	Shah (1979)		520.30	-1.83
14	Sweeny and Chato (1996)		520.30	-1.83
15	Boyko and Kruzhilin (1967)		520.76	-1.74
16	Akers et al. (1959)		520.30	-1.83
17	Bivens and Yokozeki (1994)		520.30	-1.83
18	Chen et al. (1987)		520.30	-1.83
19	Shah (2009)		520.30	-1.83
20	Cavallini et al. (2006)		520.30	-1.83
21	-		520.30	-1.83
22	-	Chato (1962)	437.86	-17.38

Table 2.9 Predicted capacities for PASCAL experiment (3/3)

No	Case		SS-750-P1		Average
			Q [kW]	δ [%]	δ [%]
	Experiment		730	-	
	Annular flow	Stratified flow			
1	Shah (1979)	Chato (1962)	698	-4.38	-7.12
2	Cavallini and Zecchin (1974)	Cavallini et al. (2006)	737.52	1.03	0.09
3	Dobson and Chato (1998)		715.68	-1.96	-1.05
4	Akers and Rosson (1960)		708.09	-3.00	-1.56
5	Traviss et al. (1973)		709.82	-2.77	-1.67
6	Fujii (1995)		704.32	-3.52	-2.00
7	Tang (1997)		702.85	-3.72	-2.04
8	Thome et al. (2003)		703.31	-3.66	-2.07
9	Tandon et al. (1995)		702.38	-3.78	-2.09
10	Kosky and Staub (1971)		700.07	-4.10	-2.20
11	Moser et al. (1998)		700.01	-4.11	-2.29
12	Cavallini et al. (2002)		699.26	-4.21	-2.31
13	Shah (1979)		700.75	-4.01	-2.38
14	Sweeny and Chato (1996)		698.92	-4.26	-2.46
15	Boyko and Kruzhilin (1967)		698.18	-4.36	-2.47
16	Akers et al. (1959)		697.79	-4.41	-2.48
17	Bivens and Yokozeki (1994)		697.78	-4.41	-2.51
18	Chen et al. (1987)		697.79	-4.41	-2.51
19	Shah (2009)		697.79	-4.41	-2.51
20	Cavallini et al. (2006)		697.79	-4.41	-2.51
21	-		697.79	-4.41	-2.51
22	-	Chato (1962)	598.40	-18.03	-16.36

Table 2.10 Comparison of capacity between NOKO experiment and MARS

Case No.	Experiment	Original MARS code		Modified MARS code	
	Q [kW]	**Q [kW]**	**δ [%]**	**Q [kW]**	**δ [%]**
1	920	851	-7.50	915	-0.54
2	1040	940	-9.62	1037	-0.29
3	1510	1400	-7.28	1464	-3.05
4	2000	1832	-8.40	1963	-1.85
5	2140	1910	-10.75	2061	-3.69
6	1410	1324	-6.10	1373	-2.62
7	1700	1560	-8.24	1603	-5.71
8	2860	2655	-7.17	2771	-3.11
9	3170	2986	-5.80	3086	-2.65
10	2310	2165	-6.28	2230	-3.46
Average **δ [%]**		-	-7.71	-	-2.70

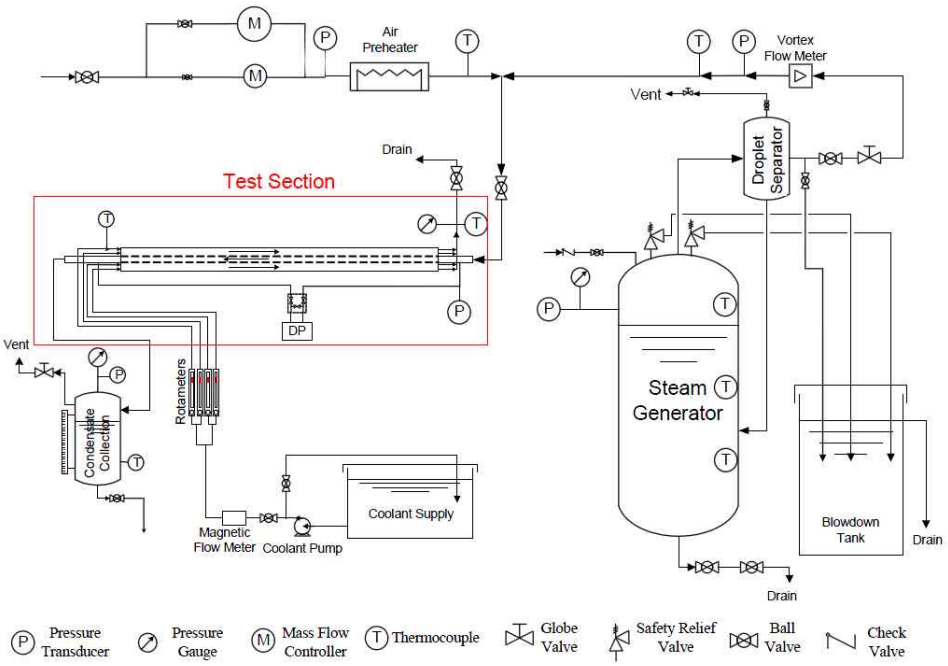

Figure 2.1 Test facility layout in Purdue University (Wu and Vierow, 2006)

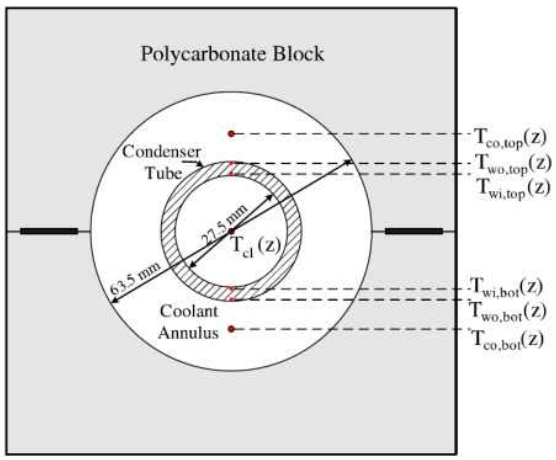

Figure 2.2 Temperature measurement cross-section (Wu and Vierow, 2006)

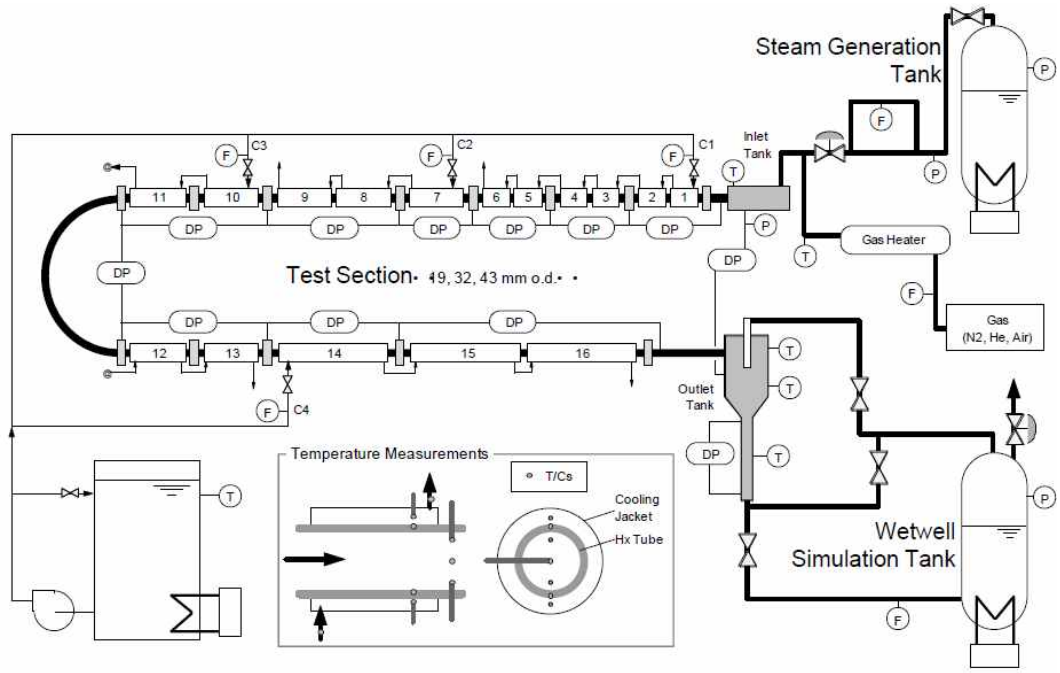

Figure 2.3 Schematic diagram of JAEA-PCCS test facility (Nakamura et al., 2000)

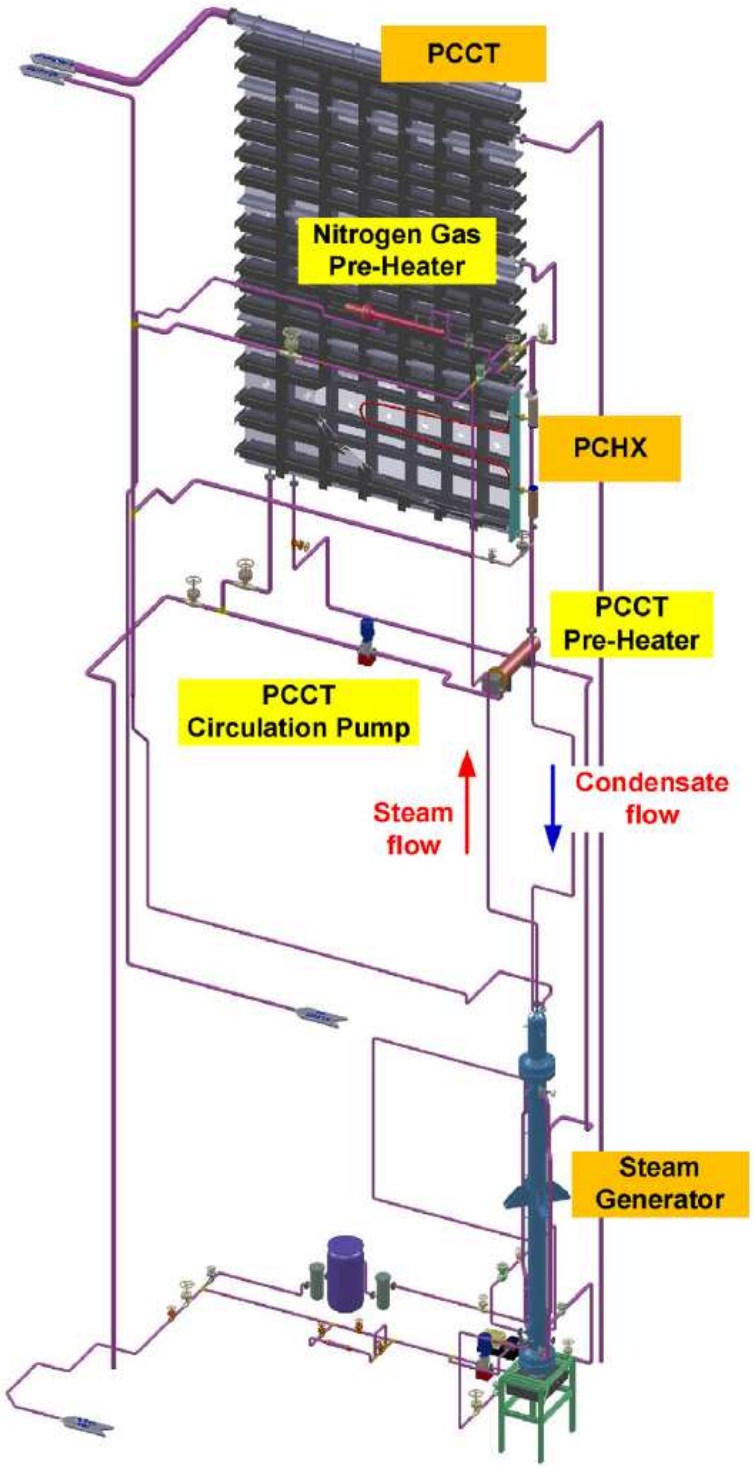

Figure 2.4 Schematic diagram of PASCAL (Kim et al., 2013)

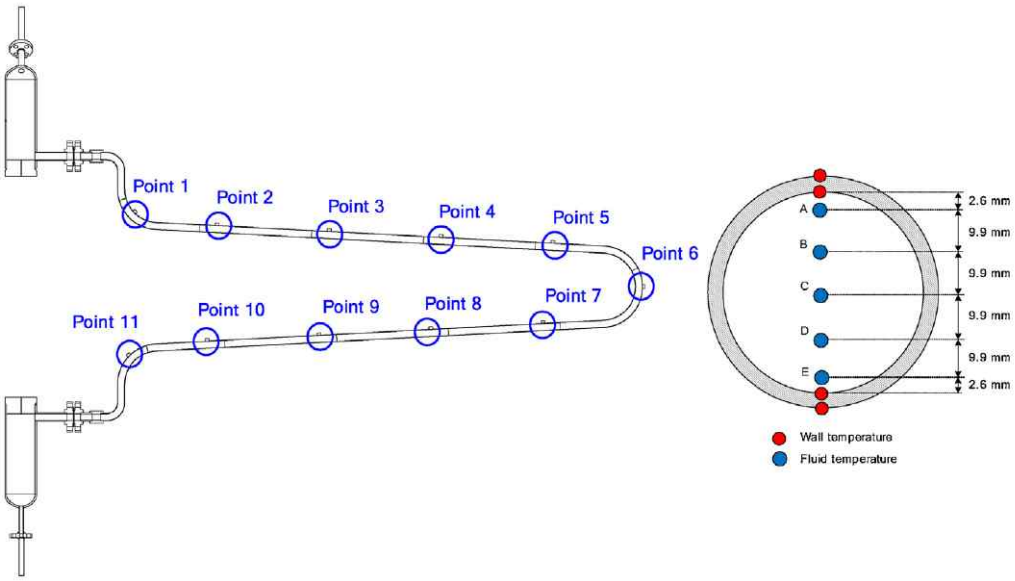

Figure 2.5 Measurement of wall and fluid temperature (Kim et al., 2013)

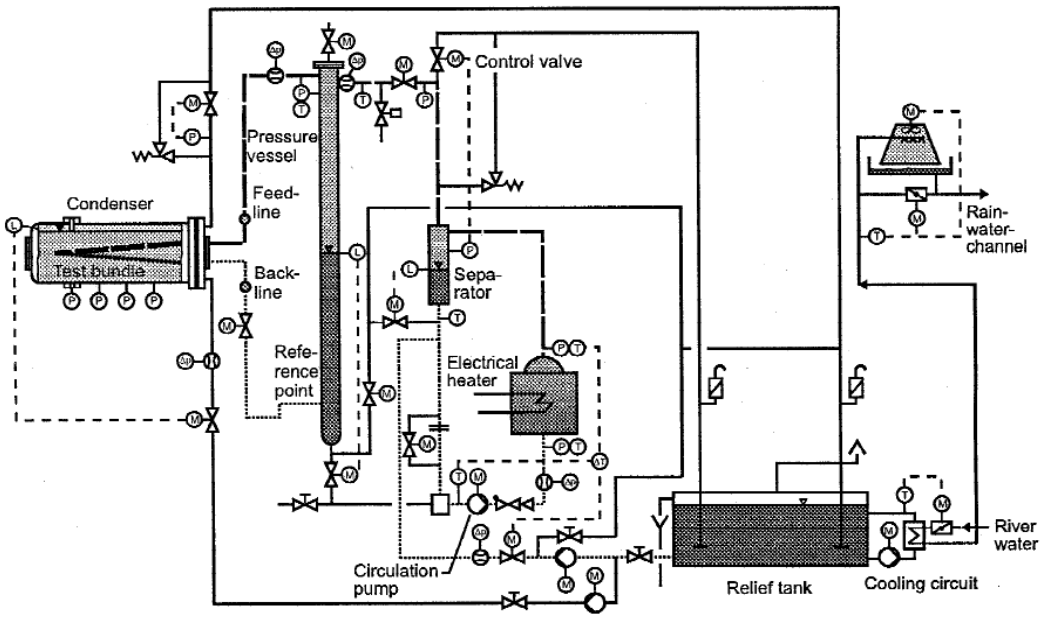

Figure 2.6 Test facility layout of NOKO (Schaffrath and Prasser, 1998)

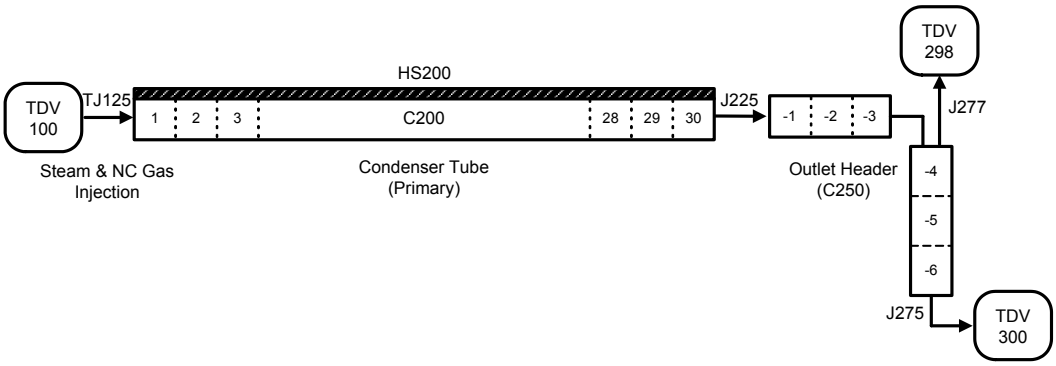

Figure 2.7 MARS nodalization for Purdue-PCCS experiment

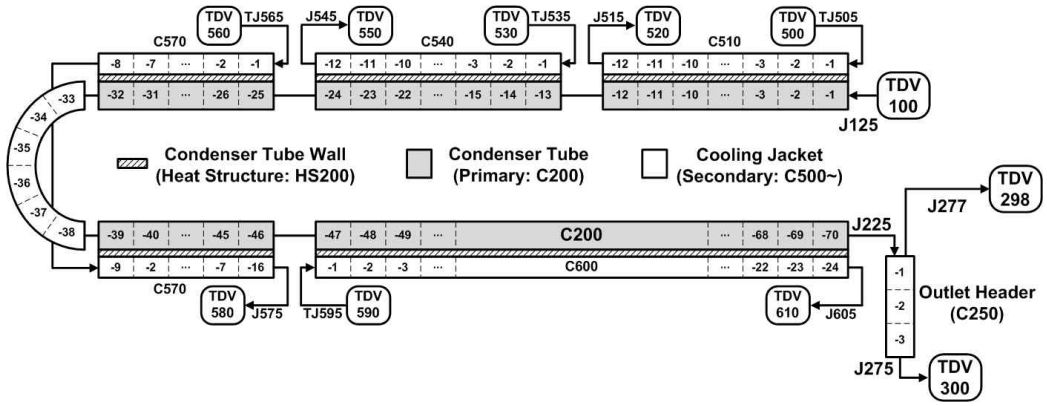

Figure 2.8 MARS nodalization for JAEA-PCCS experiment

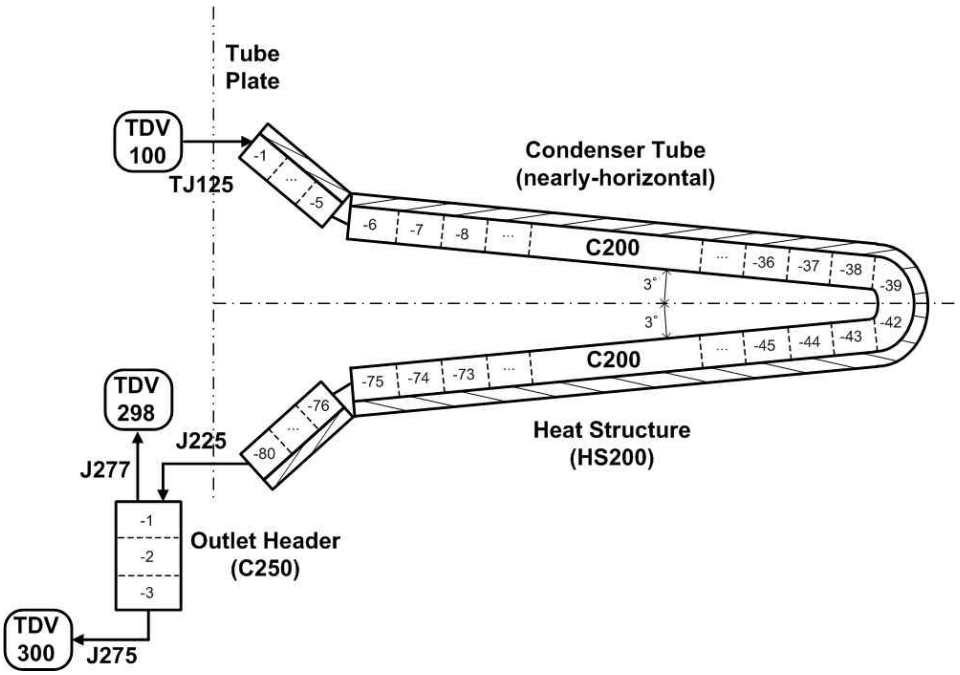

Figure 2.9 MARS nodalization for PASCAL experiment

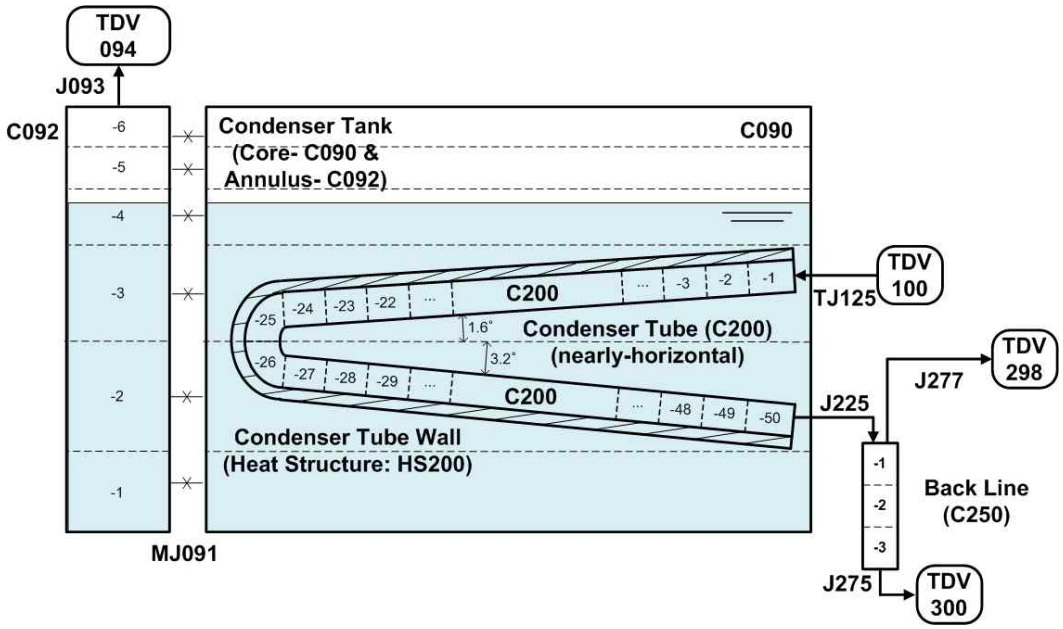

Figure 2.10 MARS nodalization for NOKO experiment

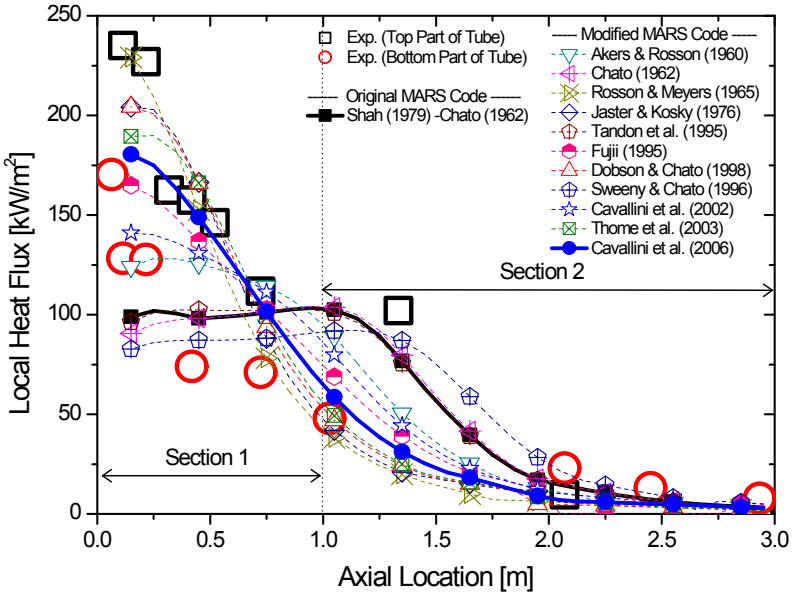

(a) Case 6

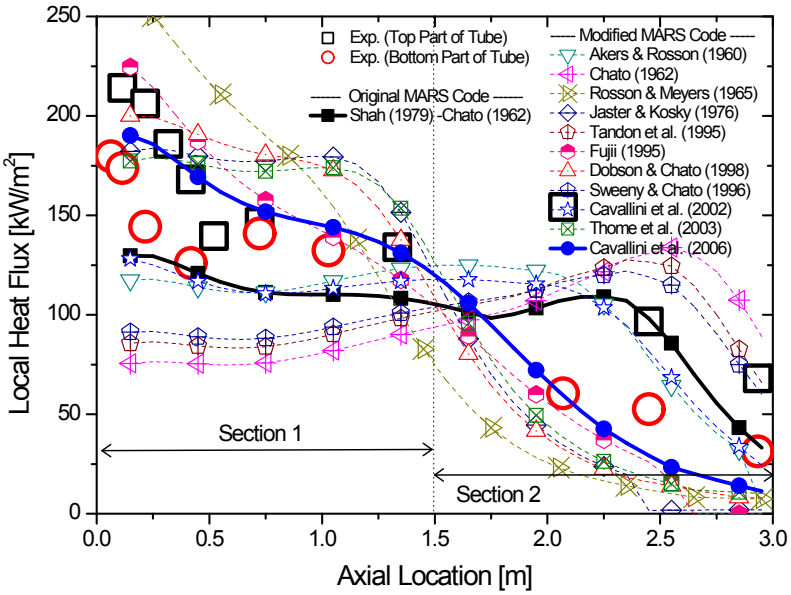

(b) Case 3

Figure 2.11 Predicted local heat flux for Purdue-PCCS (1/3)

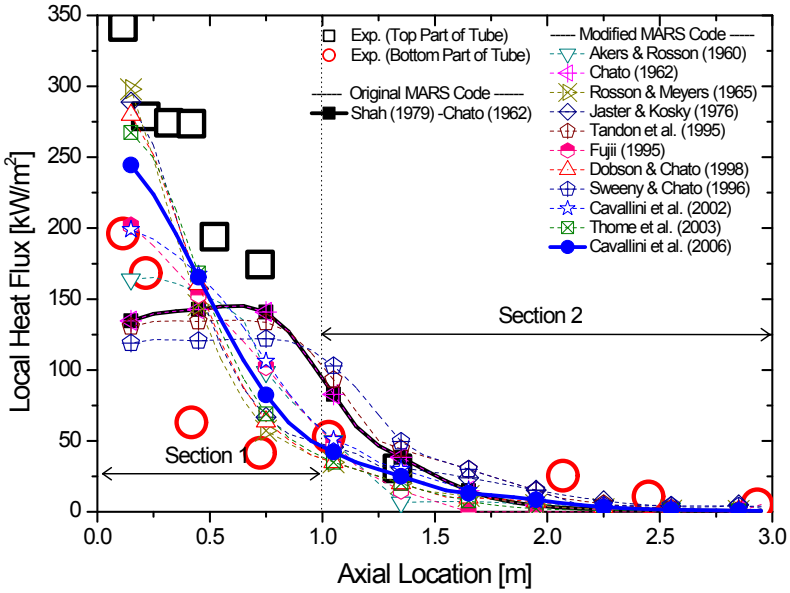

(c) Case 20

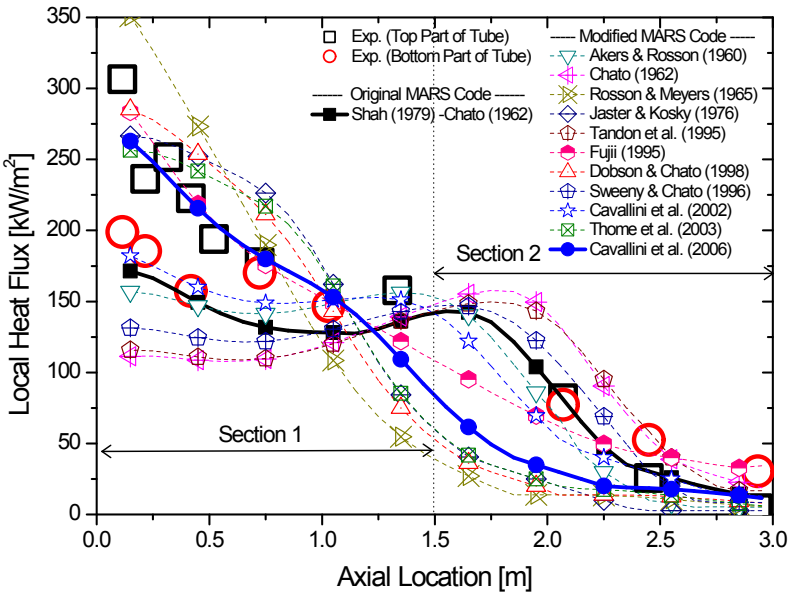

(d) Case 101

Figure 2.11 Predicted local heat flux for Purdue-PCCS (2/3)

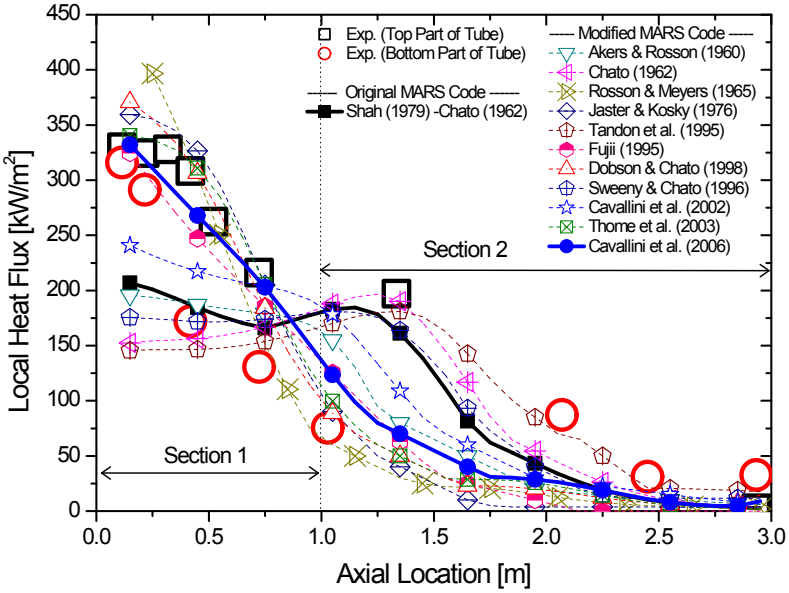

(e) Case 24

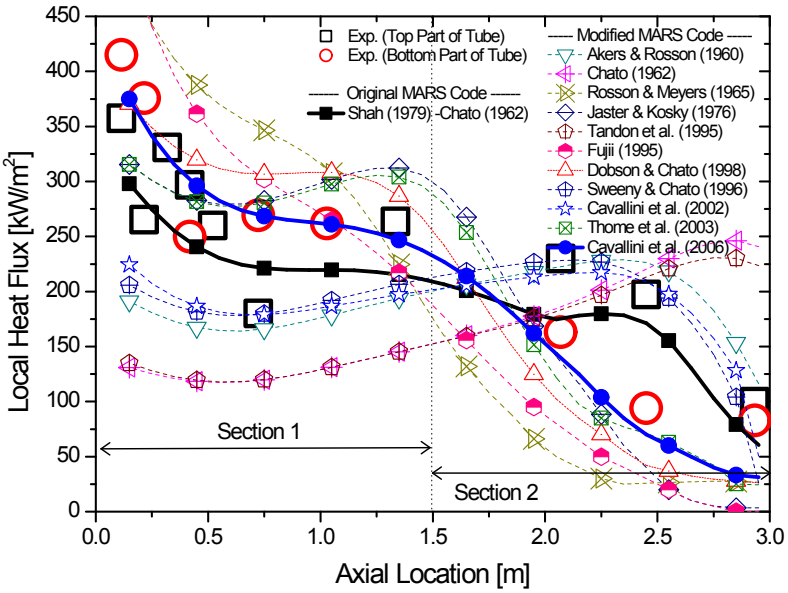

(f) Case 27

Figure 2.11 Predicted local heat flux for Purdue-PCCS (3/3)

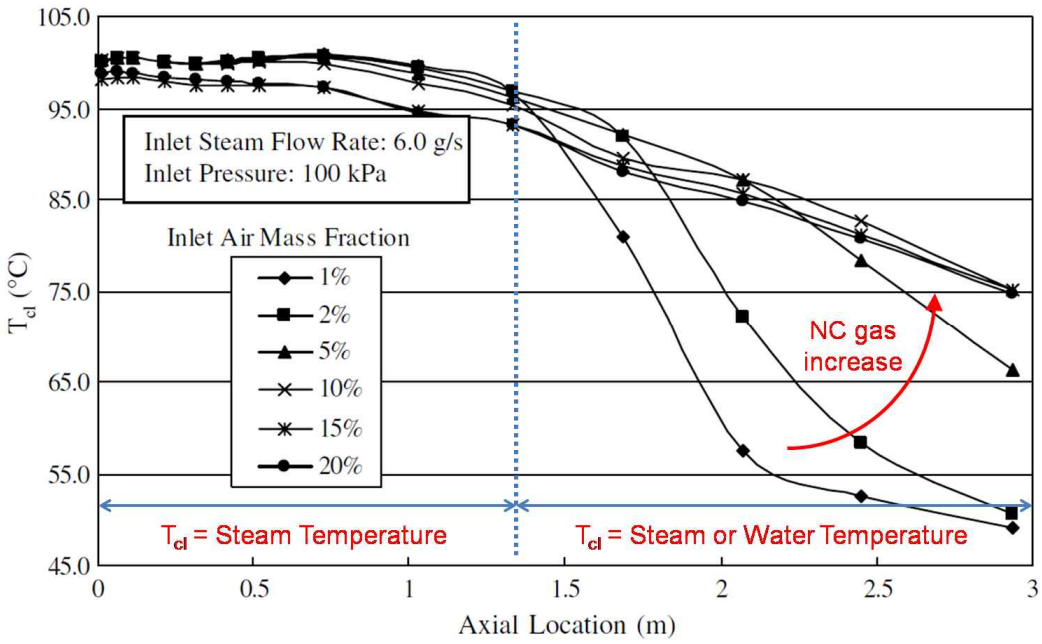

Figure 2.12 Centerline temperature profiles for inlet air mass fractions (Wu and Vierow, 2006)

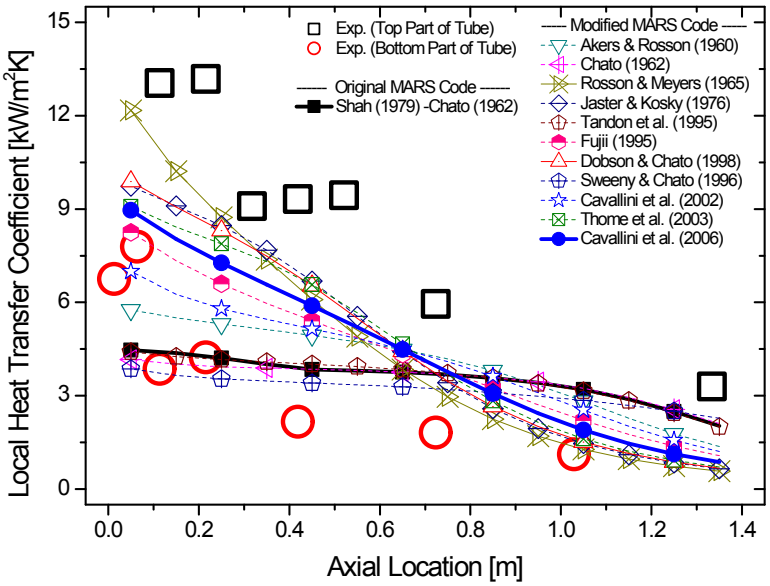

(a) Case 6

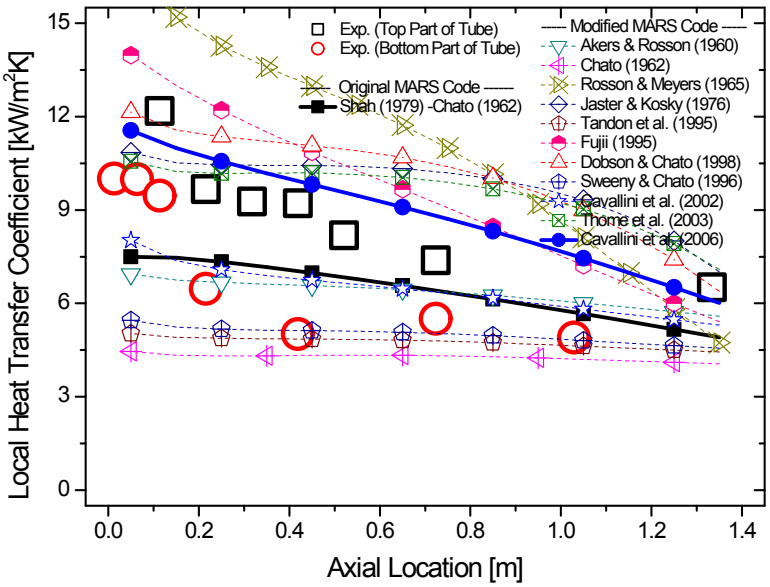

(b) Case 3

Figure 2.13 Predicted local HTC for Purdue-PCCS (1/3)

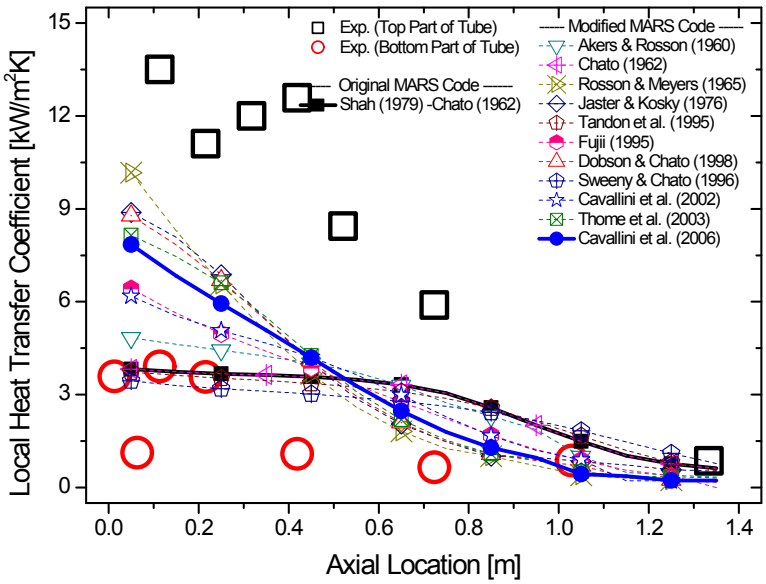

(c) Case 20

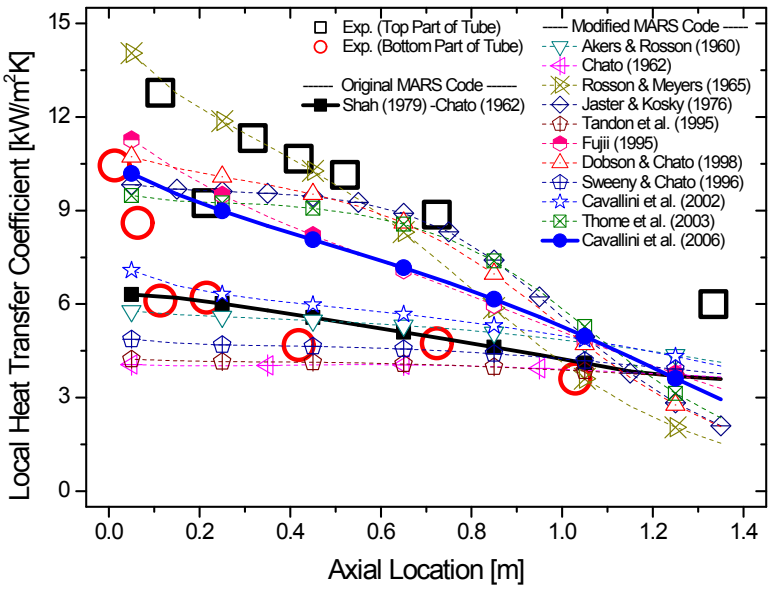

(d) Case 101

Figure 2.13 Predicted local HTC for Purdue-PCCS (2/3)

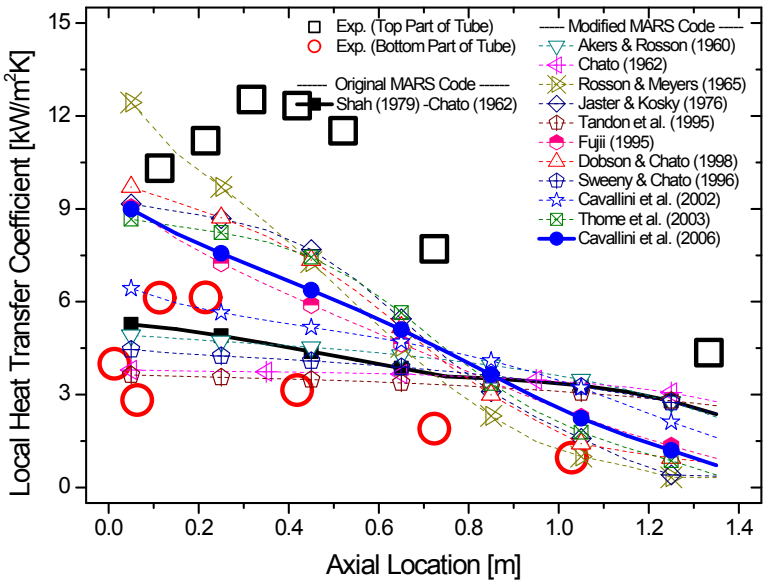

(e) Case 24

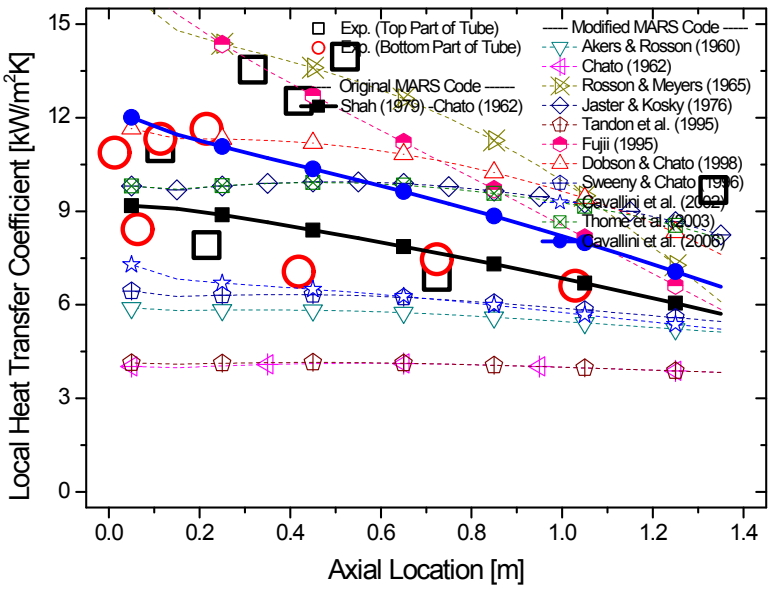

(f) Case 27

Figure 2.13 Predicted local HTC for Purdue-PCCS (3/3)

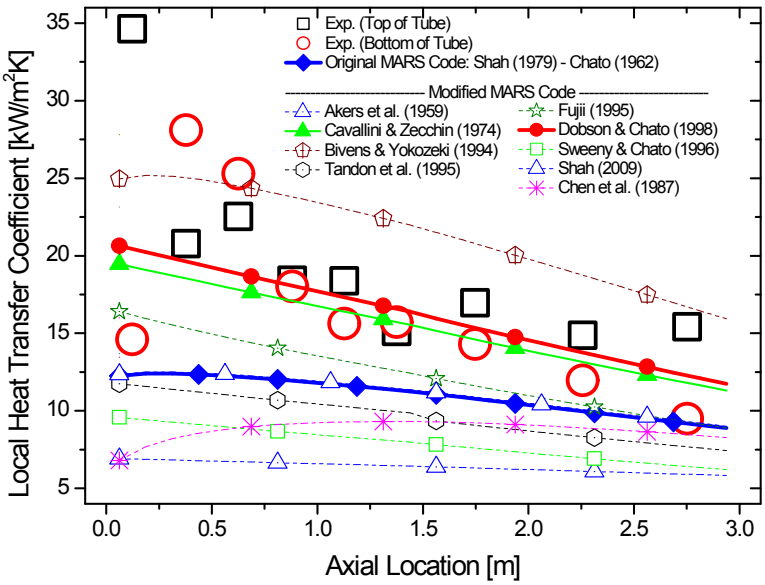

(a) Part I of 19 models

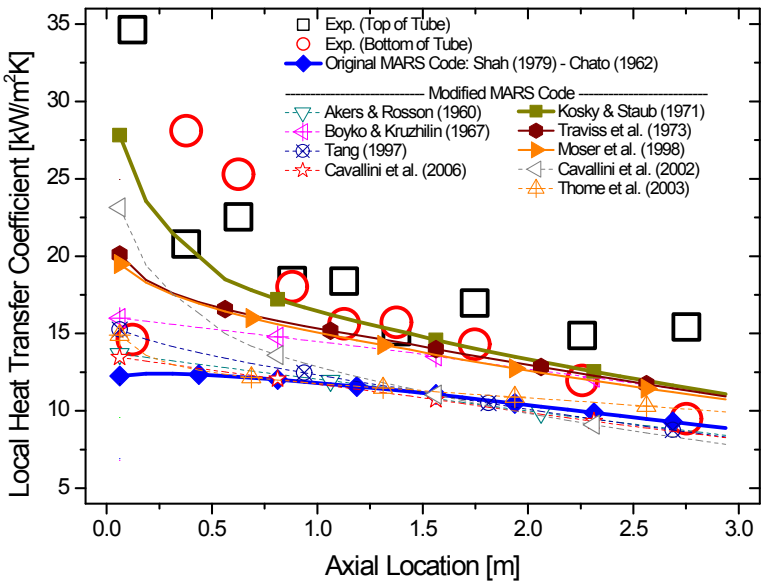

(b) Part II of 19 models

Figure 2.14 Local HTCs (JAEA-PCCS)

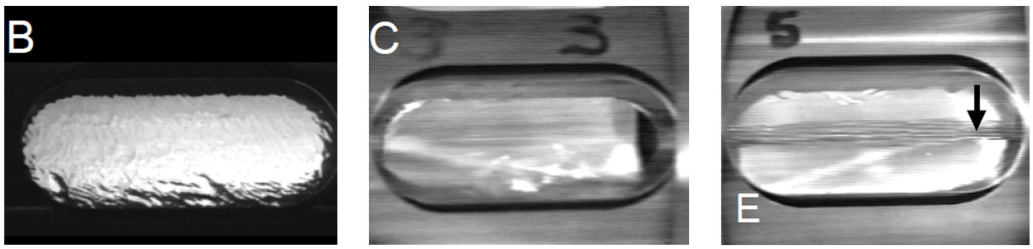

(a) Annular flow (2 m) (b) Wavy flow (4 m) (c) Stratified flow (6 m)

Figure 2.15 Observed flow regimes (Kondo et al., 2006)

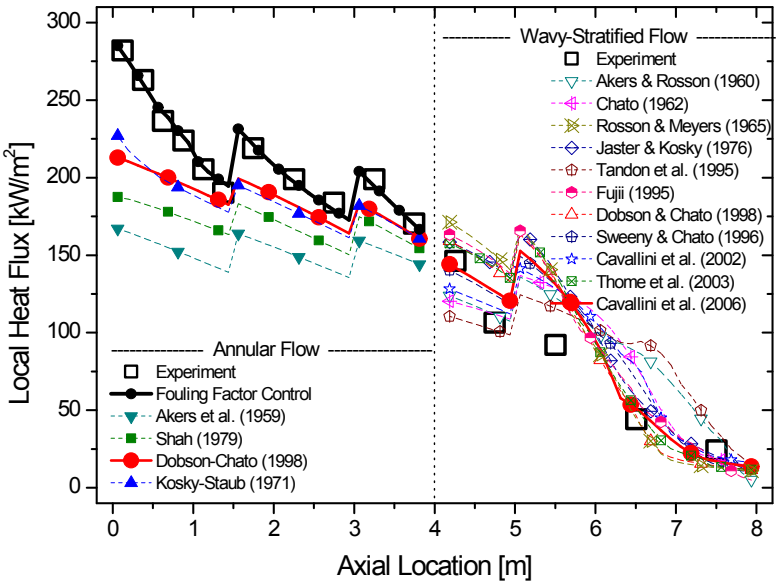

Figure 2.16 Local heat flux (JAEA-PCCS)

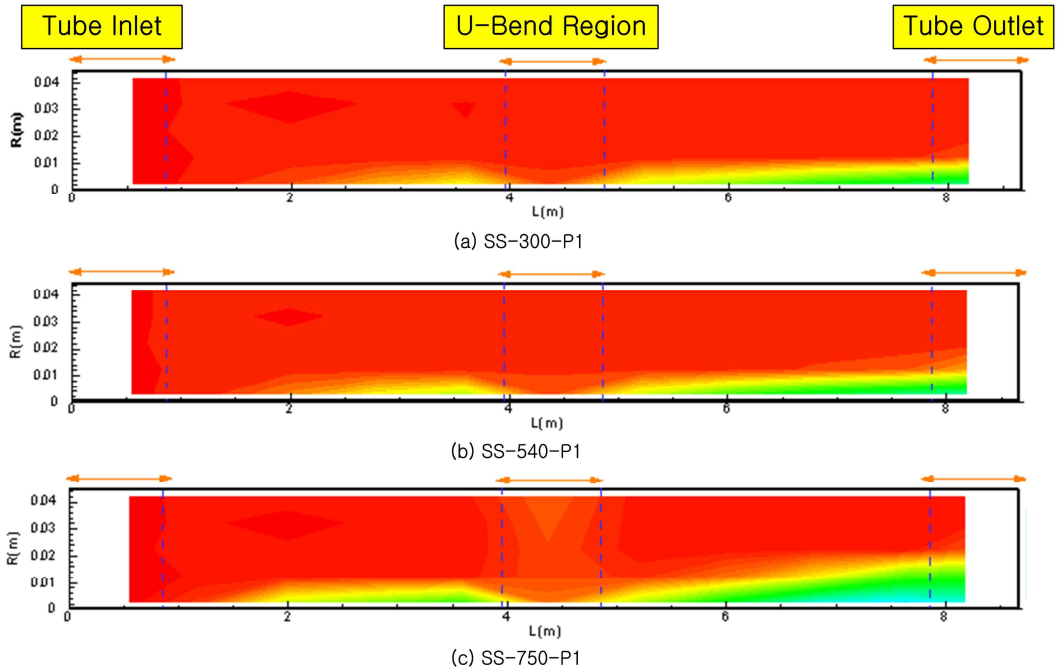

Figure 2.17 Fluid temperature distribution inside the condenser tube (MKE, 2011)

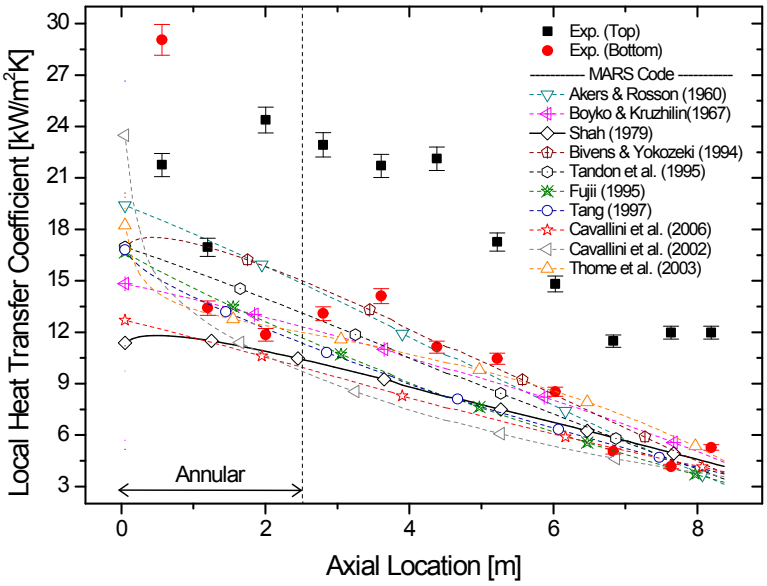

(a) SS-300-P1 (Part I of 19 models)

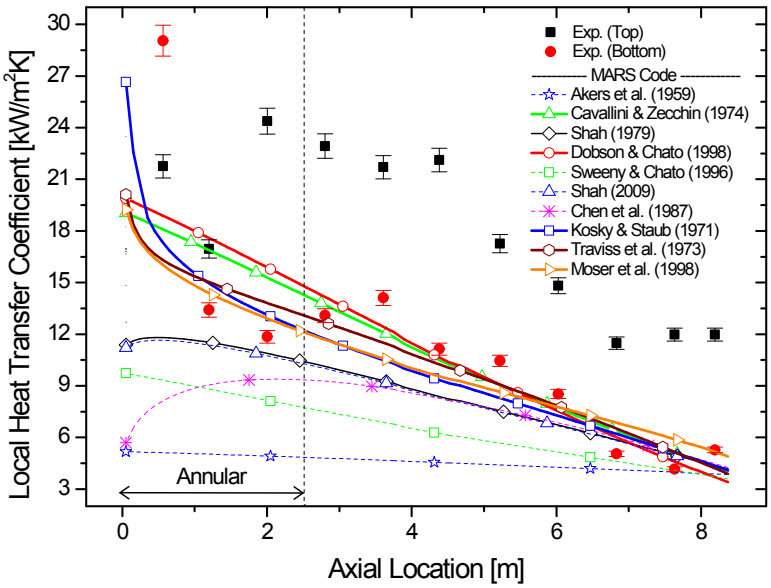

(b) SS-300-P1 (Part II of 19 models)

Figure 2.18 Predicted local HTC for PASCAL (1/3)

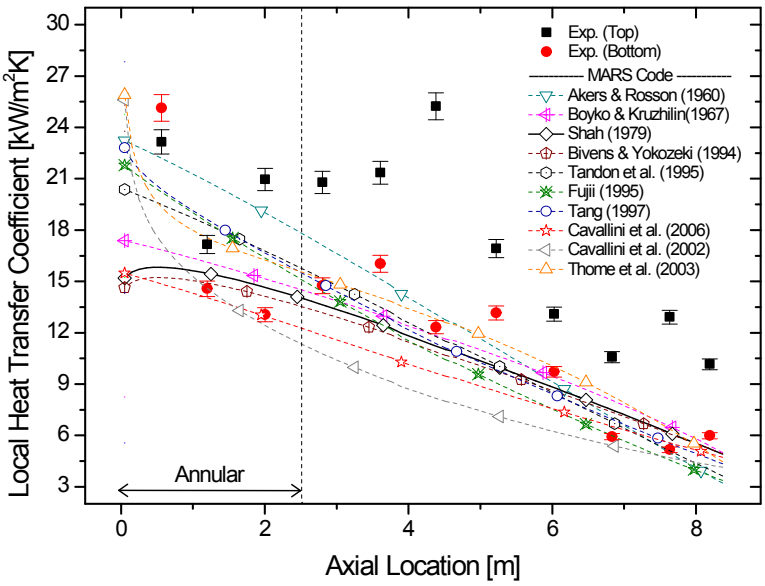

(c) SS-540-P1 (Part I of 19 models)

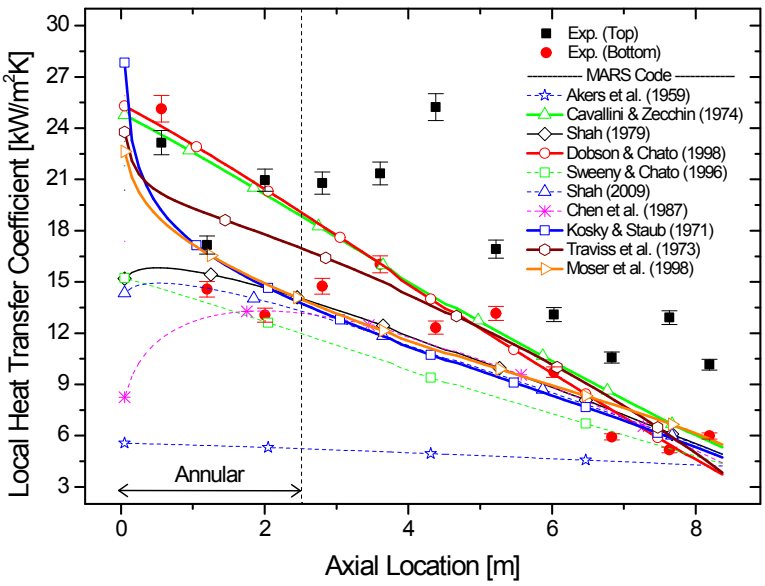

(d) SS-540-P1 (Part II of 19 models)

Figure 2.18 Predicted local HTC for PASCAL (2/3)

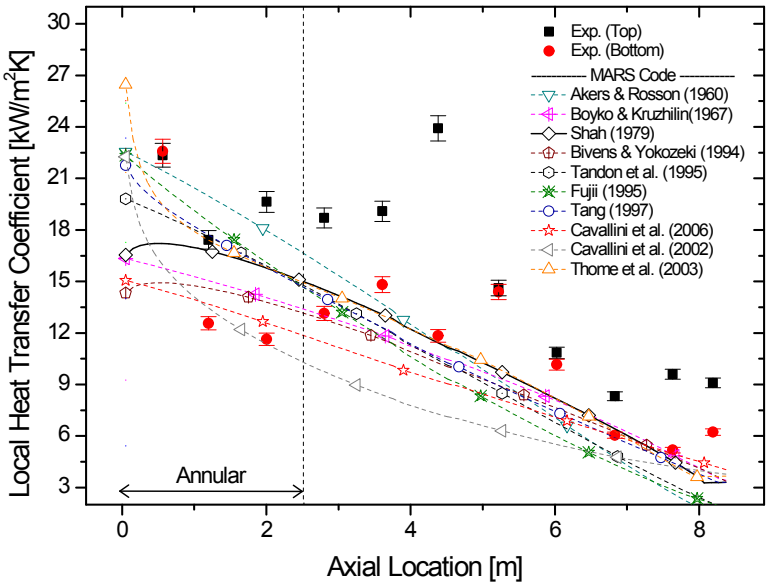

(e) SS-750-P1 (Part I of 19 models)

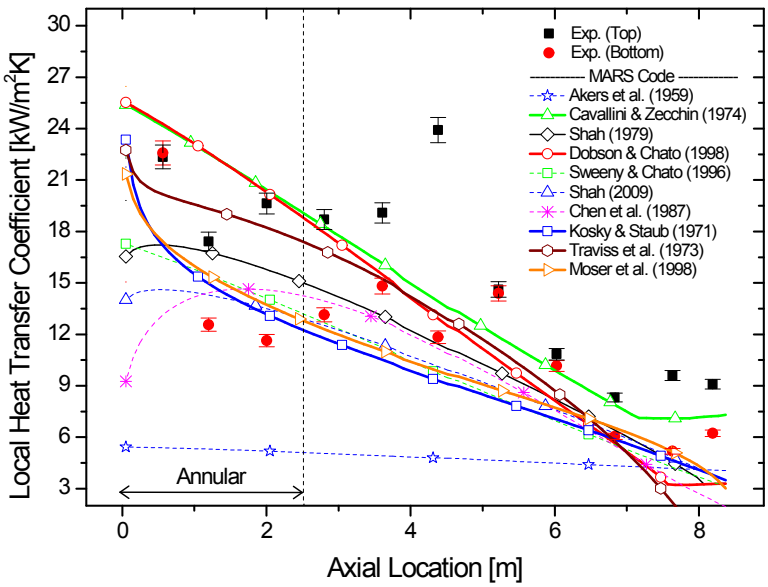

(f) SS-750-P1 (Part II of 19 models)

Figure 2.18 Predicted local HTC for PASCAL (3/3)

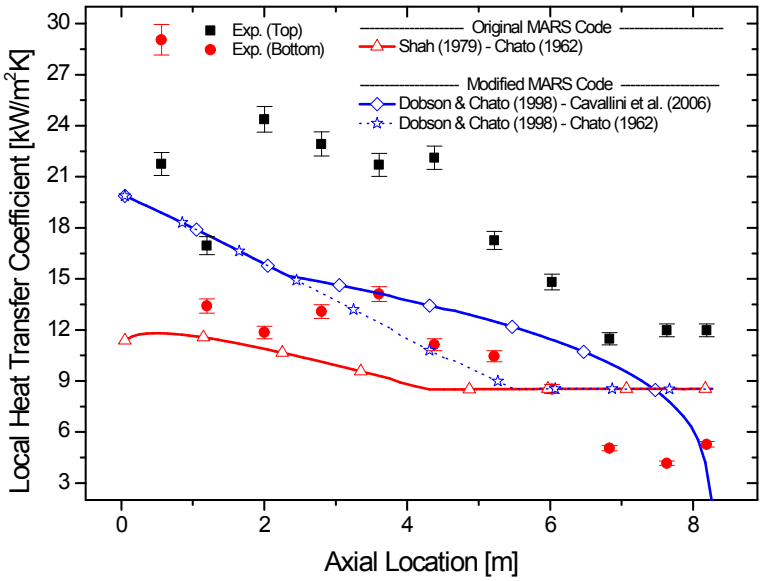

(a) SS-300-P1

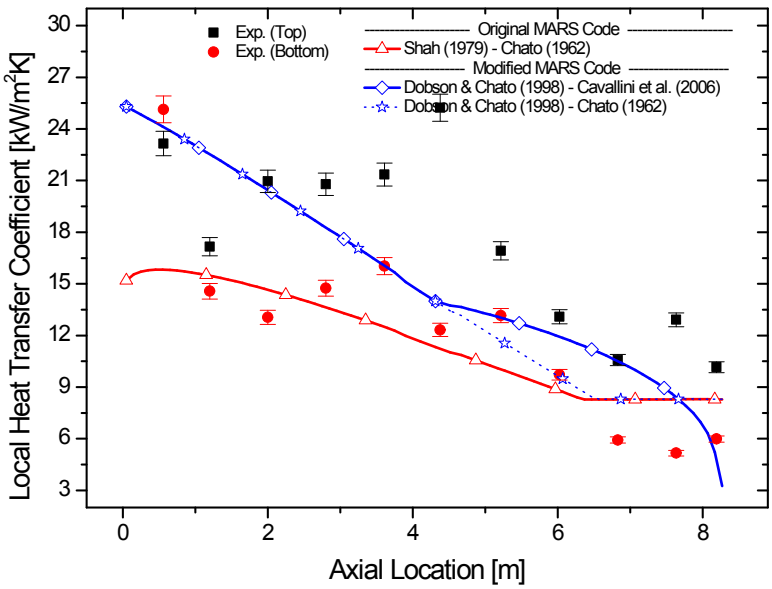

(b) SS-540-P1

Figure 2.19 Local HTCs (PASCAL) – (1/2)

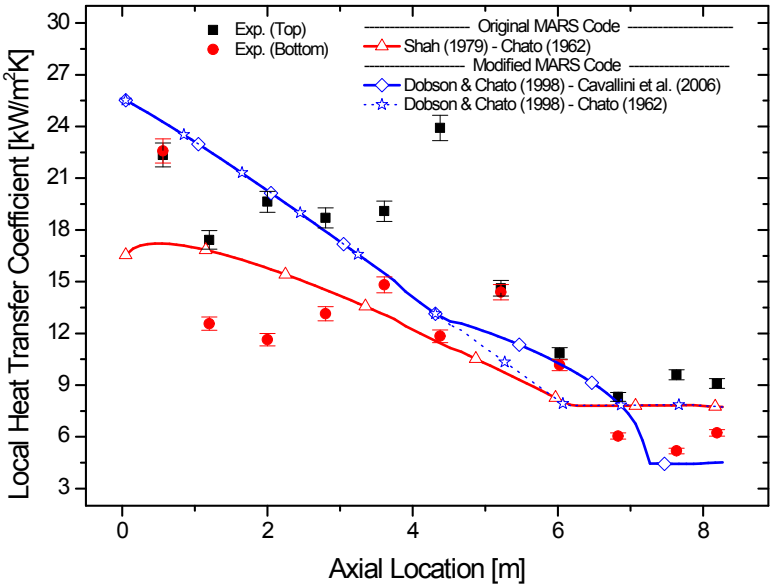

(c) SS-750-P1

Figure 2.19 Local HTCs (PASCAL) – (2/2)

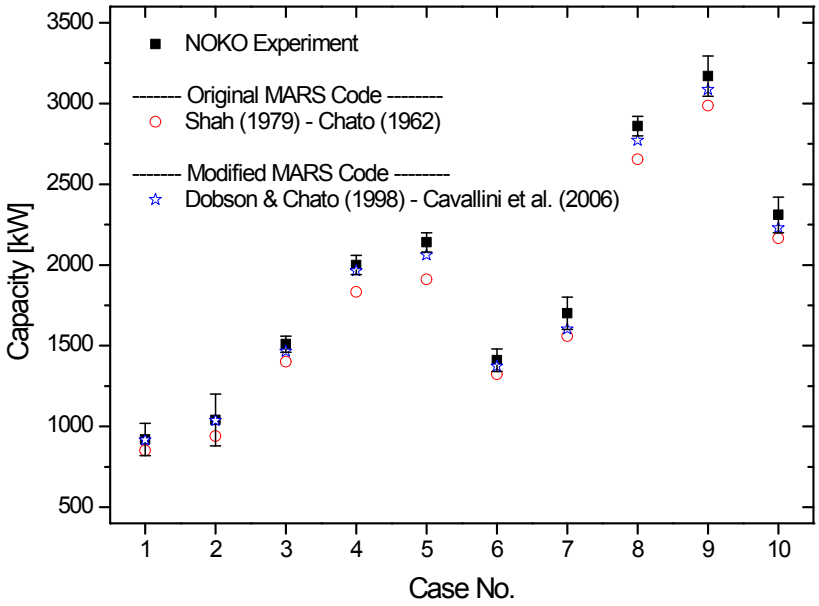

Figure 2.20 Predicted capacity for NOKO

Chapter 3

Development of Natural Convective Nucleate Boiling Model on Horizontal U-Shaped Heat Exchanger Submerged in Pool

3.1 State-of-the-Art

Nucleate boiling heat transfer on the horizontal tube is a frequent and important phenomenon encountered in many industrial applications such as evaporators in a refrigeration and air-conditioning systems, reboilers in chemical process industries, and many components in power engineering and other thermal processing plants because of its high heat transfer capability. In various engineering fields, over the past few decades, there have been many experimental and analytical researches to understand the nucleate boiling heat transfer on the horizontal tubes. A few correlations (Polley et al., 1980; Hwang and Yao, 1986; Webb and Chien, 1994; Gupta et al., 1995) have been proposed to predict the nucleate boiling heat transfer on the horizontal HX tubes. Most correlations were developed based on the superposition model by Chen (1966) established for two-phase flow in vertical tubes, and predicted their own data for the horizontal tubes

with reasonable accuracy. However, all correlations, based on the use of limited database, show a considerable deviation from the experimental data produced by different authors using different HX geometries, fluids and flow conditions.

In the TH field of nuclear engineering, there have been few researches on the prediction of the nucleate boiling heat transfer on the horizontal U-shaped HX of the passive safety systems. There have been no researches conducted on the applicability of the previous nucleate boiling models, based on the design and research experience of the reboilers or evaporators, to the HX of the passive safety systems. Furthermore, there are few nucleate boiling models developed for the horizontal U-shaped HX of the passive safety systems. Most heat transfer analyses with BE codes for the HX have been performed using the Chen (1966) correlation for the saturated forced convective boiling in vertical tubes (Arai et al., 2003; Schaffrath et al., 1999; Cho et al., 2013).

Due to the lack of the research, it is not known how to physically model the HX pool, and which correlations are suitable among the pool boiling and forced convective boiling correlations. Therefore, in order to predict the nucleate boiling heat transfer on the horizontal tube using BE codes, it is essential to assess the prediction capability of the previous nucleate boiling correlations under the operating condition of the passive safety system and to establish the prediction method. Then, if necessary, it is required to develop an appropriate heat transfer model in consideration of the main heat transfer mechanism on the horizontal U-shaped HX submerged in a pool.

3.2 Review of Previous Nucleate Boiling Heat Transfer Correlations

Various nucleate boiling heat transfer correlations on the horizontal tubes are available in the literature. Most of these correlations can be categorized as pool boiling (see Table 3.1) or forced convective boiling correlations (see Table 3.2). In this section, nucleate boiling heat transfer correlations to be assessed are presented. The understanding of the characteristics of each correlation provides a basis of the development of new boiling model described later in this Chapter.

3.2.1 Pool Boiling Correlations

Nucleate pool boiling on the horizontal tube is characterized by the bubble formation and their motion on a heated tube in a pool. It has been extensively studied and many correlations are available in the literature. Most of these correlations fall into two categories: (a) fully empirical, based on curve fittings of experimental results; and (b) semi-empirical, referring to those correlations based on a physical model of the nucleate boiling mechanism. Though the semi-empirical correlations are supported by a physical model, they are ultimately a curve fitting of experimental results (Ribatski and Jabardo, 2000).

The fully empirical correlations include the correlations by Mostinski (1963), Stephan and Abdelsalam (1980), Cooper (1984), and Gorenflo (1993). Mostinski (1963) correlation is the reduced pressure-based correlation that predicts the boiling heat transfer from the macroscopic system perspective. The author ignored surface effects and applied the principle of corresponding states to nucleate pool

boiling heat transfer, correlating data as a function of the reduced pressure of the fluid and its critical pressure. In the correlation, F_p is a non-dimensional pressure correction factor that characterizes pressure effects on nucleate boiling. This correlation gives reasonable results for a wide range of fluids and reduced pressures.

Stephan and Abdelsalam (1980) performed an analysis on 5000 experimental data existing in the literature for saturated nucleate pool boiling heat transfer in natural convection on a smooth tube. They proposed four specific correlations by employing various dimensionless groups based on the fluids physical properties, tubes properties and the operating conditions and by applying the methods of regression analysis to the following fluid classes: water, hydrocarbons, cryogenic fluids and refrigerants. The correlation by Stephan and Abdelsalam (1980) is one of the most widely quoted correlations in various engineering fields.

Cooper (1984) developed a new reduced pressure form of saturated nucleate pool boiling correlation including the roughness of the boiling surface based on an extensive database. In the correlation, the tube roughness is a parameter related to the nucleation sites size directly, and the reduced pressure and the molar mass are used to take into account the fluid physical properties important to the nucleation process.

Gorenflo (1993) proposed a fluid specific reduced pressure correlation including the effect of surface roughness using a great number of experimental data carried out with several boiling fluids on single tubes with different materials and surface roughness. The correlation by Gorenflo (1993) uses a reference HTC specified for each fluid. For water boiling, 5600 is used as the reference HTC. This method gives reliable results over a very wide range of heat flux and pressure.

The semi-empirical correlations include the correlations by Rohsenow (1952), Forster and Zuber (1955), and Cornwell and Houston (1994). Rohsenow (1952) proposed one of the first nucleate pool boiling correlations, based on the microscopic heat transfer mechanisms of the strong liquid agitation promoted by departing bubbles and the transient conduction. The correlation by Rohsenow (1952) was formulated as a single phase forced convection correlation where the characteristic length is the bubble departure diameter. In the correlation, the value of C_{sf} is an experimental constant depending on the various surface-fluid combinations.

Forster and Zuber (1955) proposed the thermo-physical properties-based correlation, on the basis of the microscopic heat transfer mechanism associated with the bubble dynamics considering the convection promoted by the expansion of bubbles during their growth. The old-established correlations by Rohsenow (1952) and Forster and Zuber (1955) are still recommended as fundamental design tools for the prediction of the boiling HTCs on the HX. Especially, the correlation by Forster and Zuber (1955) is utilized in the well-known and widely respected forced convective nucleate boiling correlation by Chen (1966).

Cornwell and Houston (1994), from the visual analysis, revealed that heat transfer mechanisms around the tube were due to traditional nucleate boiling and sliding bubble phenomena. Then, Cornwell and Houston (1994) showed that these mechanisms depended on the vapor production rate. Using the pool boiling data with water, refrigerants and hydrocarbons on single tubes having variable diameters between 8 and 50 mm, the authors proposed a new saturated pool boiling correlation including the tube diameter based on the single-phase forced convection model. Since the correlation by Cornwell and Houston (1994) also

includes the reduced pressure term in the correlation by Mostinski (1963) which has been widely used for 50 years to adequately describe the pressure dependence, it would be a correlation encompassing both the macroscopic and the microscopic system perspectives.

3.2.2 Forced Convective Boiling Correlations

Forced convective boiling on the horizontal tube is characterized by the convection heat transfer by two-phase flow around the tube as well as the nucleate pool boiling. It has been extensively studied and a few correlations are available in the literature. Most of these correlations fall into two categories according to the concepts for combining the (micro-convective) nucleate boiling and the (macro-convective) liquid convective contributions: (a) the superposition model-based; and (b) asymptotic model-based. The superposition model was initially proposed by Rohsenow (1952) as shown in Eq. (3.1).

$$h = h_{nb} + h_{cv} \tag{3.1}$$

Later, Chen (1966) advanced the superposition model (see Eq. (3.2)) by introducing the nucleate boiling suppression term, S, and the enhancement factor, F, to the Eq. (3.1).

$$h = S \cdot h_{npb} + F \cdot h_l \tag{3.2}$$

The asymptotic model was initially proposed by Kutateladze (1961). Compared to the superposition model, it has an exponent, n (n>1), as shown in Eq. (3.3); referentially, if the exponent is a value of unity, the asymptotic model can be regarded as the superposition model.

$$h = \left(h_{nb}^{n} + h_{cv}^{n} \right)^{1/n} \tag{3.3}$$

The asymptotic model has the merit of inhibiting the smaller of the contributing components such as h_{nb} and h_{cv}. However, there is no theoretical basis for selection of the exponent, n. Researchers have simply tried different values, and selected the exponent that gave the best fit of the data (Webb and Gupte, 1992).

The superposition model-based correlations include the correlations by Chen (1966), Polley et al. (1980), Singh et al. (1985), Hwang and Yao (1986), and Gupta et al. (1995). Chen (1966) proposed the superposition model-based correlation for the saturated forced convective boiling in vertical tubes. In the correlation by Chen (1966), the correlation by Forster and Zuber (1955) was used to calculate the nucleate pool boiling HTC term, h_{npb}, and the single-phase forced convection coefficient, h_l, term was predicted by the empirical correlation by Dittus-Boelter (1930) for single-phase turbulent flow in tube. For the suppression factor S, Chen (1966) argued that flow velocity acted to suppress the nucleate boiling, and correlated the suppression factor ($S < 1$) as a function of the two-phase Reynolds number ($Re_{TP}=F^{1.25}Re_l$) related to the convection. Furthermore, Chen (1966) argued that the convection heat transfer was enhanced by the two-phase flow, and proposed the enhancement factor, F (> 1), by assuming that the enhancement factor could be correlated as a function of the Martinelli parameter for two-phase friction, because the enhancement factor was a flow parameter. The correlation by Chen (1966) is most successful and widely used for the forced convective boiling in vertical tubes.

Polley et al. (1980) were the first to use the superposition model by Chen (1966) to evaluate the heat transfer on the outside of the tubes in a 36-tube

horizontal bundle with vertical flow in which R-113 was boiling. In the correlation by Polley et al. (1980), followings were different from that by Chen (1966): 1) For the nucleate pool boiling HTC, h_{npb}, the pool boiling correlation by Voloshko (1972) was used. It was developed specifically for pool boiling of R-113. 2) The nucleate boiling suppression factor, S, was assumed as a value of unity because they did not have sufficient information to conclude that the convection suppresses the nucleate boiling in a horizontal bundle. 3) The single-phase, forced convection coefficient, h_l, was obtained by a 1973 ESDU cross-flow correlation (KAERI, 2009) for the horizontal tube bundle. 4) For the enhancement factor, F, the authors developed a new equation instead of using that of Chen (1966) correlation because the pressure loss in the horizontal bundle is dominated by form loss instead of wall friction. They assumed that the liquid-phase flows as a film on the tubes wall and that the vapor-phase flows in space between tubes. They further assumed that the ratio of the two-phase HTC to the single-phase coefficient was inversely proportional to the ratio of the liquid volumetric flow to the total volumetric flow. They finally supposed that the velocity profile of the liquid film complied with $1/7^{th}$ power law and deduced a very simple expression for the enhancement factor as a function of the void fraction.

The correlation by Polley et al. (1980) was modified and incorporated in the MARS code (KAERI, 2009) as a nucleate boiling model for horizontal tube bundles. For the nucleate pool boiling correlation, the pool boiling correlation by Forster and Zuber (1955) was implemented instead of the correlation by Voloshko (1972) because the correlation was not validated with the boiling data of water. Additionally, in the modified correlation by Polley et al. (1980), this study changed the 1973 ESDU cross-flow correlation for the horizontal tube bundle to

the 1969 ESDU cross-flow correlation (KAERI, 2009) for the single horizontal tube. This is because the 1973 ESDU cross-flow correlation for the horizontal tube bundle was inadequate to use for the prediction of the HTCs on the single horizontal U-shaped tube due to the pitch-to-diameter term. Consequently, this modified correlation by Polley et al. (1980) was used in this study.

Singh et al. (1985) studied the effects of cross-flow on the boiling heat transfer for R-12 on single horizontal tube. The authors assumed the bulk flow of the boiling liquid causes additional agitation of the liquid by the bubbles, which was responsible for augmentation of pool boiling component, and the heat transfer effect of bulk flow could be added to the augmented pool boiling heat transfer. Then, the authors proposed a forced convective boiling correlation based on the superposition model by Rohsenow (1952). In the correlation by Singh et al. (1985), the nucleate pool boiling HTC, h_{npb}, was obtained by the nucleate pool boiling correlation by Rohsenow (1952), and the single-phase forced convection coefficient, h_l, was obtained by the empirical equation for forced convection normal to a single cylinder (Gupta and Prakash, 1976). Finally, they deduced the augmented term for the pool boiling heat transfer considering the effective vapor velocity. The correlation by Singh et al. (1985) showed good agreement with their own experimental data.

Hwang and Yao (1986) carried out experimental studies for the cross-flow boiling on a horizontal tube at various mass fluxes, local flow qualities and geometric arrangements. To predict their heat transfer data of a single tube in a channel or in a tube bundle, the authors established the Chen (1966) type correlation. In the correlation by Hwang and Yao (1986), followings were different from that by Chen (1966): 1) The pool boiling HTC, h_{npb}, of the

horizontal tubes was obtained by the self-developed pool boiling correlations for a single tube in a channel or in a tube bundle, respectively. 2) The nucleate boiling suppression factor S was estimated by the equation developed by Bennett et al. (1980) for both in-tube and shell-side cross-flow forced convective boiling by leaving the geometry influence. 3) The single-phase, forced convective correlations, h_l, for the single tube in a channel and in a tube bundle were taken by the empirical correlations by Bitter (1972) and Hwang and Yao (1984), respectively. 4) The enhancement factor, F, was obtained by the equation developed by Polley et al. (1980). The correlation by Hwang and Yao (1986) showed good agreement with the various experimental data at the cross-flow, refrigerants boiling conditions.

Gupta et al. (1995) carried out an experimental investigation for the cross-flow boiling heat transfer in small tube bundles consisting of horizontal tubes in a vertical column of saturated distilled water at atmospheric pressure. They observed that there was no significant effect of the bundle geometry on the HTC of the bottom tube compared to that of the single tube, but the HTCs on the upper tubes were increased by the vapor bubbles rising from the lower tubes and agitating the liquid around the upper tubes. Then, the authors proposed forced convective boiling correlations for each of the bottom and the upper tubes of the bundle. To predict the HTC of the bottom tube of the bundle, the authors used the asymptotic model by Kutateladze (1961). In the correlation by Gupta et al. (1995), the nucleate pool boiling HTC, h_{npb}, was obtained by the self-developed pool boiling correlation for a single tube, and the single-phase, forced convection HTC, h_l, was determined by the cross-flow correlation by Whitaker (1972) for single cylinders. With the exponent, n=1, the correlation by Gupta et al. (1995) was

reasonably well correlated with their own data. For the upper tubes, Chen (1966) type correlation was proposed; however, this correlation is inadequate to use for the prediction of the HTCs on the single horizontal U-shaped tube because the enhancement factor, F, consists of the pitch-to-diameter (P/D) and the number of tubes below the tube. Therefore, this study excluded this correlation and solely used the correlation for the bottom, or single, tube.

Webb and Chien (1994) conducted an evaluation study on which model was better between the superposition and the asymptotic models using various cross-flow boiling data of refrigerants to predict the forced convective boiling HTCs on banks of plain tubes. Then, they proposed the correlation based on the asymptotic model (exponent of 3) because their data were correlated better by the asymptotic model than by the superposition model. In the correlation, the h_{npb} was taken from the experimental data for one heated tube in a bundle, and the h_l term was predicted using the correlation by Zhukauskas (1972) for the single-phase flow normal to tube banks. The enhancement factor, F, was obtained by the equation developed by Bennett and Chen (1980) which was a function of the Martinelli parameter and the Prandtl number. For the suppression factor, S, Chen (1966) originally proposed this concept; however, many works by Steiner and Taborek (1992), Cornwell and Scoones (1988), Kenning and Cooper (1989), and Webb and Gupte (1992) have argued against the use of a suppression factor and there was uncertainty regarding whether the fluid velocity suppresses nucleate boiling. The issue of whether S=1 or S<1 is still unresolved; therefore, Webb and Chien (1994) assumed the suppression factor as a value of unity (S=1) and instead developed the correlation based on the asymptotic model in which the effect of suppression can be inherently included by the presence of the exponent term. Meanwhile, in

the paper by Webb and Chien (1994), the correlation for the nucleate pool boiling term had not been presented; consequently, this study obtained it from the nucleate pool boiling correlation by Forster and Zuber (1955).

Shah (2005) developed a simple dimensionless correlation for the heat transfer during subcooled boiling on a single tube and in tube bundles with forced cross-flow. Shah assumed the forced convective boiling heat transfer process could be calculated from that in single-phase flow of the liquid by introducing a suitable two-phase multiplier given as a function of the following parameters: heat flux, latent heat, mass flux, wall-, bulk fluid- and saturation temperatures. The correlation by Shah (2005) uses three correlating parameters: $\Delta T_{sub}/\Delta T_{sat}$ (this study will call this parameter as dimensionless subcooling number), boiling number Bo, and Bo-related parameter Ψ defined by Shah. Shah classified the experimental data according to the subcooling degree, and proposed the correlations for each of both high and low subcooling regimes. Four fluids (water, R-11, R-12, and R-113) were tested, with subcooling from 0 to 93℃, and upstream velocities ranging from 0.001 to 6.9 m/s. The correlation by Shah (2005) showed good agreement with 715 data points with the mean deviation of 12.5 %.

3.3 Analysis Approach

3.3.1 Description of Collected PAFS-Related Experiments

With an aim of validating the cooling and operational performance of the PAFS, an experimental program was progressed at KAERI, which is composed of

two kinds of tests; the separate effect test and the integral effect test (Kang et al., 2012). Both experiments provided the detailed heat transfer data for the horizontal U-shaped tube submerged in a pool. Details are as follows.

A. PASCAL Experiment

The PASCAL experiment, introduced in Chapter 2.3.1, provides the quasi-steady state data for nucleate boiling heat transfer under the low subcooling conditions (ΔT_{sub}=13 to 1 K) with the slow decrease of PCCT water level (ranging from 10.0 to 3.5 m) as shown in Fig. 3.1. Furthermore, it provides the detailed local heat transfer data at the high subcooling conditions of the PCCT. Therefore, it can be used to investigate the prediction capability of the nucleate boiling models and the natural convection model.

In order to assess the nucleate boiling correlations on the horizontal tubes, For the heat transfer analysis on the horizontal tubes, this study used the experimental HTCs in 8 measured positions (points 2 to 5 and 7 to 10), which correspond to the nearly horizontal part of the condenser tube (see Fig. 2.5).

From the measured temperatures, the local HTCs at the top and bottom of the tube were separately obtained as follows: 1) The local heat fluxes at the top and bottom of the tube are separately calculated as

$$q''_{wo,*}(z) = \frac{k_w \left(T_{wi,*}(z) - T_{wo,*}(z) \right)}{r_{wo} ln \left(\frac{r_{wo}}{r_{wi}} \right)} \tag{3.4}$$

2) The local HTCs at the top and bottom of the tube are respectively derived as

$$h_*(z) = \frac{q''_{wo,*}(z)}{T_{wo,*}(z) - T_b(z)} \tag{3.5}$$

In Eqs. (3.4) and (3.5), z is defined as the length from the start of the heat transfer region, T_b is the PCCT water temperature near each measurement point of the tube, and the subscript '*' indicates the "top" or "bottom" of the tube.

B. ATLAS-PAFS Experiment

To investigate the TH behavior in the primary and secondary systems of the APR+ during a transient when PAFS is actuated, KAERI performed the integral effect test using the ATLAS (Advanced Thermal-hydraulic test Loop for Accident Simulation)-PAFS facility (Kang et al., 2012). Figure 3.2 shows a schematic diagram of the ATLAS-PAFS facility. The ATLAS is a scaled-down facility of the APR+. The PAFS was connected to the SG-2 of ATLAS. Using this facility, the anticipated accident scenarios such as the feedwater line break (FLB), the main steam line break (MSLB), and SG tube rupture (SGTR) were simulated.

Figure 3.3 shows a schematic diagram of the PCHX and the PCCT of the ATLAS-PAFS facility. Contrary to the use of a single tube in the PASCAL test, the PCHX in the ATLAS-PAFS has three tubes whose dimension was scaled-down to consider the scaling methodology applied to the ATLAS design.

Geometrical data of the test section is as follows (see Table 3.3). The PCHX is composed of three U-tubes. The average tube length is 4.77 m, the inner diameter is 30.8 mm, and the wall thickness is 3 mm. The U-tube is composed of two 1.806 m straight parts and the inclination is 3.0° in both upper and lower straight parts. The PCCT was designed as a rectangular pool whose dimensions are: length 5.065 m, width 0.34 m, and height 6.5 m.

In a manner similar to the PASCAL test, to estimate the wall heat flux and the HTC, the tube inner/outer wall temperatures were measured at five points along the tube length (see Fig. 3.3). The fluid temperature profile inside the PCHX was measured by installation of the thermocouples in a radial direction and the local water temperatures were measured at 48 positions of PCCT. From the measured temperatures, the local HTCs at the top and bottom of the tube were separately obtained in a similar way to the PASCAL test.

The ATLAS-PAFS experiment provides the transient-state data for nucleate boiling heat transfer under the subcooled conditions (ΔT_{sub}=30 to 1 K); however, the local HTCs do not change rapidly because the increase of the pool temperature is not rapid as ~ 1 K/min. Therefore, the transient-state data of the ATLAS-PAFS could be used to validate the prediction capability of the nucleate boiling model.

3.3.2 MARS Modeling of Collected Experiments

A. MARS Nodalization for PASCAL Experiment

The PASCAL experimental data of the quasi-steady state condition was used to analyze the nucleate boiling heat transfer on the horizontal U-shaped HX submerged in a pool. Figure 3.4 shows the MARS nodalization scheme for the simulation of the PASCAL experiment. In order to effectively simulate the multi-dimensional natural convection flow and heat transfer phenomena in the PCCT, the PCCT was modeled using the multi-dimensional component, MULTID-200. The number of cell is 1, 16 and 29 for x, y and z-directions, respectively. A time-dependent volume, TDV-100, was used to provide the pressure boundary condition where the steam produced in the PCCT flows out. The heat structure,

HS-200, was used to calculate the heat transferred from the condenser tube wall to the cold water in the PCCT.

In order to examine the nucleate boiling heat transfer on the U-shaped tube in the PCCT, other parts such as conduction in the tube wall or condensation heat transfer in the condenser tube must be accurately modeled. In this nodalization scheme, the tube side was not modeled, and the measured inner wall temperatures were used directly in the heat structure as a boundary condition to remove the undesirable effects or uncertainties caused by the tube-side condensation heat transfer model as much as possible.

B. MARS Nodalization for ATLAS-PAFS Experiment

The ATLAS-PAFS experimental data was used to analyze the nucleate boiling heat transfer on the horizontal U-shaped HX submerged in a pool. Figure 3.5 shows the MARS nodalization scheme for the simulation of the ATLAS-PAFS experiment. The PCCT was modeled using the MULTID-200. The number of cell is 1, 12 and 27 for x, y and z-directions, respectively. The time-dependent volume, TDV-100, was used to provide the pressure boundary condition where the steam produced in the PCCT flows out. The heat structures, HS-200, 202 and 204 were used to calculate the heat transferred from the wall of each U-shaped tube in HX bundle to the cold water in the PCCT. Like the PASCAL nodalization, the tube side was not modeled in this ATLAS-PAFS nodalization, and the measured inner wall temperatures of each tube were used directly in the heat structure as a boundary condition to remove the undesirable effects due to the tube-side condensation heat transfer model as much as possible.

3.3.3 Applicability of MARS MULTID Component

In this study, the pool is modeled as a MULTID component in MARS. In order to obtain a reliable prediction of the boiling HTCs on the HX tube, it is required to confirm the simulation capability of MULTID in MARS on the multi-dimensional pool mixing phenomena. This is because the total pool mixing phenomena affect the local water temperature and the natural convection flow velocity near the HX, and finally influence the local boiling HTCs.

To confirm the simulation capability of MULTID in MARS, this study used the PASCAL experiment which provided the detailed local water temperature distribution in the large pool. Figure 3.6 shows the comparison of temperature contour between experimental data and MARS prediction under 750 kW of SG power and 9.0 m of PCCT water level condition. Since the local natural convection flow velocity was not measured in the experiment, the quantitative comparison for the flow velocity was not performed in this study. In addition, there was uncertainty due to the intrinsic difficulty of the code simulation for the two-phase natural convection phenomena. However, the temperature distribution predicted by MARS was similar with the experimental data (see Fig. 3.6), and the velocity field was similar to that predicted from a 3D TH code CUPID simulation (Cho et al., 2014) for the PASCAL experiment. Furthermore, according to the MARS simulations for the PAFS by Cho et al. (2012), the use of MULTID provides more stable results for the system parameters than the use of one dimensional component. Therefore, this study concluded that MULTID had the simulation capability of the multi-dimensional pool mixing phenomena appropriately and performed the heat transfer analysis on the horizontal HX

submerged in a pool using MULTID in MARS.

The prediction capability of MULTID in MARS for the natural convection velocity in a pool is presented in Appendix A additionally.

3.4 Assessment of Previous Nucleate Boiling Correlations

The heat transfer analysis was performed with MARS to predict the nucleate boiling heat transfer on the horizontal U-shaped HX submerged in a pool. In order to investigate the applicability of the previous nucleate boiling correlations to the horizontal U-shaped HX submerged in a pool, 15 nucleate boiling correlations presented in Tables 3.1 and 3.2 were incorporated into MARS. Using the MARS code with implemented correlations, simulations of PASCAL experiment were performed under various PCCT water level conditions ranging from 9.0 to 3.5m. Then, the comparison between experimental data and MARS predictions by each correlation was performed. This evaluation process is important because, in previous researches for the prediction of the boiling heat transfer on the horizontal U-shaped HX in a pool, it has not been clearly identified whether the approach by the pool boiling correlation is valid or the approach by the forced convective boiling correlation is appropriate.

The correlations were assessed through local HTCs. The local heat transfer rate is the critical parameter considered to be in the optimum design of the HX. The correlation which predicts the local HTCs on both upper and lower parts of the U-shaped HX well can be evaluated as an applicable correlation.

In the first step, this study has compared the HTCs with the pool boiling

correlations. Figure 3.7(a) shows the comparison between the experimental data and MARS calculation results for local HTCs under 9.0 m of PCCT water level and 750 kW of constant SG power condition as a representative condition for the PASCAL experiment. The comparison between each correlation and experimental data showed a significant dispersion. The correlations by Rohsenow (1952), Mostinski (1963), Cooper (1984) and Gorenflo (1993) generally over-estimated the experimental local HTCs. The correlation by Stephan-Abdelsalam (1980) similarly-predicted the HTCs on the upper part, but over-predicted the data on the lower part of the U-tube. On the contrary to this, the correlations by Forster-Zuber (1955) and Cornwell-Houston (1994) slightly over or closely predicted the HTCs on the lower part, but under-estimated the data on the upper part of the U-tube.

In the second step, this study has compared the HTCs with the forced convective boiling correlations. These correlations differ from the pool boiling correlations by considering the effect of two-phase flow such as local velocity and the local void fraction on the tubes. Figure 3.7(b) shows the comparison between the experimental data and MARS calculation results for local HTCs under 9.0 m of PCCT water level and 750 kW of constant SG power condition. The comparison between each correlation and experimental data showed a large scattering. The correlations by Singh et al. (1985) and Gupta et al. (1995) generally over-estimated the experimental local HTCs. The bundle correlation by Hwang-Yao (1986) similarly-predicted the HTCs on the upper part of the U-tube, but over-predicted the data on the lower part. On the contrary to this, the correlations by Shah (2005) and the single tube correlation by Hwang-Yao (1986) generally under-estimated the experimental local HTCs. The correlations by Chen (1966), Polley et al. (1980), and Webb-Chien (1994) under-predicted the HTCs on

the upper part of the U-tube, but over-estimated the data in the lower part of the U-tube.

From these results, several comments could be made. The introduced pool boiling correlations had been developed or validated using the water boiling data on a single horizontal tube and similarly, the PASCAL experiment incorporates a single tube submerged in a water pool. Considering that the HX is submerged in a pool, the prediction approach by pool boiling correlation might be reasonable. However, there are no correlations which can predict the HTCs on both upper and lower parts of the U-tube in PASCAL experiment well enough. This may be attributed to the HX geometry of the U-shaped tube which may have different heat transfer characteristics from the single horizontal tube. The U-shaped tube can be regarded as the connection of two horizontal tubes installed in a vertical row and then the interaction between the two tubes may cause the different heat transfer characteristics. In addition, all pool boiling correlations were developed under the saturated boiling condition but the PASCAL data were obtained under the low subcooled boiling conditions (ΔT_{sub}=1 to 13 K). Since the heat flux of pool boiling is determined by Eq. (3.6) below, MARS calculations by pool boiling correlations do not consider the subcooling effect on local HTCs. Therefore, the application of pool boiling correlation solely to the PASCAL might be inadequate.

$$q'' = h_{npb}\left(T_w - T_{sat}\right) \tag{3.6}$$

For the forced convective boiling correlations, the local flow velocity and void fraction were considered as well as the nucleate pool boiling heat transfer. Emphasizing that the heat transfer is affected by the multi-dimensional flow near the HX, the approach by forced convective boiling correlation may provide better prediction. However, there are no correlations which can predict the PASCAL

data of the HTCs on both upper and lower parts of the U-tube well enough. This is possibly because the introduced forced convective boiling correlations do not consider the heat transfer mechanisms on the U-shaped tube submerged in a pool. Most correlations have been developed based on the design and research experience of reboilers and evaporators. Therefore, the simple application of previous forced convective boiling correlations to the PASCAL may be inadequate.

With regard to estimate the boiling heat transfer on the horizontal U-shaped HX submerged in a pool, it is required to figure out which approach is most valid. From the MARS simulations of the PASCAL experiment, it is clearly evidenced that the prediction with the previous approach cannot describe fully the boiling heat transfer on the U-shaped HX in a pool. All previous correlations showed considerable differences in the prediction of local HTCs. There are appropriate pool boiling or forced convective boiling correlations to predict the HTCs on the upper or lower parts of the U-shaped HX well, but there is no single correlation that can be universally applied to the prediction of the local HTCs on both upper and lower parts of the U-shaped tube. From this study, it is obvious that a better heat transfer analysis with MARS requires a new approach to the horizontal U-shaped HX submerged in a pool.

3.5 Boiling Heat Transfer Mechanism of Horizontal U-Shaped HX Submerged in Pool

In this study, a target passive safety system is a PAFS which has four bundle

heat exchangers deeply submerged in a pool of water. In the heat exchanger pool of the PAFS, a steam-water two-phase flow is formed by the gravity-induced natural circulation. The flow is multi-dimensional, which has the combined velocity components normal and parallel to the HX tubes, and the boiling occurs at the pool side of the HX tubes. The overall boiling phenomena are very complicated. However, the nucleate boiling heat transfer on a tube in the bundle can be approached by the fundamental understanding of the heat transfer characteristics of the unit HX tube as a building block of a bundle HX (Hwang and Yao, 1986), except the bundle effect due to vapor bubbles generated from lower tubes rising and causing turbulence around the upper tubes (Gupta et al., 1995).

The PASCAL facility has a single U-shaped HX as a unit HX of the PAFS. Since the PASCAL experiment was conducted at a natural convective boiling condition with a preserved HX power level and pool size environment for the PAFS, this study investigated the nucleate boiling heat transfer mechanism on the horizontal U-shaped HX in the PAFS considering the PASCAL experimental data, MARS simulations and literature survey comprehensively and had several insights.

Figures 3.8(a) and 3.8(b) present typical experimental data obtained from the PASCAL experiment (Bae et al., 2013). These figures represent the local HTCs versus the PCCT water level at constant SG power of 750 kW. Two heat transfer characteristics are observed. The first characteristic is that HTCs increase at all measured points as the PCCT water level decreases by evaporation (see Fig. 8(a)). It can be explained by the subcooling decrease of water in the PCCT. In the PASCAL experiment, the HX is deeply submerged in the PCCT. Due to the static

head, the pressure of water near the HX is higher than that near the surface of water. Until the HX is uncovered by the water level decrease, it is operated under the low subcooled boiling condition (ΔT_{sub}=13 to 1 K). In this situation, a decrease in water level induces a decrease of saturation temperature and subcooling degree of water near the HX. The decrease of subcooling degree induces the increase of the generation of large bubbles. Moreover, the flow velocity around the HX is increased because the driving force of the natural circulation depends on the bubble generation rate. Therefore, the decrease of PCCT water level increases the nucleate boiling heat transfer.

The second characteristic is that the difference of HTCs between upper and lower parts of U-shaped HX is too large to be predicted by the single correlation (see Fig. 3.7). Moreover, the difference increases as the water level decreases (see Fig. 3.8(b)). This implies that the different heat transfer mechanism acts on each part of U-shaped HX. Figure 3.9 shows the boiling heat transfer mechanisms on the horizontal U-shaped HX submerged in a pool. The base heat transfer mode outside the HX tube is a nucleate pool boiling heat transfer. However, the upper part is influenced by the effect of gravity-induced natural convection velocity due to the heat transfer from the lower part of U-tube additionally. As the PCCT water level decreases, more bubbles are generated from the lower part of U-tube and the effect of flow velocity on the upper part of U-tube increases further. Since the turbulence around the upper part of U-tube increases more due to the liquid agitation by the bubbles generated from the upper part of U-tube, the HTCs on the upper part increases more rapidly than those on the lower part. Meanwhile, the HTCs on the lower part increases slowly. It is deduced that the lower part is not affected by the multi-dimensional flow significantly. According to Reymond et al.

(2008), in the natural convection experiment using a pair of vertically aligned horizontal cylinders in a pool, the lower cylinder is unaffected by the presence of the upper cylinder. Therefore, the heat transfer mechanism on the lower part of U-tube is different from that on the upper part of U-tube.

3.6 Prediction Method with BE Code

From the analysis of heat transfer mechanisms, following approaches are drawn to predict the nucleate boiling heat transfer on the U-shaped HX submerged in a pool: 1) Since the subcooling degree and the local flow velocity near the HX affects the local HTCs, for the reliable prediction of the local variables, it is recommended that the pool is modeled by using the multi-dimensional component in BE code such as MULTID of MARS. 2) In the upper and lower parts of U-tube, different heat transfer correlations should be applied because the phenomenological difference exists in the heat transfer mechanism on the upper and lower parts of the U-tube. 3) For the lower part of U-tube, it is reasonable to predict the heat transfer using the nucleate pool boiling correlation which considers the effect of subcooling since the lower part of U-tube experiences subcooled nucleate boiling. 4) For the upper part of U-tube, the base heat transfer mode is the subcooled nucleate pool boiling, but it is reasonable to predict the heat transfer using the forced convective boiling correlation because the effect of natural convection velocity from the lower part on the upper part of the U-tube should be considered. Moreover, in the correlation, it is required to consider the effect of void fraction around the upper part of U-tube because the effect of flow

velocity induced from the lower part on the upper part increases due to the increase of turbulence due to the liquid agitation by the bubble around the upper part.

3.7 Development of Nucleate Boiling Model on Horizontal U-shaped Heat Exchanger Submerged in Pool

According to the proposed prediction method with the BE code, it is required to develop a new boiling model. Since the nucleate boiling heat transfer on the U-tube submerged in a pool is governed by two heat transfer mechanisms: subcooled nucleate pool boiling for the lower part of U-tube and subcooled forced convective boiling for the upper part of U-tube, this study proposed new correlations for each part of U-tube.

3.7.1 New Subcooled Pool Boiling Correlation

A general heat flux equation of the pool boiling is expressed as shown in Eq. (3.6). It does not include the term of subcooling degree. To develop a subcooled pool boiling correlation, this study introduced the suppression term into the pool boiling equation as shown in Eq. (3.7).

$$h_{nb} = S \cdot h_{npb} \tag{3.7}$$

Previously, this suppression term has been used in the forced convective boiling correlation to consider the decrease of the nucleate boiling heat transfer

due to the flow velocity. This study borrowed the concept from the suppression term of the forced convective boiling correlation to consider the effect of subcooling degree on the decrease of the nucleate boiling heat transfer.

In order to develop a subcooled nucleate pool boiling correlation, it is essential to select the appropriate saturated nucleate pool boiling correlation first. Since the heat transfer mode in the lower part of U-tube corresponds to the nucleate pool boiling, this study compared the PASCAL data on the lower part of U-tube and MARS predictions by seven pool boiling correlations identified in the literature survey (see Table 3.1). As shown in Fig. 3.7(a), the correlations by Forster-Zuber (1955) and Cornwell-Houston (1994) presented similarly or slightly over estimated the experimental HTCs on the lower part of U-tube. On the contrary to this, the correlations by Rohsenow (1952), Mostinski (1963), Cooper (1984), Gorenflo (1993) and Stephan-Abdelsalam (1980) over-estimated the experimental HTCs on the lower part of U-tube generally and showed significant dispersion. At this level, this author determined the correlation by Cornwell-Houston (1994) as the most appropriate pool boiling correlation for the analysis of PASCAL experiment because it gave the reasonable results generally, and it was the latest nucleate pool boiling correlation for the horizontal tube encompassing both the macroscopic and the microscopic system perspectives physically as described in Chapter 3.2.1.

Figure 3.10 shows the MARS predictions by the Cornwell-Houston (1994) correlation versus the experimental HTCs on the lower part of U-tube for all selected PCCT water level conditions. The saturated pool boiling correlation by Cornwell-Houston (1994) gave similar results with the experimental HTCs for the subcooled nucleate pool boiling within a deviation of ±20 %. Since the bubble

generation mechanism in the subcooled condition is fundamentally same with that in the saturated condition, it is judged that the saturated pool boiling correlation may be applicable to the low subcooled condition in the PASCAL experiment. However, in order to obtain any better prediction of HTCs physically, it is required to develop the suppression term, S (≤1), which can decrease the HTC as the degree of subcooling increases.

In Fig. 3.7(a), the MARS code with the saturated pool boiling correlation by Cornwell-Houston (1994) slightly over-predicted the experimental HTCs under the high PCCT water level of 9 m. In this condition, the effect of subcooling cannot be ignored because the degree of subcooling is relatively high, ~13 K. To develop the suppression term due to the subcooling degree, this study borrowed the dimensionless subcooling number from the Shah (2005) correlation for the subcooled boiling (see Table 3.2). The suppression term can be expressed as Eq. (3.8) by non-dimensionalizing the degree of subcooling using the wall superheat.

$$S = \left(1 + \frac{\Delta T_{sub}}{\Delta T_{sat}} \right)^{a} \tag{3.8}$$

The coefficient, a, in Eq. (3.8) was determined as –0.167 by comparing the calculated HTCs with the PASCAL experimental data at the lower part of U-tube. As a result, new subcooled nucleate pool boiling correlation can be obtained as Eq. (3.9) by adding the suppression term for the subcooling degree to the saturated pool boiling correlation by Cornwell-Houston (1994).

$$h_{nb} = 9.7 \cdot P_c^{0.5} \cdot \frac{k_l}{D} \cdot F_p \cdot \left(\frac{\dot{q}'' D}{\mu_l h_{fg}} \right)^{0.67} \cdot Pr_l^{0.4} \cdot \left(1 + \frac{\Delta T_{sub}}{\Delta T_{sat}} \right)^{-0.167} \tag{3.9}$$

3.7.2 New Subcooled Forced Convective Boiling Correlation

The heat transfer mode in the upper part of the U-tube corresponds to the subcooled forced convective boiling. To develop a subcooled forced convective boiling correlation which takes into account the effects of subcooling degree and multi-dimensional two-phase flow in a pool, this study used the superposition model (see Eq. (3.2)) by Chen (1966), because it has been known that the Chen-type correlation predicted the experimental data for the horizontal tubes with reasonable accuracy.

In Chen-type correlation, it is required to determine the each term of h_{npb}, S, h_l, and F appropriately. The nucleate pool boiling HTC, h_{npb}, of the correlation can be obtained from the correlation by Cornwell-Houston (1994) applied to the lower part of U-tube. For the suppression factor S, which represents the suppression of the nucleate pool boiling contribution, many previous researches have used the relation of suppression by the convection flow. However, visual observations of bubbly and frothy flow made by Cornwell (1989), Leong and Cornwell (1979), and Cornwell et al. (1980) do not show an evidence of a suppression of nucleate boiling in a bundle. In addition, cross-flows over single tubes do not show effects of boiling suppression according to the finding of Steiner and Taborek (1992). Thus, Collier (1994) concluded that the boiling suppression factor should be set equal to 1.0 for a tube bundle. Therefore, this study ignored the suppression due to the convection flow. Meanwhile, the PASCAL experiment was performed under the subcooled boiling condition. Since the suppression due to the degree of subcooling is clear in this situation, this study used Eq. (3.8) as a suppression factor for the subcooling degree instead of the previous suppression factor due to

the flow velocity.

The liquid-only HTC, h_l, can be obtained from the single-phase, forced convective heat transfer correlation. Previously, in dealing with the forced convective boiling on the horizontal tubes, many researches have considered the cross-flow only. However, in passive safety systems such as PAFS and PCCS, the HX tubes are submerged in a large pool. Near the HX tubes, the flow direction is not fixed and the multi-dimensional flows having the parallel-, cross-, and inclined flows to the HX tubes are likely (see Figs. 3.6(b)). In the multi-dimensional flow, although the flow speed is the same, both the parallel and normal velocity components become different (see Fig. 3.11) and finally, the HTC changes according to the flow direction. Using the BE code, in order to predict the out-tube convection heat transfer in the pool, the heat transfer correlation which can estimate the convection HTCs for the parallel-, cross-, and inclined flows appropriately is required. For the parallel and cross flows, many correlations exist in previous literatures; however, there is no correlation validated for the inclined flow. Therefore, it is required to develop the heat transfer correlation for the multi-dimensional flow.

To develop the single-phase convection correlation for the multi-dimensional flow, this study used the asymptotic method suggested by Kutateladze (1961). This method of averaging uses the square root of the sum of the squares in order to weight the answers more toward the larger of the two values mathematically (USNRC, 2006). When the two heat transfer modes are combined and it is difficult to know the HTC by each heat transfer mode, this method has provided the reasonable predictions. It has been used to correlate the forced convective and nucleate boiling results (see Eq. (3.3)) or the combined natural and forced

convection heat transfer results frequently. Similarly, the multi-dimensional flow can be regarded as a kind of mixed flow of the parallel- and cross flows. In this situation, the liquid-only HTC can be determined by averaging the HTCs caused by flow parallel to the tubes and flow perpendicular to the tubes (USNRC, 2006). Therefore, the single-phase forced convective HTC on the HX submerged in the pool where the multi-dimensional flows exist can be expressed as follows:

$$h_l = \left(h_{l,cross}^n + h_{l,parallel}^n \right)^{1/n} \tag{3.10}$$

In this study, single-phase forced convective HTCs for cross flow and parallel flow are determined from the correlations proposed by Whitaker (1972) of Eq. (3.11) and Dittus-Boelter (1930) of Eq. (3.12), respectively, as given below:

$$h_{l,cross} = \left(0.4 Re_l^{1/2} + 0.06 Re_l^{2/3} \right) \left(Pr_l \right)^{0.36} \left(\frac{\mu_l}{\mu_v} \right)^{0.25} \left(\frac{k_l}{D} \right) \tag{3.11}$$

$$h_{l,parallel} = 0.023 Re_l^{0.8} Pr_l^{0.4} \left(\frac{k_l}{D} \right) \tag{3.12}$$

The exponent, n, in Eq. (3.10) was determined as 2 from the CFD analysis. The validation of the proposed convection correlation for the multi-dimensional flow is presented in Appendix B.

The remaining element of the prediction is calculation of the enhancement factor, F. It accounts for the enhancement of the single-phase liquid convective HTC due to the turbulence created by the bubble formation and their motion on the tube. It can be obtained from the equation analytically deduced by Polley et al. (1980) as given below:

$$F = \left(\frac{1}{1 - \alpha_v} \right)^{0.744} \tag{3.13}$$

Since the void fraction effect on the single-phase convection HTC can be

considered appropriately, Polley et al. (1980) and Hwang and Yao (1986) have used this equation to develop the forced convective boiling correlation.

Finally, using Eqs. (3.8) and (3.13) for the S and F factors, together with Eqs. (3.9) and (3.10), a new subcooled nucleate forced convective boiling correlation could be obtained.

3.7.3 Validation of Proposed Nucleate Boiling Model

The validation of the proposed model was performed with the MARS simulations of the PASCAL and ATLAS-PAFS experiments. Figure 3.12 shows the comparison between the experimental data and MARS calculation results for local HTCs under 9.0 and 4.0 m of PCCT water level and 300, 540 and 750 kW of constant SG power conditions in the PASCAL experiment. Including the MARS default correlation by Chen (1966) for in-tube forced convective boiling, the modified correlation by Polley et al. (1980) for the forced convective boiling on the horizontal tube and the saturated pool boiling correlation on the horizontal tube by Cornwell-Houston (1994) did not predict the HTCs on both the upper and lower parts of the U-tube. However, the proposed boiling model generally well predicted the experimental data at all measured points by applying the new subcooled pool boiling correlation and the new forced convective boiling correlation to the lower and upper parts of the U-tube, respectively.

Figure 3.13 presents the MARS calculation results of the local HTCs for the PASCAL experiment as a function of the PCCT water level. As the PCCT water level decreased, the local HTCs increased and the difference of HTCs between upper and lower parts of U-tube increased gradually. At low PCCT water level

(below ~5.0 m), as the void fraction increased, the local HTCs on the upper part of U-tube did not increase stably due to the oscillation of the flow velocity and tube surface temperature; however, the predicted HTCs were generally similar to the experimental HTCs in Fig. 3.8(b).

Figure 3.14 shows a comparison of the proposed boiling model with the experimental data for PASCAL, together with the data for ATLAS-PAFS. Applying the in-tube boiling correlation by Chen (1966) to the horizontal parts of the U-shaped tube yields poor results. The correlation by Chen (1966) uses the relation of suppression by the convection flow, the enhancement factor based on the wall friction, and the single-phase correlation for the in-tube forced convection. However, for the heat transfer on the horizontal tube HXs, the suppression due to the flow velocity has not been identified (Leong and Cornwell (1979); Cornwell et al. (1980); Cornwell and Scoones (1988); Kenning and Cooper (1989); Cornwell (1989); Steiner and Taborek (1992); Webb and Gupte (1992); Collier (1994)), the pressure loss is dominated by form loss instead of wall friction, and the single-phase heat transfer is governed by an external flow outside the horizontal tube not an internal flow. For this reason, it is concluded that the correlation by Chen (1966) is not physically valid to be applied to the prediction of the boiling heat transfer on the horizontal tubes.

Meanwhile, the proposed boiling model predicted the experimental HTCs much better than the correlation by Chen (1966). For PASCAL experiment, 288 data points were predicted with a mean deviation of 7.9 %. For ATLAS-PAFS experiment, 78 data points were predicted with a mean deviation of 8.7 %. Only 7 of total 366 data points from 2 sources (PASCAL and ATLAS-PAFS) had deviation greater than 19 %. The experimental HTCs on both upper and lower

parts of U-shaped tubes were correlated very satisfactorily by the developed boiling model. Therefore, it is expected that the proposed nucleate boiling model will be usable to the reliable design and the safety analysis of the passive safety system using the BE code.

3.8 Development of Natural Convective Nucleate Boiling Model on Horizontal U-shaped HX Submerged in Pool

The proposed nucleate boiling model was validated at low subcooling conditions (up to around 30 K); however, when the passive safety system starts to operate, the water temperature in the HX pool is low as the room temperature, ~300 K, and the subcooling is significantly high (about 90 K for the PAFS). Considering that the heat flux from the HX tube surface is high (hundreds of kW/m^2 for the PAFS) at the initial phase of the NPP accident, the nucleate boiling model is expected to be applied to the high subcooling conditions as well; however, emphasizing that the subcooling is high in the HX pool, the heat transfer outside the HX tube surface may be governed by the natural convection. In order to complete the modeling of the heat transfer outside the horizontal HX tube, it is required to secure the heat transfer model to be applicable to a full time operation of the passive safety system including the high subcooling conditions. Therefore, this study assessed the prediction capability of the nucleate boiling models and the MARS default natural convection model using the HTC data at high subcooling conditions in the PASCAL experiment and developed the natural convection model on the horizontal U-shaped HX submerged in a pool suitable for high

subcooling conditions. Finally, this study developed the natural convective nucleate boiling model on the horizontal U-shaped heat exchanger submerged in a pool by combining the proposed nucleate boiling model and the natural convection model.

3.8.1 MARS Nodalization for PASCAL Experiment

Figure 3.15 shows the MARS nodalization scheme for the simulation of the PASCAL experiment. The time-dependent volume, TDV-100, was used to provide the inlet boundary condition for the pure saturated steam. The inlet flow rate of the steam was controlled by the time-dependent junction, TDJ-125. The pipe component, PIPE-150, was used to model the condenser tube, PCHX. The time-dependent volumes, TDV-190, was used to provide the boundary conditions for the pressure outlet. The condensate water is drained into the TDV-190 through the PIPE-180. The heat structure, HS-150, was used to calculate the heat transferred from the steam to the cold water in the PCCT through the condenser tube wall. The PCCT was modeled using the multi-dimensional component, MULTID-200, to effectively simulate the multi-dimensional natural convection flow and heat transfer phenomena in the PCCT. The number of cell is 1, 16 and 29 for x, y and z-directions, respectively. A time-dependent volume, TDV-210, was used to provide the pressure boundary condition where the steam produced in the PCCT flows out.

3.8.2 Assessment of Natural Convection and Nucleate Boiling Models

The heat transfer analysis on the horizontal U-shaped HX submerged in a pool was performed using the MARS code implemented with the improved condensation heat transfer model. In order to investigate the applicability of previous out-tube heat transfer models to the high subcooling conditions, this study used the nucleate boiling models by Chen (1966) and this author, and the MARS default natural convection model by Churchill and Chu (1975) for a horizontal cylinder. Simulations of PASCAL experiment were performed under various PCCT water temperature conditions ranging from 310 to 370 K as shown in Table 3.4. Then, the comparison between experimental data and MARS predictions by each model was performed. This evaluation process is important because, in previous researches for the prediction of the heat transfer on the horizontal U-shaped HX in a pool, it has not been clearly identified whether the approach by the nucleate boiling model is valid to the high subcooling conditions or the approach by the natural convection model is appropriate.

Figures 16(a) and 16(b) show the comparison between the experimental data and MARS calculation results for local HTCs at positions 3 and 7 (see Fig. 2.5) under the SS-540-P1 test condition, respectively. The nucleate boiling models by Chen (1966) and this author similarly-predicted the HTCs for the low subcooling conditions ($\Delta T_{sub} < \sim 40$ K), but significantly under-estimated the data for the high subcooling conditions ($\Delta T_{sub} > \sim 40$ K). Meanwhile, the natural convection model by Churchill and Chu (1975) considerably under-predicted the experimental data for all test conditions.

From these results, several comments could be made. Considering the high

heat flux from the HX tube surface, it was originally expected that the nucleate boiling model could be applicable to the high subcooling conditions. However, including the Chen model (1966), the nucleate boiling model proposed in this study was not valid to be applied to the high subcooling conditions. Furthermore, the application of the well-known natural convection model by Churchill and Chu (1975) to the operating conditions of the PAFS was also inadequate.

To investigate the heat transfer regime, this study analyzed the PCCT water and PCHX outer wall temperatures and found that the PCHX wall temperature is below the saturation temperature in the initial phase of the HX operation (ΔT_{sub} > ~40 K). This means that the heat transfer regime is governed by the natural convection in the high subcooling region and the onset of nucleate boiling (ONB) occurs in the transition region between the natural convection region and the subcooled nucleate boiling region. Therefore, it is obvious that a better heat transfer analysis with MARS requires a new natural convection heat transfer model to be applied to the high subcooling conditions of the HX pool in the passive safety system.

3.8.3 New Natural Convection Model

According to the heat transfer analysis of the U-shaped tube (see Chapter 3.6), different heat transfer correlations should be applied in the upper and lower parts of U-tube because the phenomenological difference exists in the heat transfer mechanism on the upper and lower parts of the U-tube. The base heat transfer mode outside the HX tube is a natural convection heat transfer; however, the upper part is influenced by the effect of gravity-induced natural convection

velocity due to the heat transfer from the lower part of U-tube additionally. Therefore, this study developed the natural convection model by separating the upper and lower parts of the U-tube.

According to Morgan (1975), the natural convection heat transfer data for the circular cylinder can be simply correlated by the Rayleigh number, Ra_D, as shown in Eq. (3.14) below.

$$Nu_D = CRa_D^n \tag{3.14}$$

This study developed Morgan-type natural convection correlations for each horizontal part of U-tube using the PASCAL data for various PCCT water temperature conditions (310 to 350 K). Figure 3.17 shows the Nusselt number, Nu_D, versus the Rayleigh number. The Nusselt number increases with the Rayleigh number and the Nu_D data of the upper part of U-tube are generally larger than those of the lower part of U-tube. The natural convection correlations for each horizontal part of U-tube are obtained as follows.

$$h_{upper} = 0.0405 Ra_D^{0.471} \frac{k_l}{D} \tag{3.15}$$

$$h_{lower} = 0.0117 Ra_D^{0.514} \frac{k_l}{D} \tag{3.16}$$

The mean deviation for the upper part of U-tube data is 10.6 % and that for the lower part of U-tube data is 14.6 %. Only 8 of total 134 data points from PASCAL had deviation greater than 33.2 % (see Fig. 3.18). All experimental HTCs on both upper and lower parts of U-shaped tubes were correlated satisfactorily by the developed natural convection model with a mean deviation of 12.9 %.

3.8.4 Development of Natural Convective Nucleate Boiling Model

Figures 3.19(a) and 3.19(b) show the comparison between the experimental data and MARS calculation results for local HTCs at positions 3 and 7 (see Fig. 2.5) under the SS-540-P1 test condition, respectively. The proposed natural convection model similarly-predicted the HTCs for the high subcooling conditions ($\Delta T_{sub} > \sim 40$ K), but significantly under-estimated the data for the low subcooling conditions ($\Delta T_{sub} < \sim 40$ K). On the other hand, the proposed nucleate boiling models similarly-predicted the HTCs for the low subcooling conditions, but significantly under-estimated the data for the high subcooling conditions. During a full time operation of the HX, to obtain a reliable prediction of the HTCs using the BE code, it is required to combine the natural convection model with the nucleate boiling model exquisitely. For the smooth transition between both models, this author determined the HTCs from the maximum of the values predicted by the proposed natural convection model and the proposed nucleate boiling model using Eq. (2.5) and finally developed the natural convective nucleate boiling model for the horizontal U-shaped HX submerged in a pool. As a result, the HTCs calculated by the proposed natural convective nucleate boiling model showed good agreement with the experimental data, compared to those by the original MARS code.

3.9 Discussion

3.9.1 Low HTC at Position 2 in PASCAL Experiment

Given that the heat transferred from the tube-side by the steam condensation decreases along the tube length, it is expected that the nucleate boiling HTC might be highest at the tube inlet region. However, in PASCAL experiment, it is observed that the local HTC at position 2 is significantly smaller than that at positions 3, 4, and 5 and it is slightly larger than the local HTC at position 7 (see Fig. 3.8(b)). This is possibly because the forced convection effect from the lower part of the U-tube does not appear at position 2 due to the following reasons: (1) The HTC at position 2 may be influenced by the effect of gravity-induced natural convection flow due to the heat transfer from position 10. Since the condensation heat transfer decreases along the tube length, the heat transfer at position 10 is lower than those at positions 7, 8, and 9. Consequently, the gravity-induced natural convection flow generated from the position 10 may be significantly low. (2) The position 2 is located close to the PCCT wall. Due to the wall friction, the gravity-induced natural convection velocity from the lower part of U-tube may decreases. (3) The distance between the positions 2 and 10 is further than that between the positions 5 and 7. Hence, the effect from the lower part of U-tube is relatively small at position 2. (4) In the PCCT, due to the buoyancy, the heated water rose up and the natural circulation occurred in clockwise direction (Cho et al., 2014) as shown in Fig. 3.20. While there is uncertainty, the gravity-induced natural convection flow from the lower part of U-tube might not pass the position 2. At this point, the position 2 might be under the vortex flow as shown in Fig.

3.20 because the width of PCCT is quite narrow and the position 2 is located near the curved region of the U-tube.

For reasons mentioned above, this author assumed that the HTC at position 2 is not influenced by the effect of gravity-induced natural convection flow from the lower part of U-tube and then predicted the HTC at position 2 using the subcooled nucleate pool boiling correlation developed for the lower part of U-tube. The calculated results showed good agreement with the experimental data (see Fig. 3.12).

3.9.2 Applicability of Proposed Boiling Model to Bundle HX in PAFS

The HX of prototype PAFS consists of 3×20 U-shaped tube bundles as shown in Figs. 1.3 and 3.21. In the bundle HX, a bundle effect, which increases the heat transfer compared to the single tube, occurs as one of the key heat transfer mechanisms. However, the proposed boiling model was developed based on the data of single U-shaped tube of PASCAL corresponding to the unit HX of the bundle HX in PAFS and so the bundle effect was not reflected in the proposed model. Therefore, the proposed model may under-predict the boiling heat transfer in the bundle HX of PAFS.

In order to confirm the applicability of the proposed model to the bundle HX of the prototype PAFS, it is required to investigate the main flow direction near the HX bundle because the magnitude of the bundle effect is closely linked with the number of tube under the flow direction. In PAFS, near the bundle HX, a multi-dimensional flow occurs. If a lateral flow is dominant against the HX as shown in (1) of Fig. 3.21, the bundle effect might be large but if a vertical flow is

dominant as shown in (2) of Fig. 3.21, the bundle effect might be small. To investigate the bundle effect in PAFS, this study simulated the TH phenomena in the PCCT of the prototype PAFS.

Figure 3.22 shows the top view of bundle HX layout in PCCT. For the region marked with the red line, 3D simulation was performed with MARS MULTID. Figure 3.23 qualitatively shows the 3D simulation results for the flow velocity field in PCCT. It is found that the main flow direction is vertical to the bundle HX. Given that the PAFS has three tubes bundle in vertical row (see Fig. 1.3), the bundle effect may not be relatively large in the PAFS. Therefore, it is concluded that the proposed model can be applied to predict the nucleate boiling HTC in HX of PAFS.

However, for the optimum design of the HX in various passive safety systems, a direct application of the proposed model to the tube bundles is still limited. To supplement the proposed model and to obtain a reliable HTC in the bundle HX, the following approach may be effective. In relation to the bundle effect, a simple method for estimating bundle boiling coefficients has been presented by Palen (1983). In the method, the bundle effect was considered by introduction of the bundle boiling factor, which acted as a multiplier for the nucleate boiling HTC, determined by the experimental data. Up to now, the bundle effect has not been investigated systematically to relate the single U-shaped tube heat transfer to the heat transfer of a U-shaped tube in a bundle, and the available experimental data is extremely limited. Throughout the further research of the bundle effect in the passive safety system, if the bundle boiling factor can be deduced as suggested by Palen (1983) and consequently it is applied to the proposed model, the optimum design of the passive safety system with the BE code may be possible.

Table 3.1 Main nucleate pool boiling correlations

1	Rohsenow (1952)
	$h = \frac{1}{C_{sf}} \frac{C_{p,l} q''^{0.67}}{h_{fg}^{0.67}} \left(\frac{1}{\mu_l} \sqrt{\frac{\sigma}{g(\rho_l - \rho_v)}} \right)^{-0.33} Pr_l^{-1}$ (where $C_{sf} = 0.013$)
2	Forster and Zuber (1955)
	$h = 0.00122 \left[\frac{k_l^{0.79} C_{p,l}^{0.45} \rho_l^{0.49}}{\sigma^{0.5} \mu_l^{0.29} h_{fg}^{0.24} \rho_v^{0.24}} \right] (T_w - T_{sat})^{0.24} \Delta P_{sat}^{0.75}$
3	Mostinski (1963)
	$h = 0.00417 q''^{0.7} P_c^{0.69} F_p$ (where $F_p = 1.8 P_r^{0.17} + 4 P_r^{1.2} + 10 P_r^{10}$; $P_c\,[kPa]$)
4	Stephan and Abdelsalam (1980)
	$h = 0.246 \times 10^7 \left(\frac{D_b^{-0.967} T_{sat}^{0.587} q''^{0.673} C_{p,l}^{0.62} k_l^{0.967} (\rho_l - \rho_v)^{5.22}}{h_{fg}^{1.58} \rho_l^{5.86}} \right)$ (where $D_b = 0.0146 \times 45 \left(\frac{2\sigma}{g(\rho_l - \rho_v)} \right)^{0.5}$)
5	Cooper (1984)
	$h = 55 P_r^{0.12 - 0.21 log_{10} R_p} (-log_{10} P_r)^{-0.55} M^{-0.5} q''^{0.67}$
6	Gorenflo (1993)
	$h = 5600 F_{PF} \left(\frac{q''}{20000} \right)^{nf}$ (where $F_{PF} = 1.73 P_r^{0.27} + \left(6.1 + \frac{0.68}{1 - P_r} \right) P_r^2$; $nf = 0.9 - 0.3 P_r^{0.15}$)
7	Cornwell and Houston (1994)
	$h = 9.7 P_c^{0.5} F_p \left(\frac{q'' D}{\mu_l h_{fg}} \right)^{0.67} Pr_l^{0.4} \left(\frac{k_l}{D} \right)$ (where $h \left[kW/m^2 K \right]$; $h_{fg} \left[kJ/kg \right]$; $k_l \left[kW/mK \right]$; $q'' \left[kW/m^2 \right]$)

Table 3.2 Main forced convective boiling correlations (1/2)

1	Chen (1966)
	$h = Sh_{npb} + Fh_l$ (where $S = \dfrac{1}{1 + 2.53 \times 10^{-6} Re_{TP}^{1.17}}$ (where $Re_{TP} = Re_l F^{1.25}$); h_{npb} : Forster-Zuber correlation; $F = 1 \quad for\ X_{tt}^{-1} \le 0.1$ $= 2.35\left(0.213 + X_{tt}^{-1}\right)^{0.736} \quad for\ X_{tt}^{-1} > 0.1$; $h_l = 0.023 Re_l^{0.8} Pr_l^{0.4} \left(\dfrac{k_l}{D}\right)$)
2	Polley et al. (1980)
	$h = Sh_{npb} + Fh_l$ (where $S = 1.0$; h_{npb} : Forster-Zuber correlation; $F = \left(\dfrac{1}{1-\alpha_v}\right)^{0.744}$; $h_l = exp\left[-0.186 + 0.338 ln\, Re_l + 0.362 ln\, Pr_l + 0.0131\left(ln\, Re_l\right)^2 - 0.00926\left(ln\, Pr_l\right)^2\right]$)
3	Singh et al. (1985)
	$h = \left(1 + \dfrac{0.4 u_l}{u_{su}}\right)^{0.67} h_{npb} + h_l$ (where $u_{su} = \dfrac{q''}{\rho_v h_{fg}}$; h_{npb} : Rohsenow correlation; $h_l = \left[0.35 + 0.56\left(\dfrac{GD}{\mu_l}\right)^{0.56}\right] Pr_l^{0.3} \left(\dfrac{k_l}{D}\right)$)
4	Hwang and Yao (1986) – Single tube
	$h = Sh_{npb} + Fh_l$ (where $S = \dfrac{k_l}{Fh_l Y}\left[1 - exp\left(\dfrac{Fh_l Y}{k_l}\right)\right]$ (where $Y = 0.041\left(\dfrac{\sigma}{g\left(\rho_l - \rho_v\right)}\right)^{0.5}$); $h_{npb} = 0.224 q''^{0.67}$ (where $h_{npb}\ \left[kW/m^2K\right]$; $q''\ \left[kW/m^2\right]$); F : Polley et al relation; $h_l = 0.21 Re_l^{0.62} Pr_l^{0.38} \left(\dfrac{Pr_l}{Pr_w}\right)^{0.25} \left(\dfrac{k_l}{D}\right)$)

Table 3.2 Main forced convective boiling correlations (2/2)

5	Hwang and Yao (1986) – Bundle
	$h = Sh_{npb} + Fh_l$ (where $h_{npb} = 0.2086q''^{0.75}$, $h_l = 0.366Re_l^{0.6}Pr_l^{1/3}\left(\frac{k_l}{D}\right)$)
6	Webb and Chien (1994)
	$h = \left[h_{nb}^3 + h_{cv}^3\right]^{1/3} = \left[\left(Sh_{npb}\right)^3 + \left(Fh_l\right)^3\right]^{1/3}$ (where $S = 1.0$; h_{npb}: Forster-Zuber correlation; $F = \left(\phi_l^2 \frac{Pr_l + 1}{2}\right)^{0.346}$ where $\phi_l^2 = 1 + \frac{8}{X_{tt}} + \frac{1}{X_{tt}^2}$; $h_l = 0.27Re_l^{0.63}Pr_l^{0.36}\left(\frac{Pr_l}{Pr_w}\right)^{0.25}\left(\frac{k_l}{D}\right)$)
7	Gupta et al. (1995)
	$h = h_{npb} + h_l$ (where $h_{npb} = 13.035\left(T_w - T_s\right)^{2.881}$; $h_l = \left(0.4Re_l^{1/2} + 0.06Re_l^{2/3}\right)Pr^{0.36}\left(\frac{\mu_l}{\mu_v}\right)^{0.25}\left(\frac{k_l}{D}\right)$)
8	Shah (2005)
	$h = \psi\left(\frac{T_w - T_{sat}}{T_w - T_b}\right)h_l$ where $h_l = 0.21Re_l^{0.62}Pr_l^{0.4}$; $For\ high\ subcooling\left(St < 38Pe^{-0.38}\ \ or\ \ Bo < 2.5\times10^{-4}\right),\ \ \psi = \psi_0 + \frac{T_{sat} - T_b}{T_w - T_{sat}}$ $For\ low\ subcooling,\ \ \psi = \psi_0$ $Bo \le 0.01,\quad \psi_0 = 1 + \frac{Bo}{0.000216 + 0.041Bo - 1.53Bo^2}$ $Bo > 0.01,\quad \psi_0 = 443Bo^{0.65}$

Table 3.3 Geometrical data of ATLAS-PAFS and PASCAL facilities

Parameter		**PASCAL (Single tube)**	**ATLAS-PAFS (3 tubes)**
PCHX	Inner / Outer diameter	50.8 mm / 44.8 mm	36.8 mm / 30.8 mm
	Length	8.4 m	4.77 m
PCCT	Width	0.112 m	0.34 m
	Length	6.7 m	5.065 m
	Height	11.5 m	6.5 m

Table 3.4 Subcooling test conditions of PASCAL (SS-540-P1)

No	Pool Temperature [K]	Tube Inlet Pressure [bar]	Tube Inlet Flow Rate [kg/s]
1	310	13.16	0.1869
2	320	10.69	0.155
3	330	12.98	0.1744
4	340	17.67	0.2073
5	350	24.66	0.2499
6	360	29.87	0.2783
7	370	31.74	0.2874

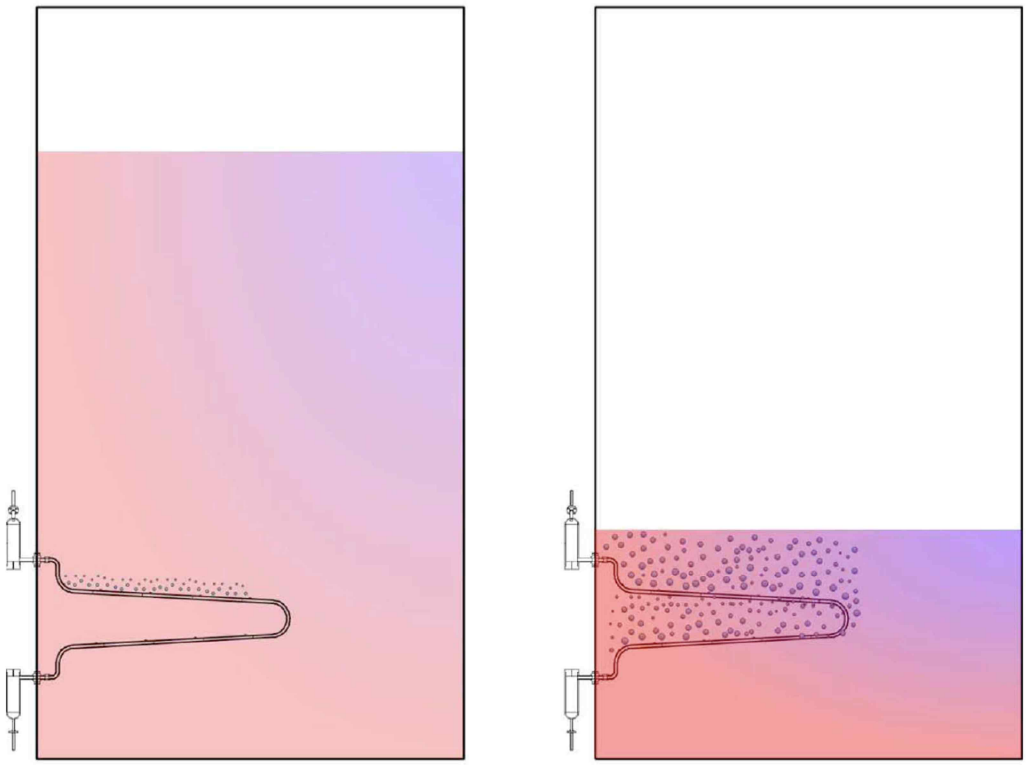

Figure 3.1 Boiling heat transfer phenomena in PCCT (Kang et al., 2012)

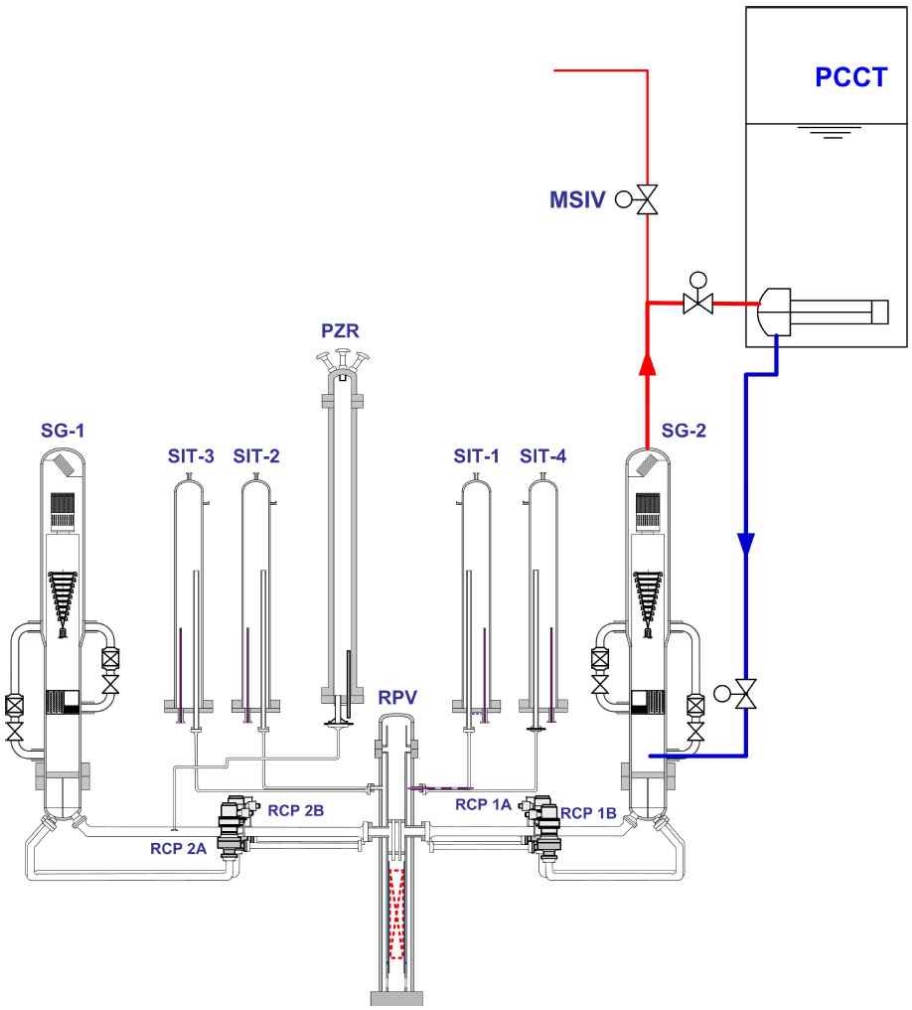

Figure 3.2 Schematic diagram of ATLAS-PAFS (KAERI, 2012)

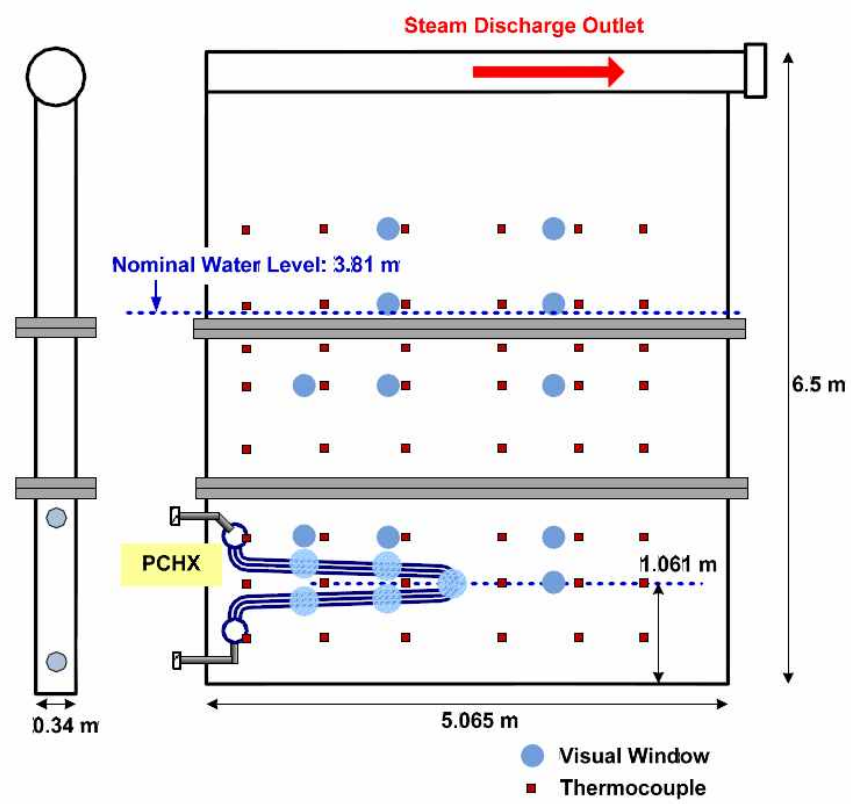

Figure 3.3 PCCT and measurement points of ATLAS-PAFS (Bae et al., 2014)

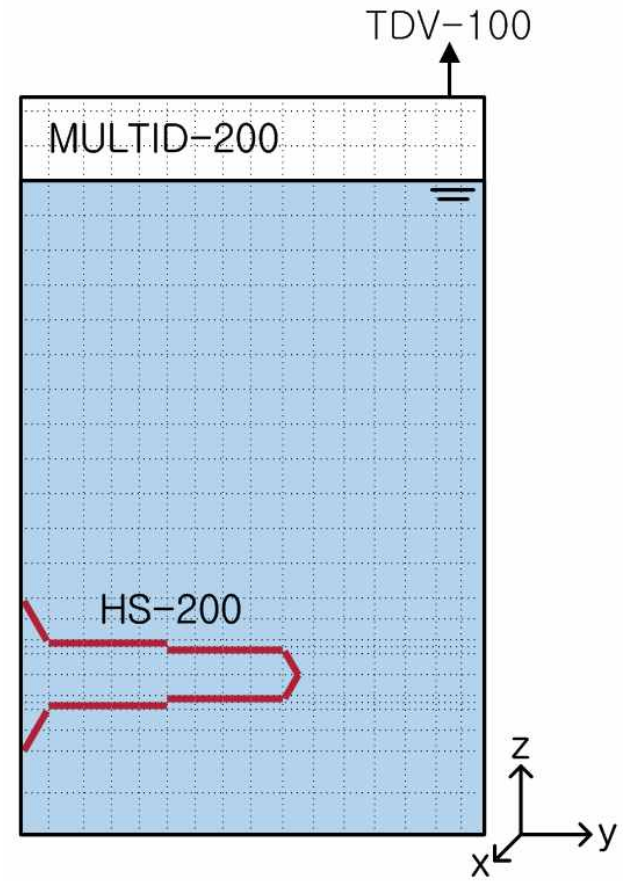

Figure 3.4 MARS nodalization of PASCAL experiment

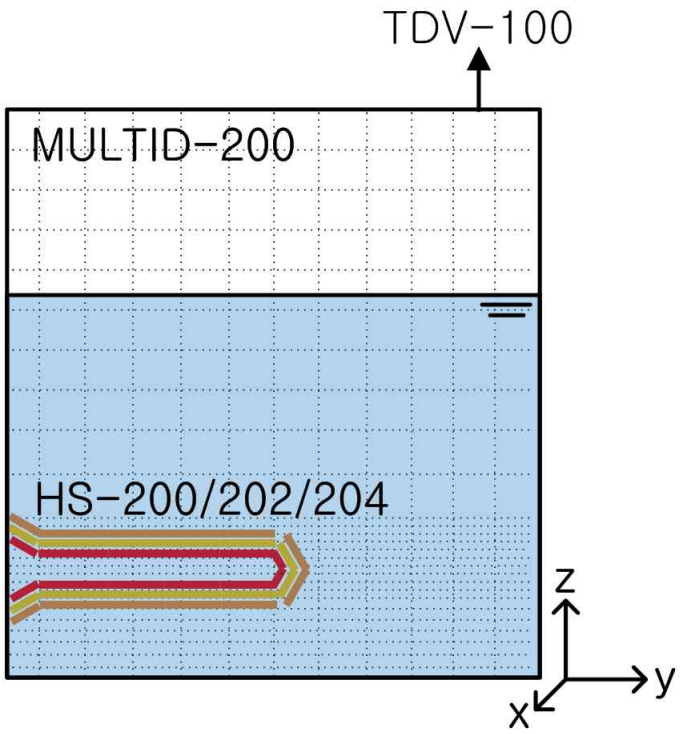

Figure 3.5 MARS nodalization of ATLAS-PAFS experiment

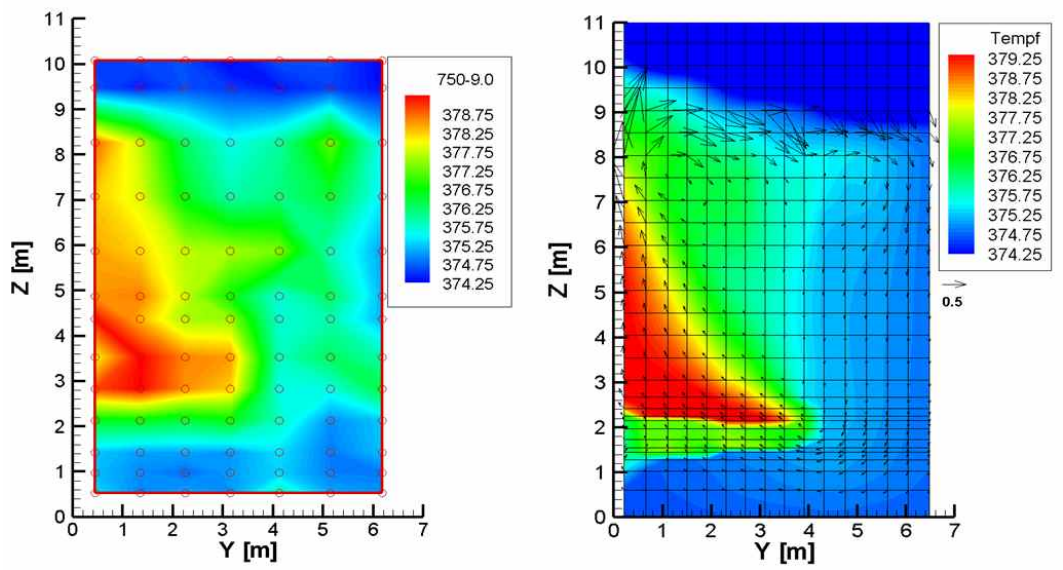

(a) Experiment (b) MARS

Figure 3.6 Comparison of temperature contour between experimental data and MARS prediction

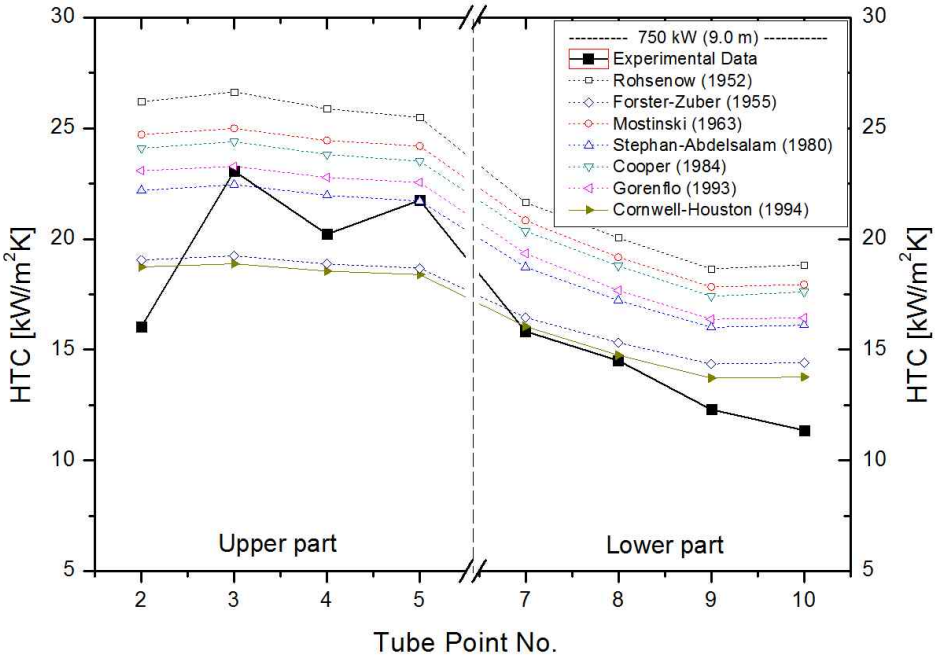

(a) Pool boiling correlations

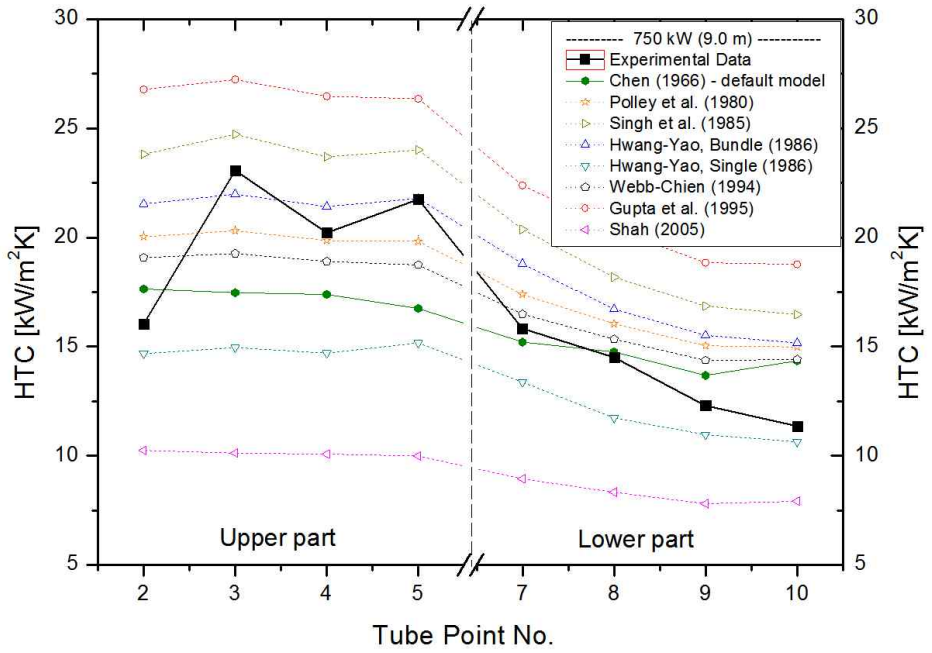

(b) Forced convection boiling correlations

Figure 3.7 Assessment results of previous nucleate boiling models

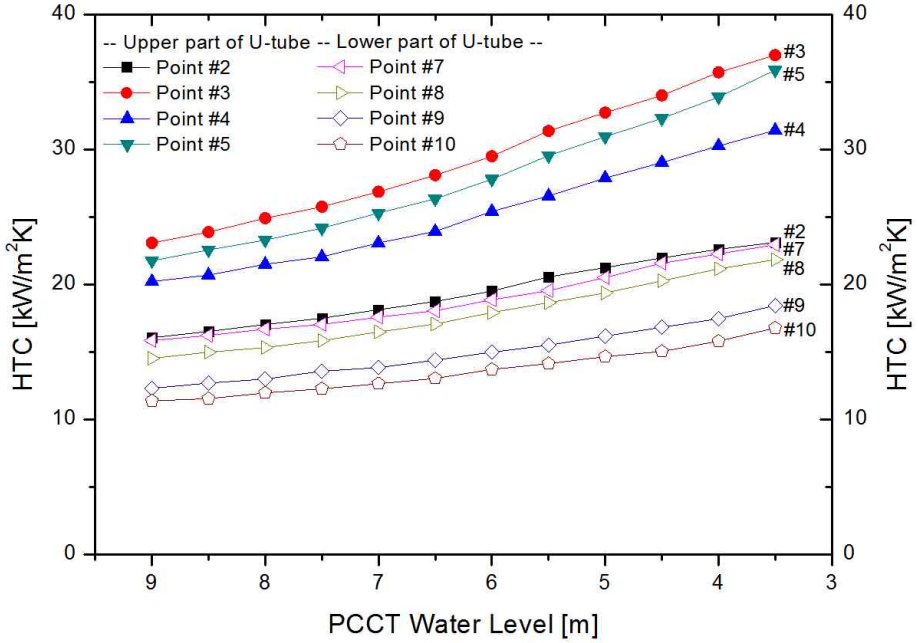

(a) Local HTCs for PCCT water level

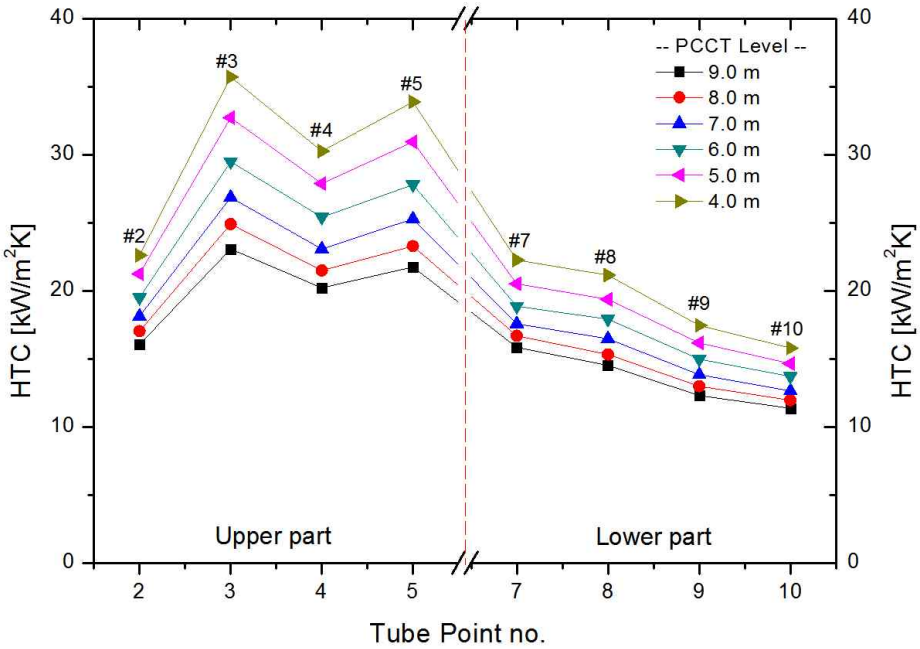

(b) Local HTCs at each measurement point

Figure 3.8 Experimental HTCs on U-shaped tube (PASCAL, SG power 750 kW)

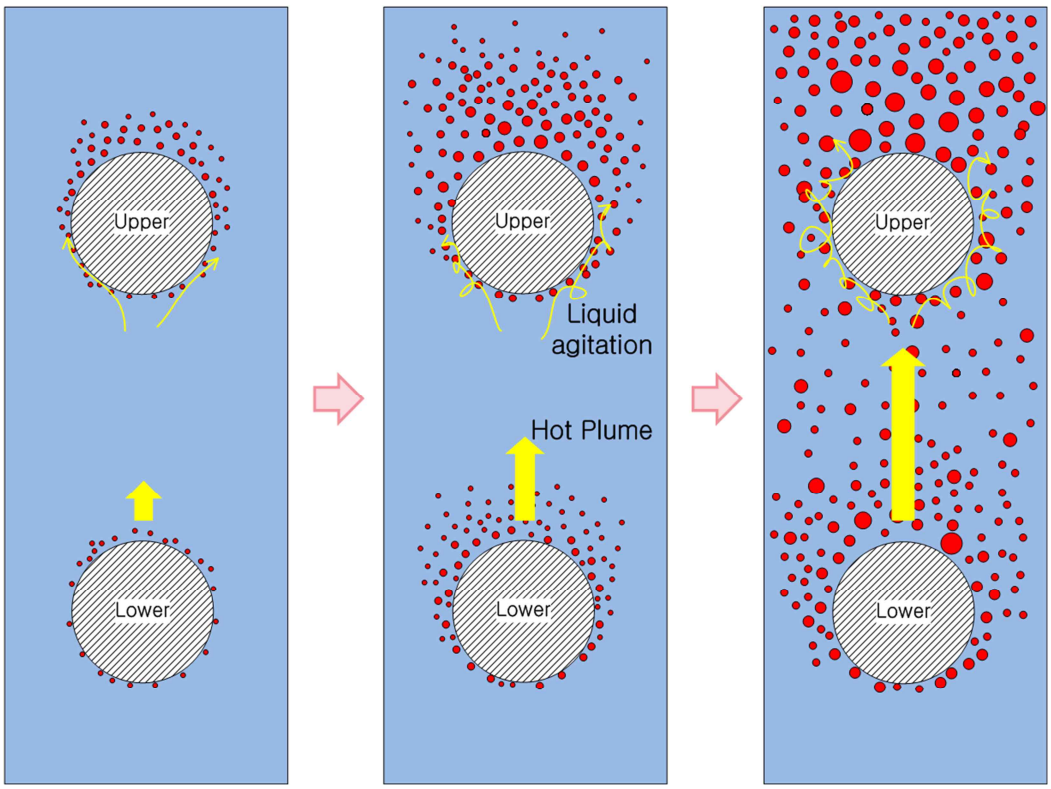

Figure 3.9 Heat transfer mechanism

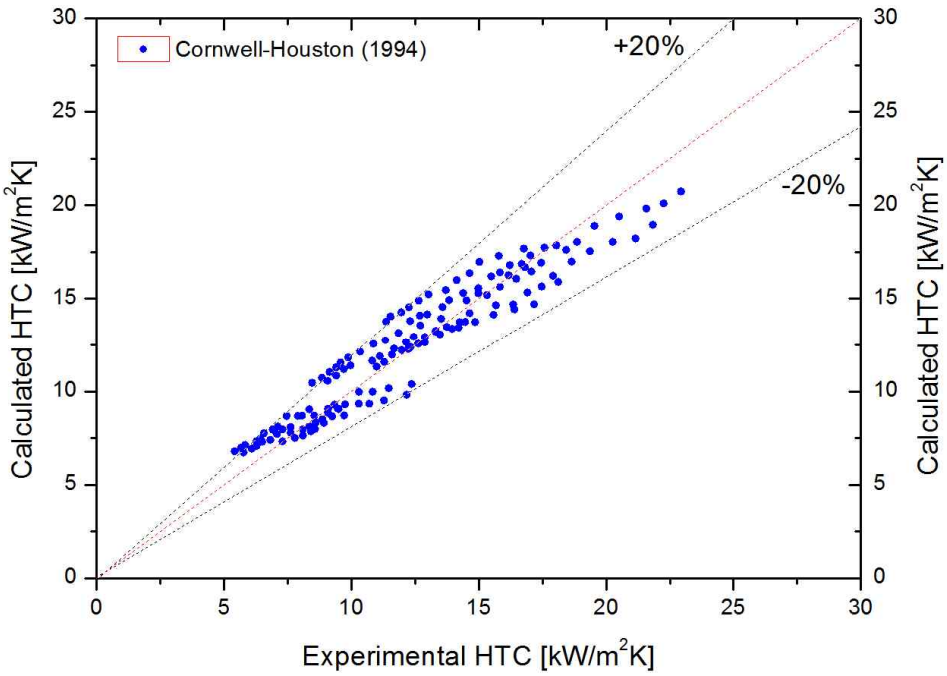

Figure 3.10 Comparison of calculated HTCs with experimental HTCs on lower part of U-tube in PASCAL

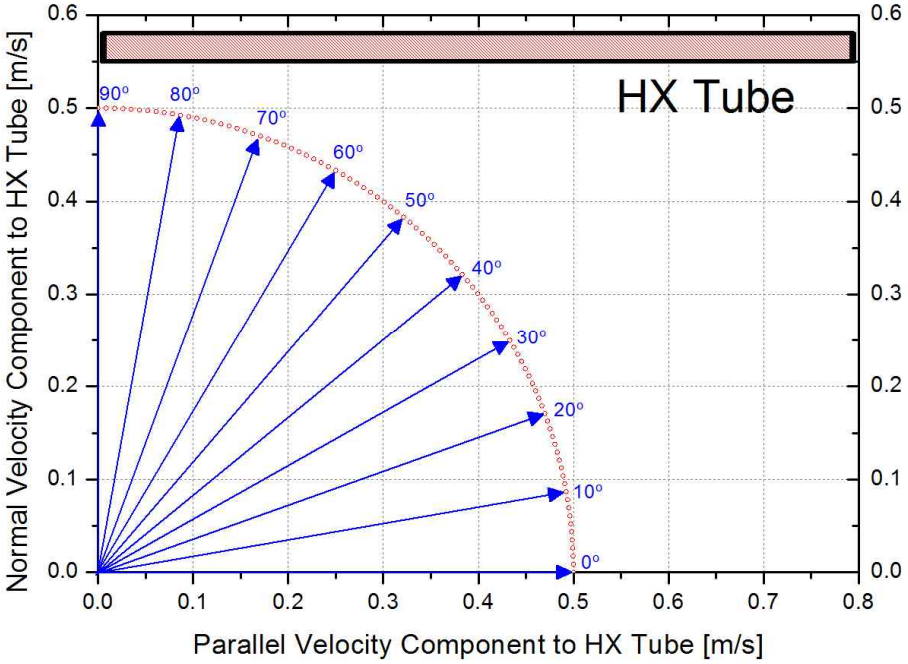

Figure 3.11 Velocity components in inclined flow at flow speed of 0.5 m/s

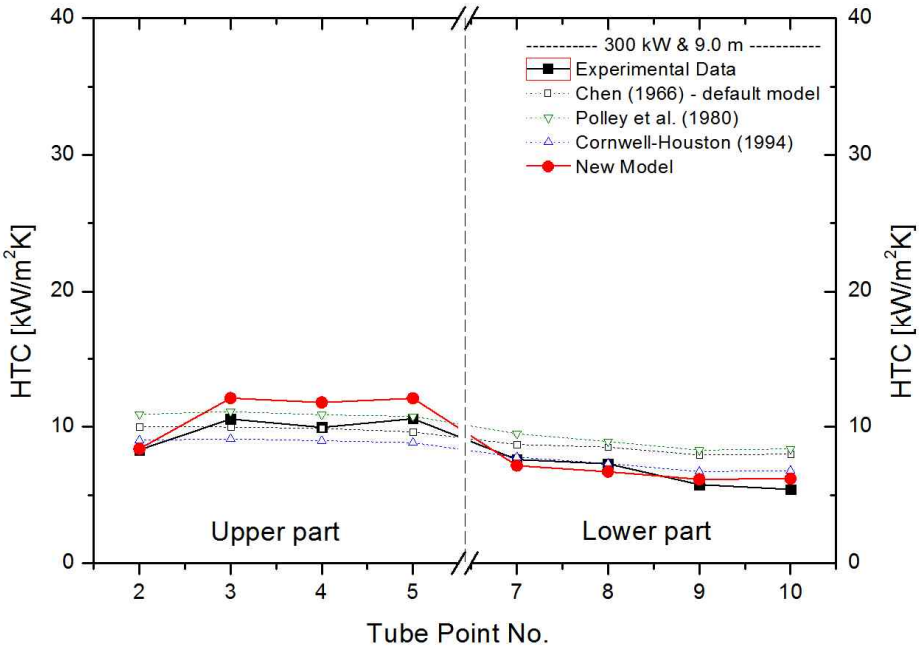

(a) SG power 300 kW and PCCT level 9.0 m

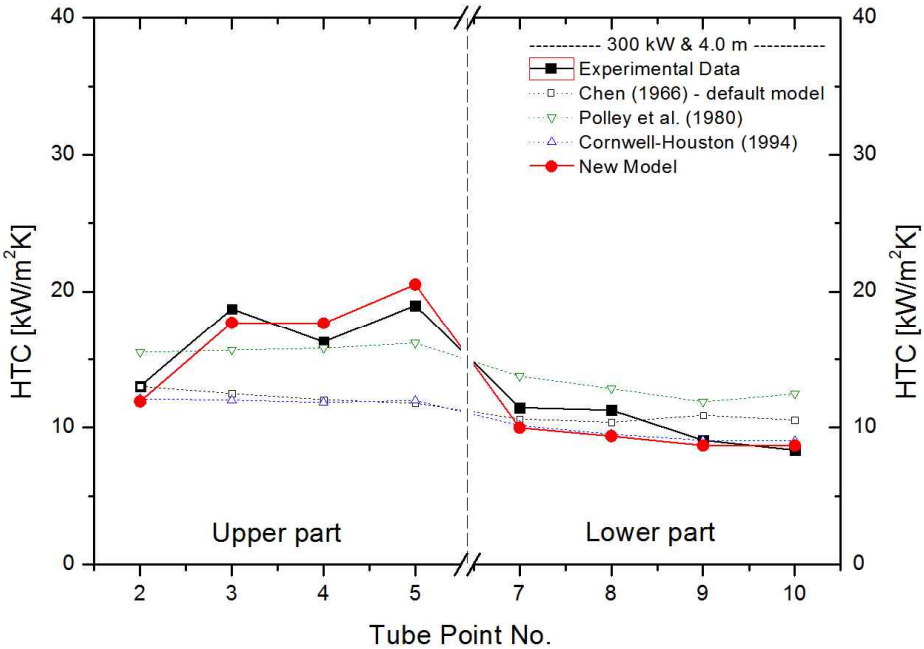

(b) SG power 300 kW and PCCT level 4.0 m

Figure 3.12 Comparison of MARS predictions with experimental HTCs (1/3)

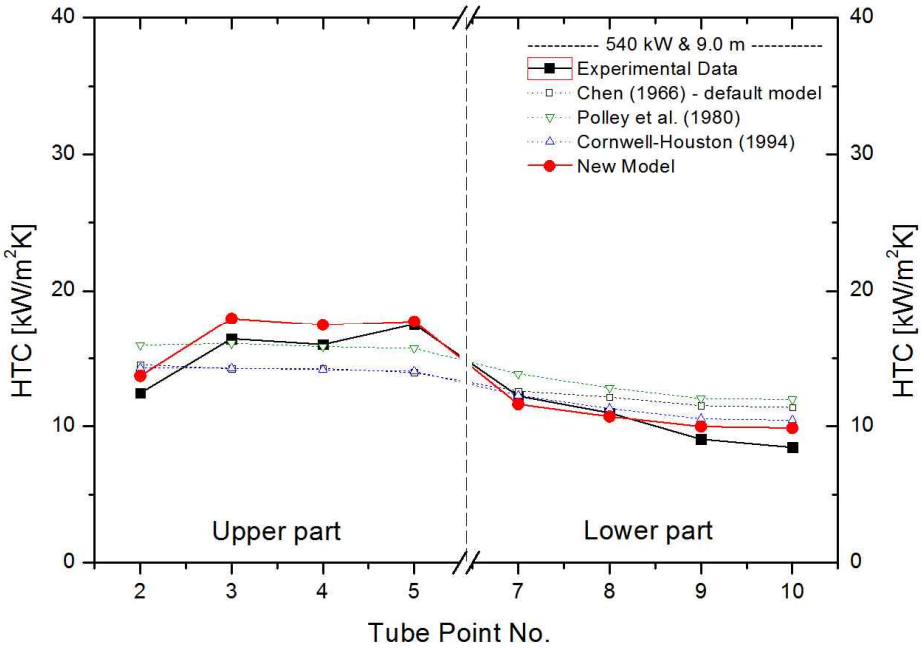

(c) SG power 540 kW and PCCT level 9.0 m

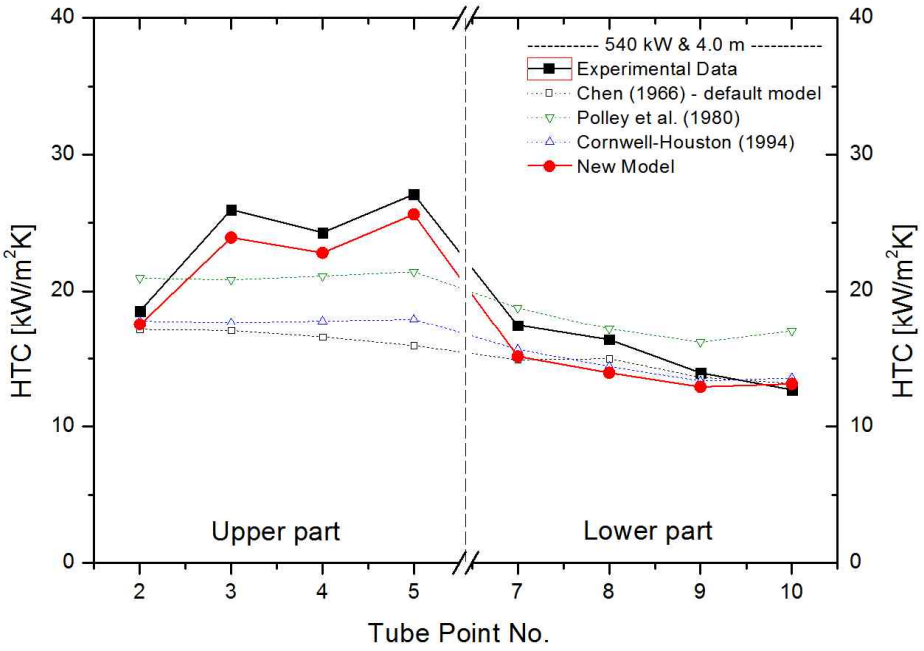

(d) SG power 540 kW and PCCT level 4.0 m

Figure 3.12 Comparison of MARS predictions with experimental HTCs (2/3)

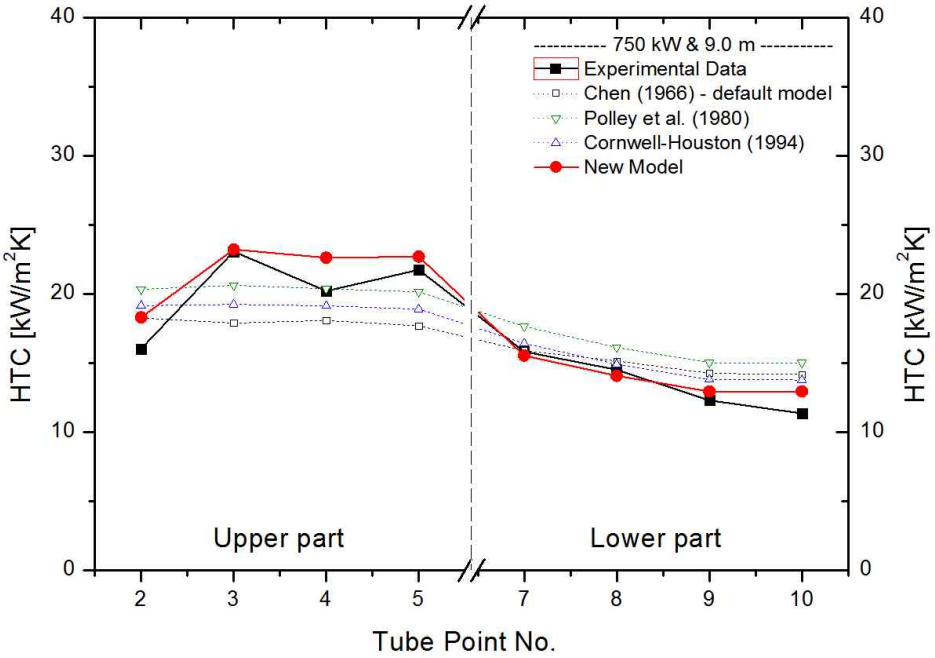

(e) SG power 750 kW and PCCT level 9.0 m

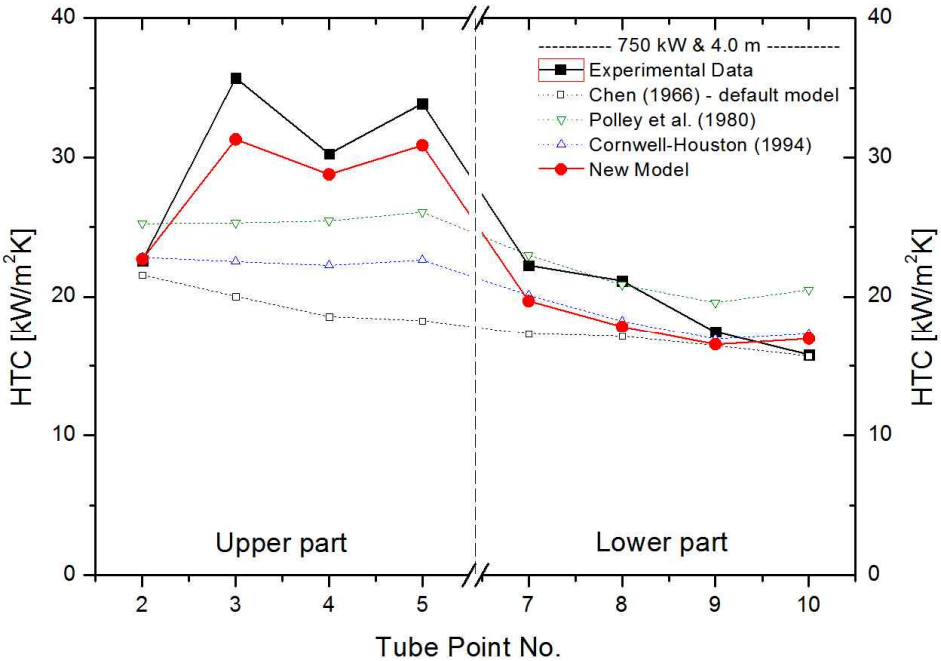

(f) SG power 750 kW and PCCT level 4.0 m

Figure 3.12 Comparison of MARS predictions with experimental HTCs (3/3)

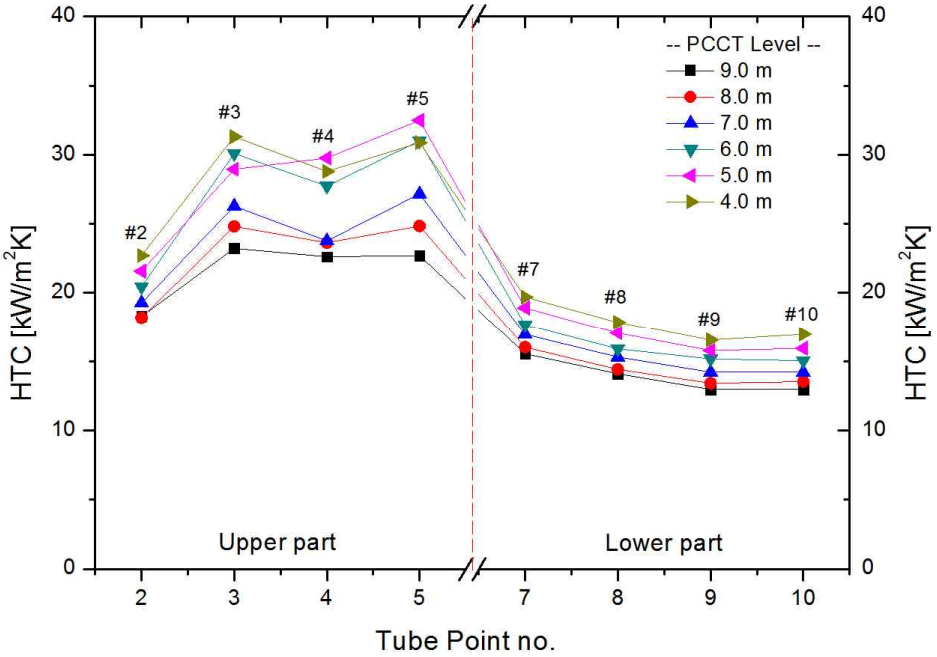

Figure 3.13 MARS predictions for local HTCs (PASCAL, SG power 750 kW)

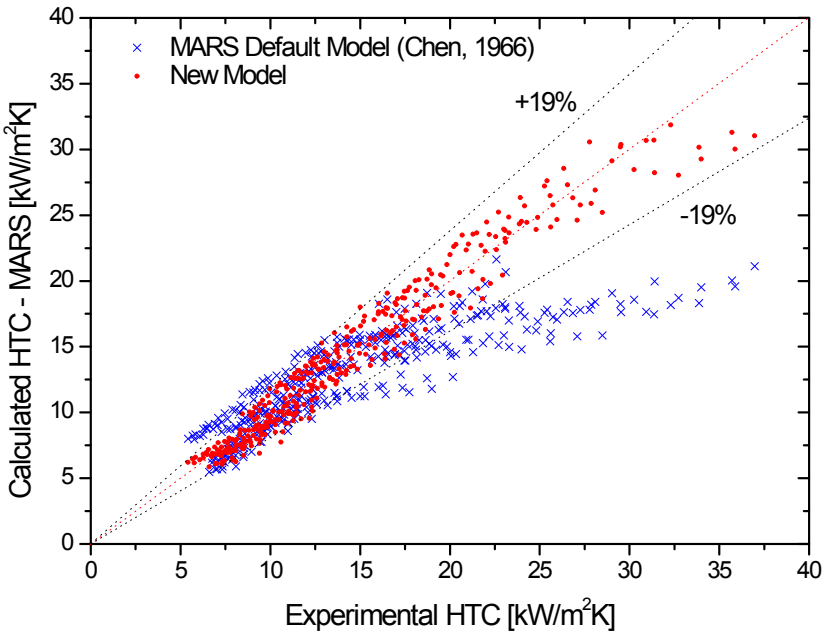

Figure 3.14 Comparison of MARS predictions with experimental HTCs for PASCAL and ATLAS-PAFS

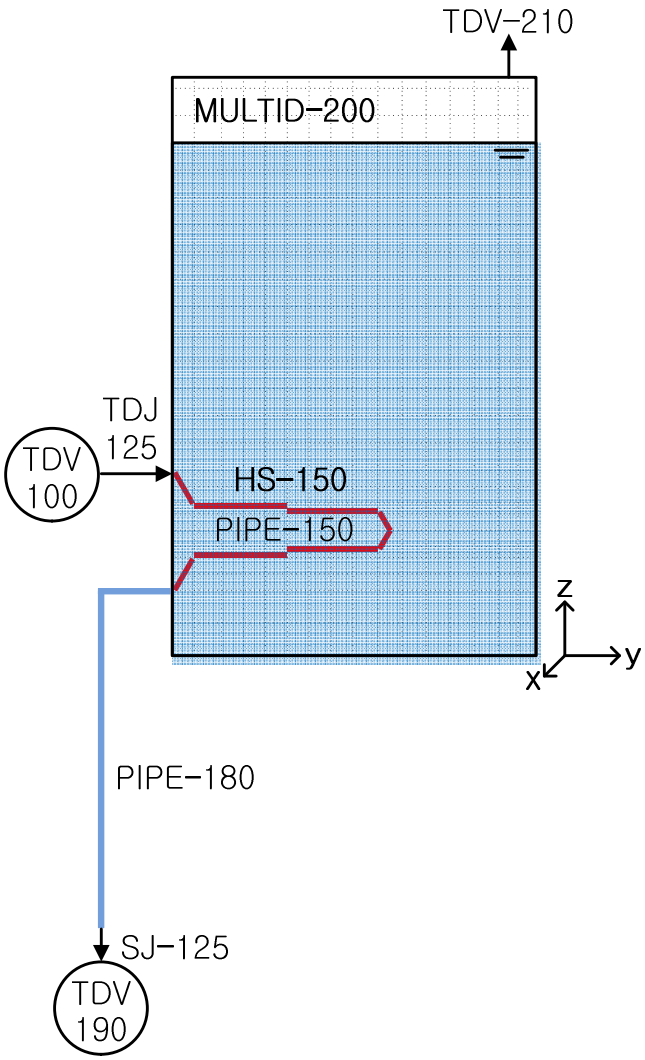

Figure 3.15 MARS nodalization of PASCAL

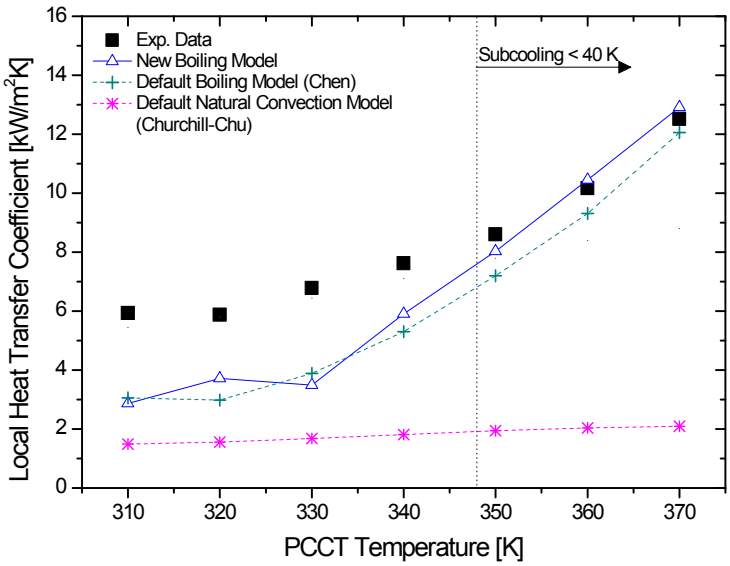

(a) Upper part of U-tube (Position 3)

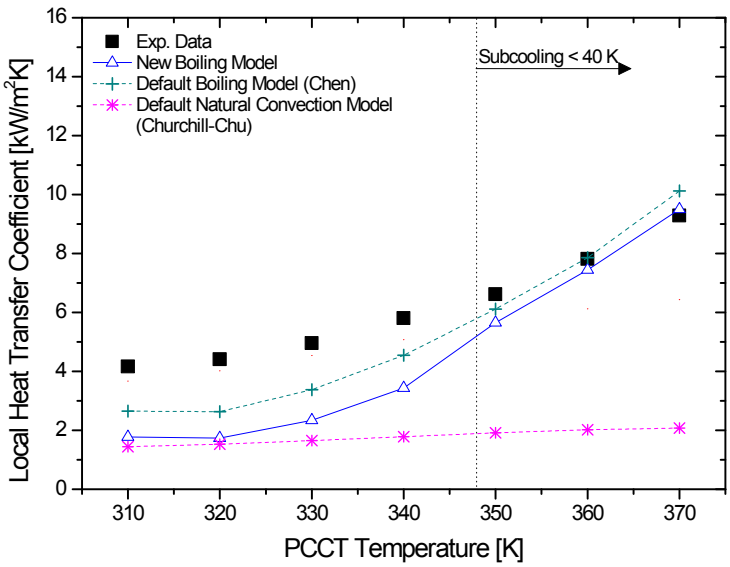

(b) Lower part of U-tube (Position 7)

Figure 3.16 Local HTCs of PASCAL – Assessment

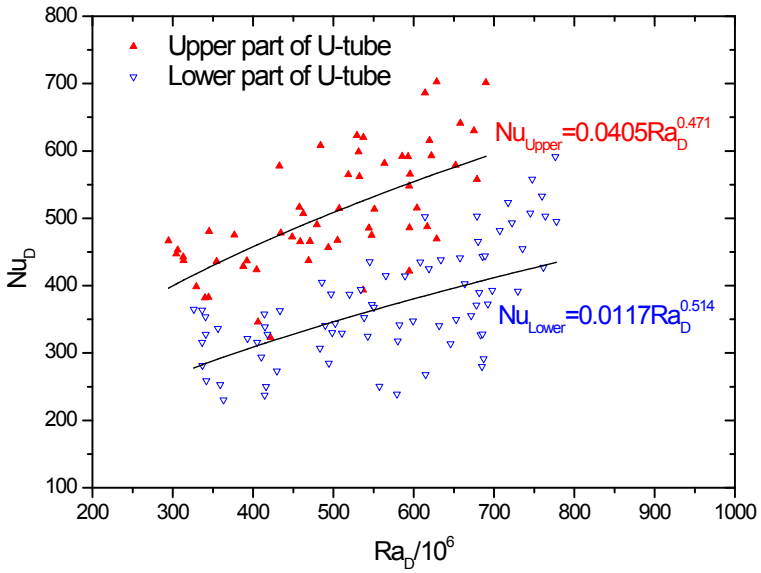

Figure 3.17 New natural convection correlations

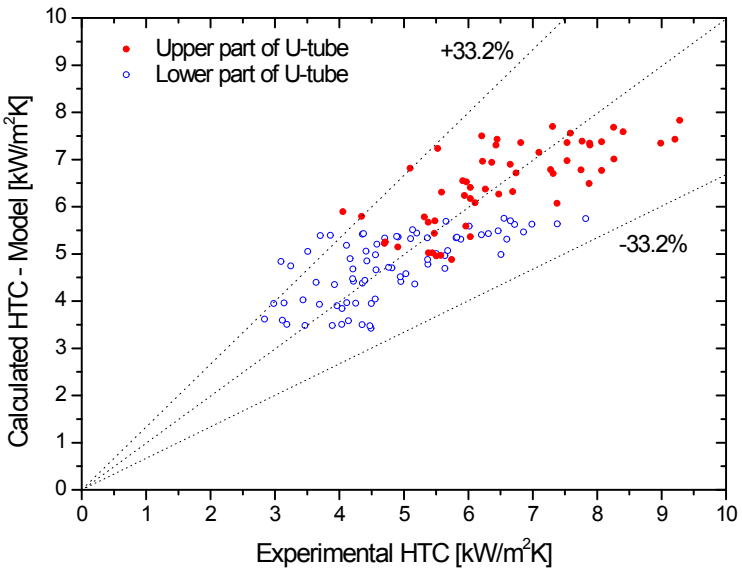

Figure 3.18 Comparison of calculated HTCs with experimental HTCs

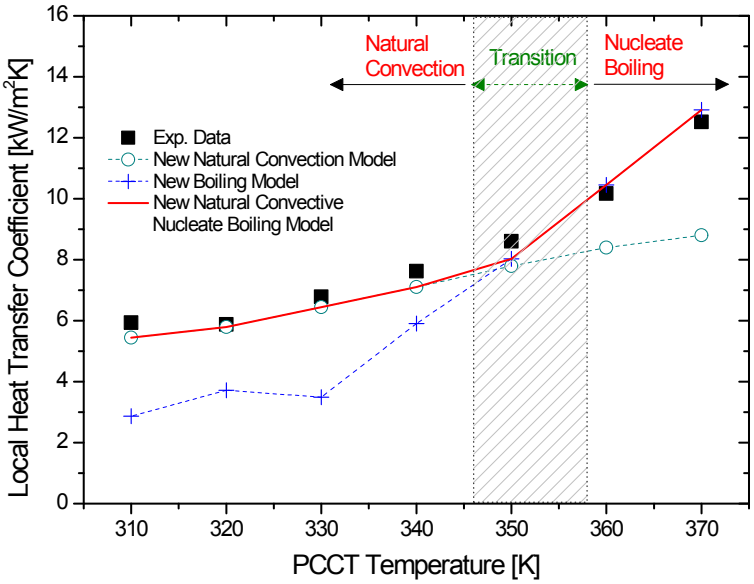

(a) Upper part of U-tube (Position 3)

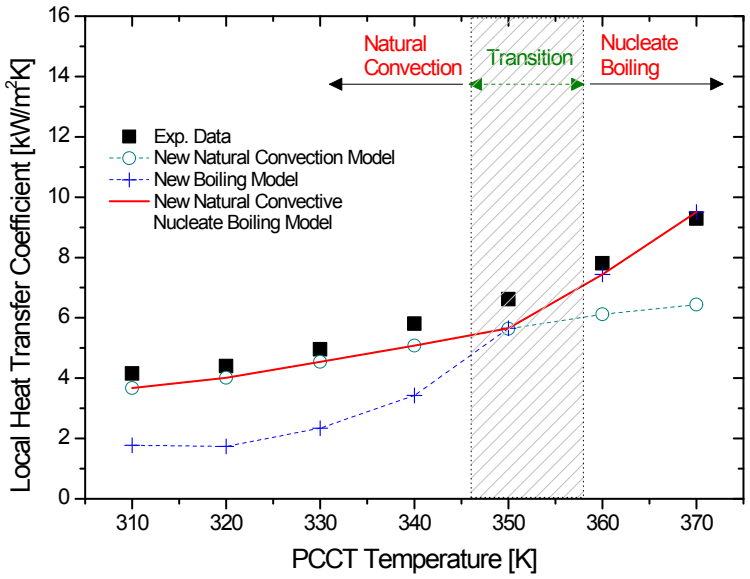

(b) Lower part of U-tube (Position 7)

Figure 3.19 Local HTCs of PASCAL - New model

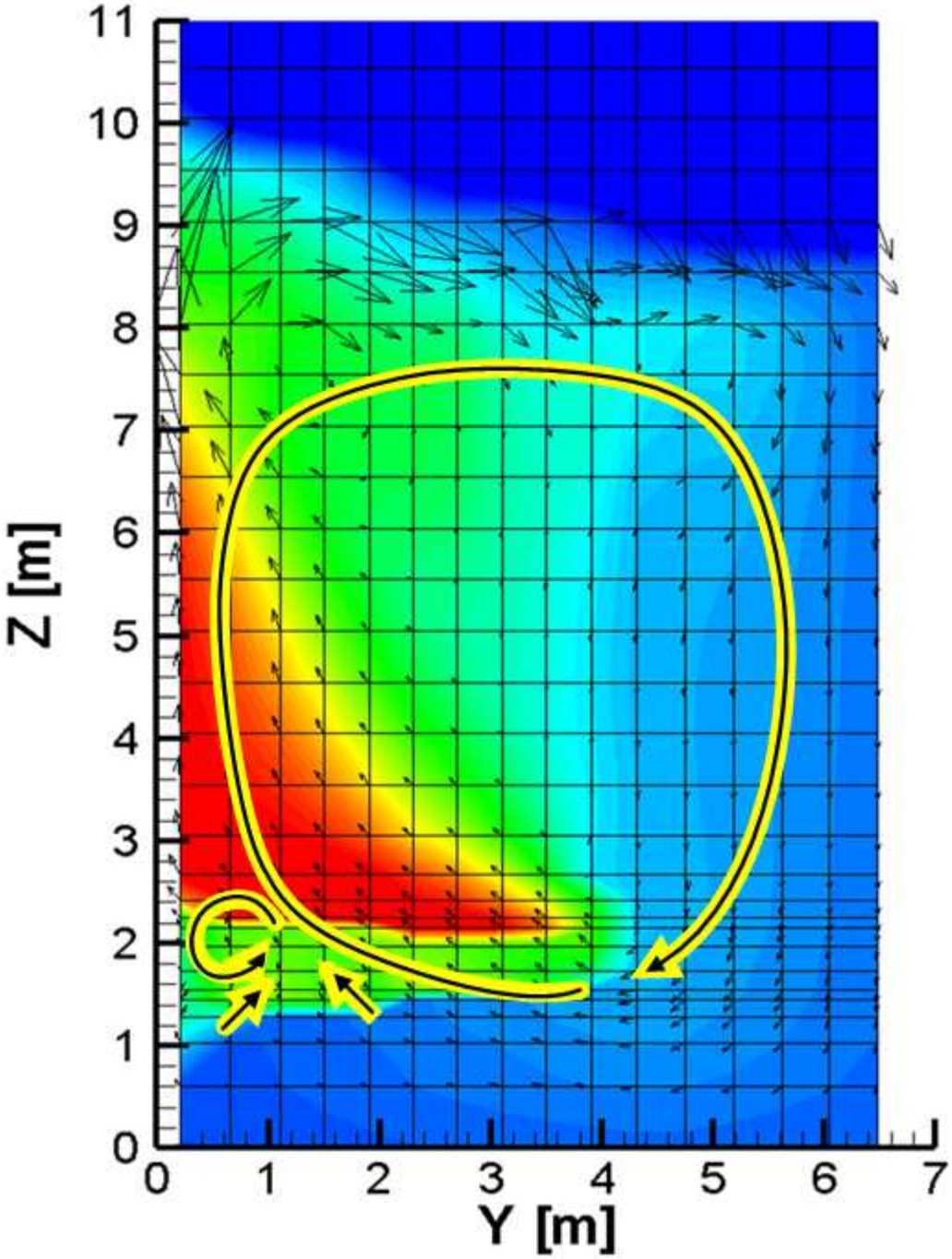

Figure 3.20 Predicted flow velocity field in PCCT of PASCAL experiment

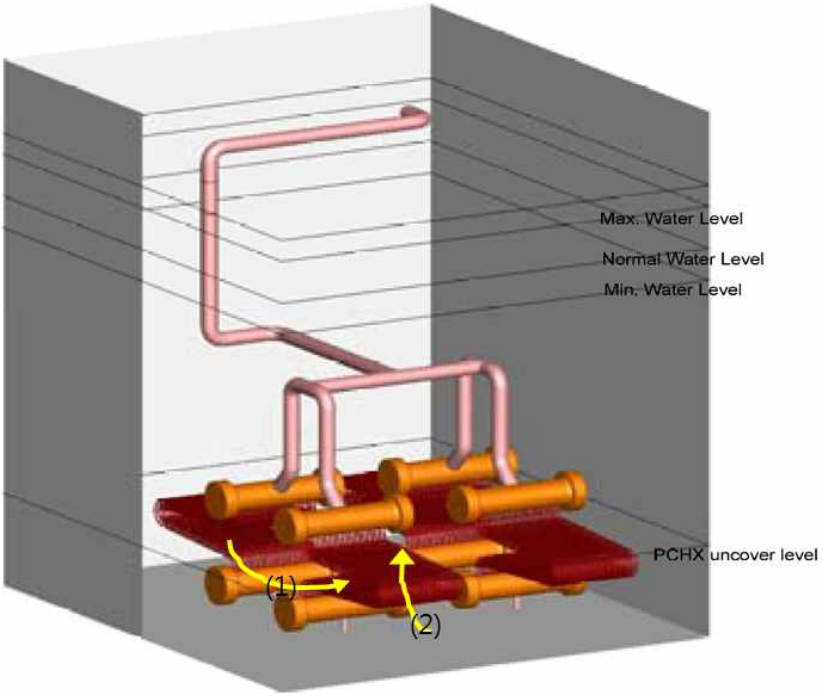

Figure 3.21 Multi-dimensional flow near bundle HX of PAFS (Choi et al., 2011)

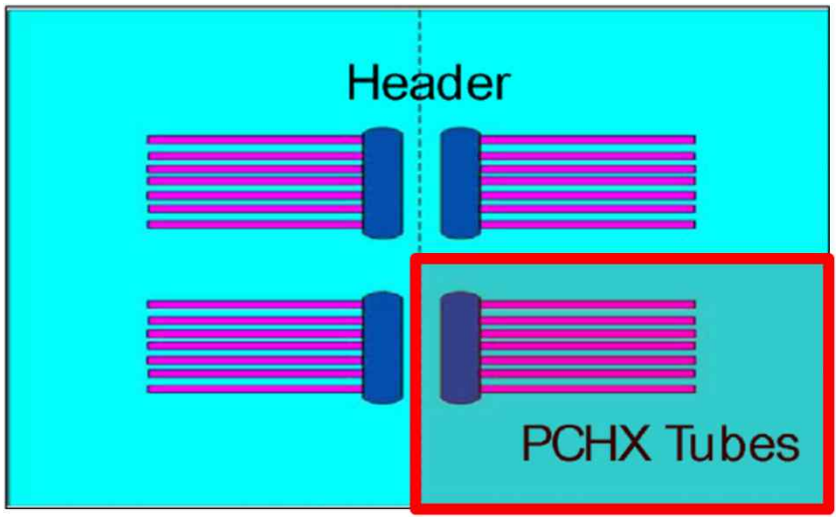

Figure 3.22 Top view of bundle HX layout in PCCT (Kim et al., 2013)

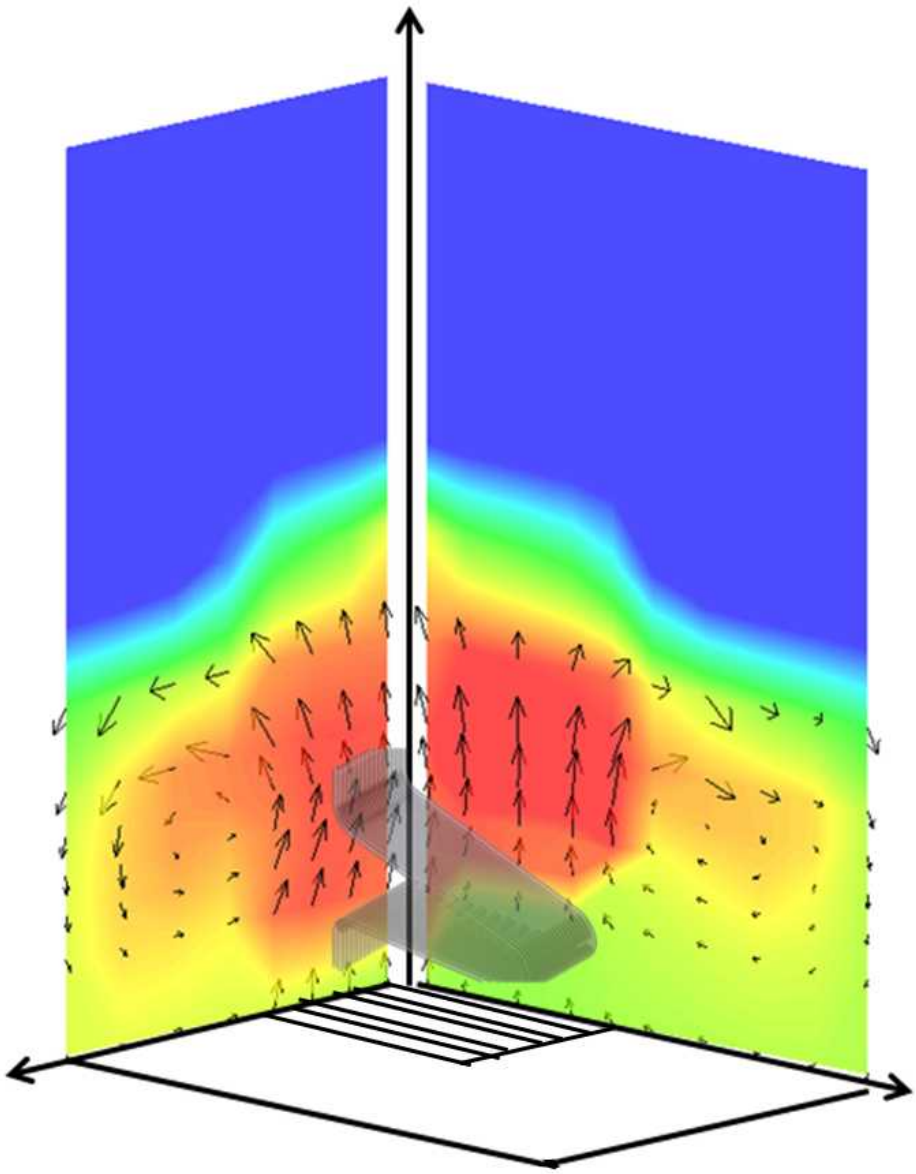

Figure 3.23 3D simulation results for flow velocity field in PCCT

Chapter 4

Validation of Heat Transfer Model for Horizontal U-Shaped HX Submerged in Pool

This study developed the heat transfer model package for the horizontal U-shaped HX submerged in the pool by combining the horizontal in-tube condensation model (see Chapter 2.5.3) and the natural convective nucleate boiling model (see Chapter 3.8.4). This heat transfer model package is implemented to the MARS code. This modified version of MARS is renamed as MARS/PAFS. This section describes the validation results of MARS/PAFS against three passive safety system-related experimental data of PASCAL (Kang et al., 2012; Kim et al., 2013; Bae et al., 2013), ATLAS-PAFS (Kang et al., 2012; Bae et al., 2014), and NOKO (Schaffrath and Prasser, 1998).

4.1 Validation for PASCAL Experiment

4.1.1 MARS Modeling of PASCAL Experiment

For the PASCAL experiment, the validation of MARS/PAFS was performed

through three items: (a) HX heat removal performance, (b) local HTCs, and (c) quasi-steady state system pressure. The heat removal performance, or the HX capacity, is the most important parameter in terms of the NPP safety analysis. The local heat transfer rate is the critical parameter considered in the optimum design of the HX. The quasi-steady state system pressure is the crucial indicator to show the HX heat removal performance through the system cooling.

For the validation of each item, two nodalization schemes were used. In approach 1 (see Fig. 3.15), the SG was not modeled to investigate the HX heat removal performance and the local HTCs. The inlet and outlet of the PCHX is modeled as boundary conditions to set the same conditions with the experiment. In approach 2 (see Fig. 4.1), all systems with SG were modeled to investigate the quasi-steady state SG pressure.

4.1.2 Simulation Results

A. HX Heat Removal Performance

For various test conditions in Table 4.1, Table 4.2 shows the comparison between the experimental data and MARS calculation results for the HX heat removal rate. While the original MARS code generally under-predicted the HX heat removal rate with a mean deviation of 10.9 %, MARS/PAFS slightly under-estimated the experimental data with a mean deviation of 1.4 %. Compared to the default model in the original MARS code, the proposed HX heat transfer model package provided the improved prediction of the HX heat removal performance.

B. Local HTCs

Figure 4.2(a) shows the comparison between the experimental data and MARS calculation results for local HTCs of the horizontal in-tube condensation along the tube axial length under the SS-540-P1 test as a representative condition. While the original MARS code, based on the combination of condensation models by Shah (1979) and Chato (1962), generally under-predicted the local HTCs, the predictions by MARS/PAFS, based on the combination of condensation models by Dobson and Chato (1998) and Cavallini et al. (2006), were well located between experimental top and bottom HTCs. Therefore, it is confirmed that the proposed condensation model can provide the improved prediction of the local HTCs compared to the default condensation model in the original MARS code.

Figures 4.2(b) to 4.2(d) show the comparison between the experimental data and MARS calculation results for local HTCs of the nucleate boiling outside the HX tube according to the decrease of PCCT water level under the SS-540-P1 test condition. While the original MARS code, based on the nucleate boiling model by Chen (1966), generally under-predicted the local HTCs on the upper part of U-tube, the predictions by MARS/PAFS, based on the nucleate boiling model, showed good agreement with the experimental data. MARS/PAFS well traced the increase of local HTCs according to the decrease of the PCCT water level. Therefore, it is found that the proposed nucleate boiling model can provide the improved prediction of the local HTCs compared to the default nucleate boiling model in the original MARS code.

C. Quasi-Steady State System Pressure

Figure 4.3 shows the comparison between the experimental data and MARS

calculation results for the SG pressure at the quasi-steady state condition, according to a variation of the SG thermal power. The original MARS code generally over-predicted the system pressure. The pressure difference between the data and predictions increased with the SG thermal power. On the other hand, MARS/PAFS well traced the increase of the system pressure with the SG power. It is revealed that the proposed HX heat transfer model package can provide the improved prediction of the heat removal performance compared to the default model in the original MARS code.

4.2 Validation for ATLAS-PAFS Experiment

The ATLAS-PAFS data can be used to validate the prediction capability of MARS/PAFS for the transient-state. Since the FLB has been pointed out as the most important accident in evaluating the cooling capability of the PAFS among FLB, MSLB, and SGTR, this study simulated the FLB accident scenario.

4.2.1 MARS Modeling of ATLAS-PAFS Experiment

Figure 4.4 shows the MARS nodalization scheme for the simulation of the ATLAS-PAFS experiment. The primary- and secondary-sides of the ATLAS facility were modeled using one-dimensional volumes and junctions (Bae et al., 2014). The break nozzle was placed on the SG-1. The PAFS was modeled similarly with the PASCAL nodalization (see Fig. 4.1). However, three HX tubes were modeled as one pipe component (PIPE-044) and one heat structure (HS-044)

where the total heat transfer area of the PCHX is maintained. The PCCT was modeled using the MULTID-090 where the number of cell is 1, 12 and 27 for x, y and z-directions, respectively. The initial and boundary conditions for the PAFS-FLB-EC-01 test (see Table 3 in the paper by Bae et al. (2014)) in the ATLAS-PAFS facility were equivalently simulated in this MARS simulation.

4.2.2 Simulation Results

According to Bae et al. (2014), MARS has a sufficient capability to quantitatively predict the FLB transient with the actuation of the PAFS; however, the authors mentioned that there was a difference between the experimental data and the code calculation for the natural circulation flow rate in the PCHX because of the deficiency in predicting the heat transfer characteristics of the PCHX. Therefore, this study simulated the FLB accident focusing on the prediction capability of MARS/PAFS for the HX heat removal performance after the PAFS actuation.

Figure 4.5(a) shows the natural circulation flow rate at the return water line of the PAFS. As time passed, the natural circulation flow rate gradually decreased due to the SG secondary side cooling by the PAFS. While the original MARS code generally over-predicted the natural convection flow rate, MARS/PAFS estimated the data well during the whole time of FLB accident.

Figure 4.5(b) shows the comparison between the experimental data and MARS calculation results for the SG secondary-side pressure. Initially, an oscillating behavior of the SG pressure is caused by the opening and closing of the main steam safety valve (MSSV). After the PAFS actuation, the SG pressure

decreased rapidly owing to the SG secondary-side cooling by the PAFS. While the original MARS code significantly over-predicted the SG pressure, MARS/PAFS considerably well predicted the system pressure behavior with the natural convection flow rate similar to the experimental data. It means that the HX heat transfer model package in MARS/PAFS estimated the heat removal performance of the PAFS well compared to the default model in the original MARS code.

4.3 Validation for NOKO Experiment

4.3.1 MARS Modeling of NOKO Experiment

The MARS nodalization scheme of the NOKO test facility is shown in Fig. 4.6. It consists of the pressure vessel and the emergency condenser system including the bundle HX, the condenser pool, and the connecting line. The pressure vessel is composed of three regions (upper -, lower -, and middle plenum). The upper and lower plenums are modeled as single volume components of V190 and V140, respectively. The middle plenum is modeled as the pipe component of V150 where the electrical heater exits. The time-dependent volume, TDV-540, is connected with the upper plenum through the valve component, J195, to control the initial system pressure and the initial water level using the boundary condition. When the emergency condenser system starts to operate, the valve, J195, is closed.

The four HX tubes were modeled as a single pipe component, V350, which are divided into 20 control volumes, and one heat structure (HS-350), which was

used to represent the heat transferred from the steam to the cold water in the condenser pool through the condenser tube wall. The steam produced from the pressure vessel is injected into this tube bundle through the steam line, V350. When the water level in the pressure vessel reaches the target level by the water boiling, the actuation valve, J395, at the feed line opens and then the natural circulation flow of the NOKO is formed. The condensate water is returned to the pressure vessel through the feed line, V400. The condenser pool was modeled using the MULTID-640 where the number of cell is 7, 7 and 11 for x, y and z-directions, respectively. TDV-650 is coupled to the pool for pressure control.

4.3.2 Simulation Results

The code simulations of NOKO were performed by controlling the electrical heater power in the pressure vessel to investigate the electrical heater power which can maintain a constant system pressure through a balance between the heater power and the emergency condenser capacity. Figure 4.7 presents the emergency condenser capacity in terms of the water level in the pressure vessel for the test conditions described in Table 4.3. A reference point of the water level is the connecting point of the emergency condenser outlet line at the pressure vessel. The bars in the capacity curves show the fluctuations of the experimental capacity during the measurement time period. The center point indicates the centered value of the bar.

In Fig. 4.7, as the water level in the pressure vessel decreases and the system pressure increases, the emergency condenser capacity increases. While the original MARS code under-predicted the emergency condenser capacity with a

mean deviation of 15.85 %, MARS/PAFS well-estimated it with a mean deviation of 4.26 % (see Table 4.4). It is revealed that the proposed HX heat transfer model package can provide the improved prediction of the heat removal performance compared to the default model in the original MARS code.

Table 4.1 Test conditions of PASCAL

No.	Tube Inlet P [bar]	Tube Inlet Flow [kg/s]	PCCT Level [m]
1	10.29	0.1455	4
2	11.57	0.1460	6
3	13.29	0.1473	9
4	26.20	0.2832	4
5	27.99	0.2885	6
6	31.92	0.2947	9
7	58.51	0.4136	4
8	62.37	0.4218	6
9	67.09	0.4305	9

Table 4.2 HX heat removal performance of PASCAL

No	Experiment	Original MARS		MARS/PAFS	
	Q [kW]	Q [kW]	δ [%]	Q [kW]	δ [%]
1	292.9	249.8	-14.7	290.2	-0.9
2	291.9	254.7	-12.8	292.5	0.2
3	288.4	257.6	-10.7	292.1	1.3
4	526.9	463.1	-12.1	516.3	-2.0
5	523.2	467.4	-10.7	519.9	-0.6
6	526.6	477.7	-9.3	524.1	-0.5
7	730.4	654.3	-10.4	709.2	-2.9
8	725.8	659.3	-9.2	711.0	-2.0
9	727.1	664.3	-8.6	711.6	-2.1
Mean deviation [%]		-	10.9	-	1.4

Table 4.3 Test conditions of NOKO

Test No.	Pressure Vessel		Condenser Pool	
	Pressure [bar]	Level above back line [m]	Pressure [bar]	Level [m]
EU-1-3	9.8	3.66	1.1	1.33
EU-2-4	9.9	2.52	1.2	1.33
EU-1-5	9.8	1.31	1.1	1.36
EU-3-3	30.1	3.64	1.1	1.43
EU-3-4	30.1	2.47	1.4	1.37
EU-3-5	30.0	1.33	1.5	1.27
EU-5-4	70.7	3.58	1.4	1.39
EU-5-5	70.6	2.41	1.8	1.26
EU-5-6	70.6	1.29	1.7	1.34

Table 4.4 HX heat removal performance of NOKO

Test No.	Experiment		Original MARS		MARS/PAFS	
	Q [kW]	Avg. Q [kW]	Q [kW]	δ [%]	Q [kW]	δ [%]
EU-1-3	800-1100	950	780	-18.09	1080	13.41
EU-2-4	960-1100	1030	740	-28.19	1090	5.77
EU-1-5	960-1210	1080	880	-18.67	1160	7.21
EU-3-3	1950-2050	2000	1730	-13.53	2020	0.96
EU-3-4	2080-2200	2140	1700	-20.49	2110	-1.31
EU-3-5	2000-2200	2100	1680	-19.90	2120	1.08
EU-5-4	2810-2930	2870	2680	-6.50	3000	4.66
EU-5-5	2950-3090	3020	2760	-8.55	3060	1.39
EU-5-6	3050-3300	3180	2900	-8.78	3260	2.54
Mean deviation [%]			-	15.85	-	4.26

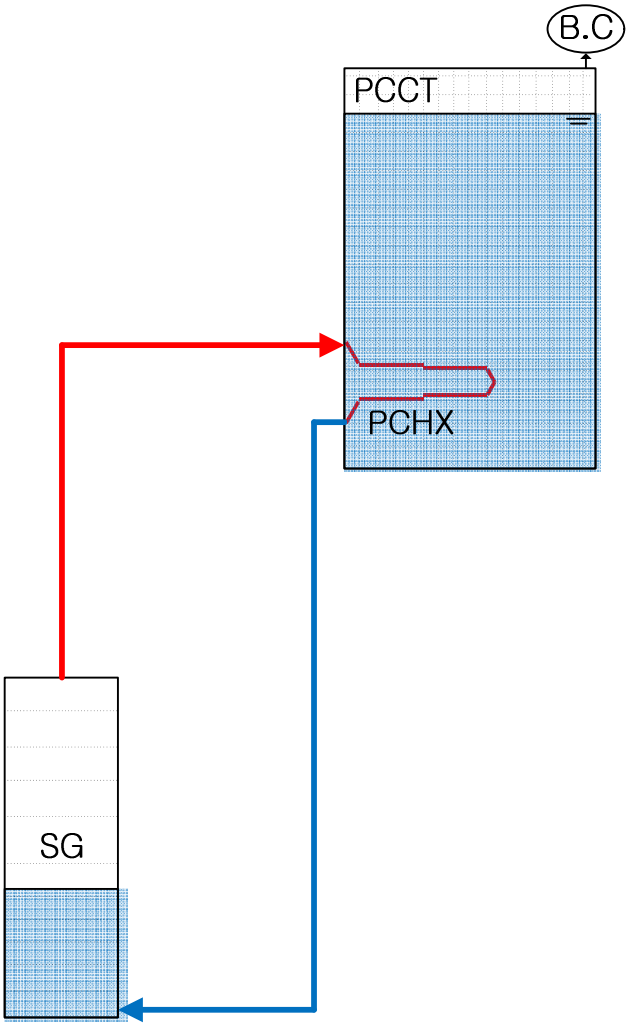

Figure 4.1 MARS modeling of PASCAL

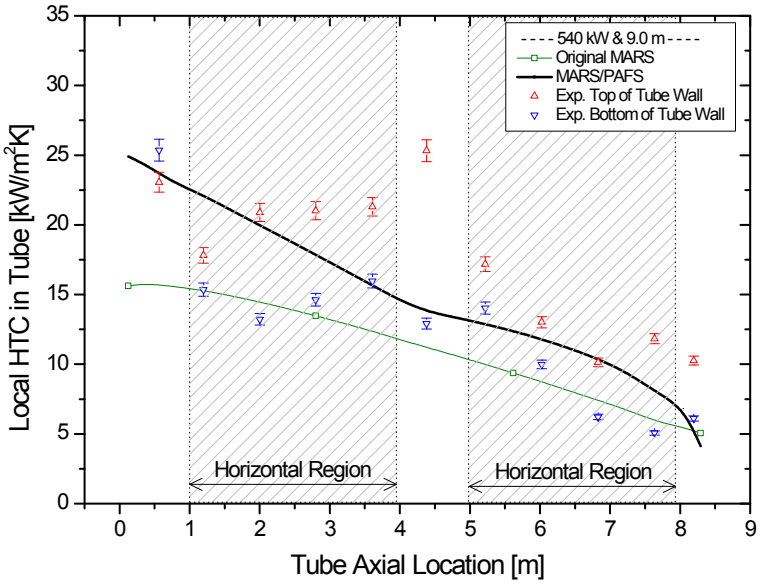

(a) Local HTCs in tube - condensation

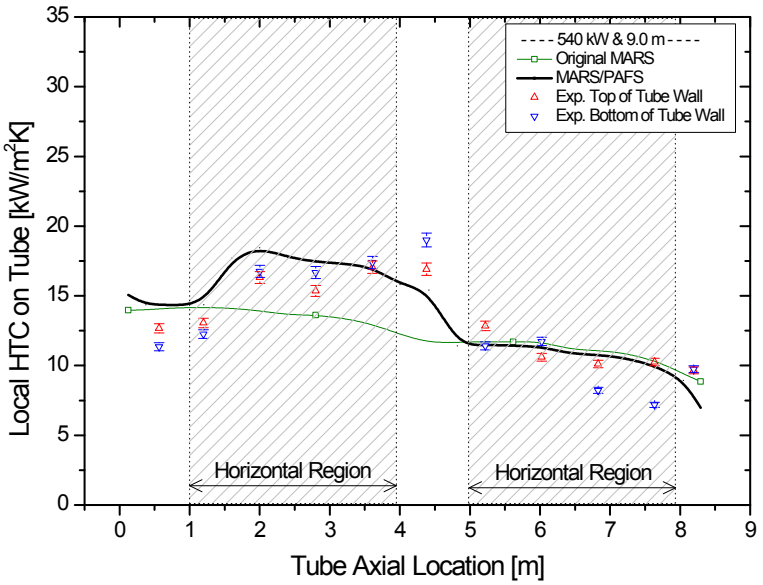

(b) Local HTCs on tube – nucleate boiling (PCCT level: 9 m)

Figure 4.2 Local HTCs of PASCAL (1/2)

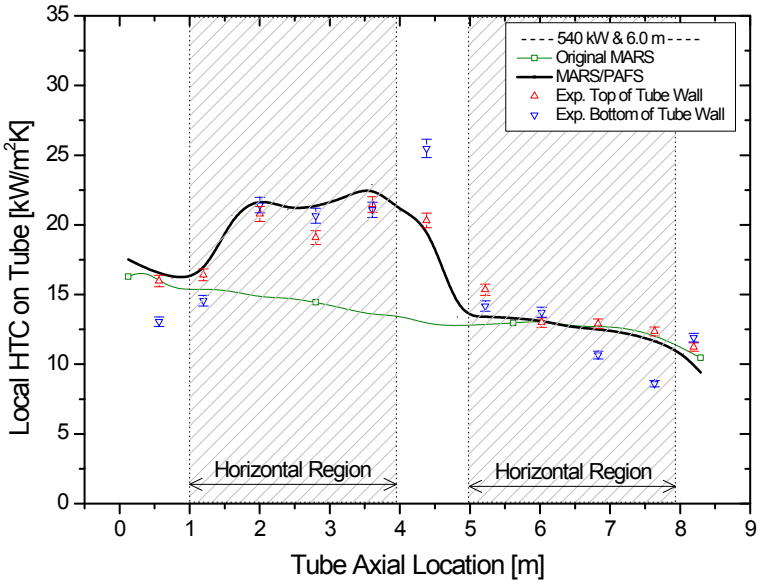

(c) Local HTCs on tube – nucleate boiling (PCCT level: 6 m)

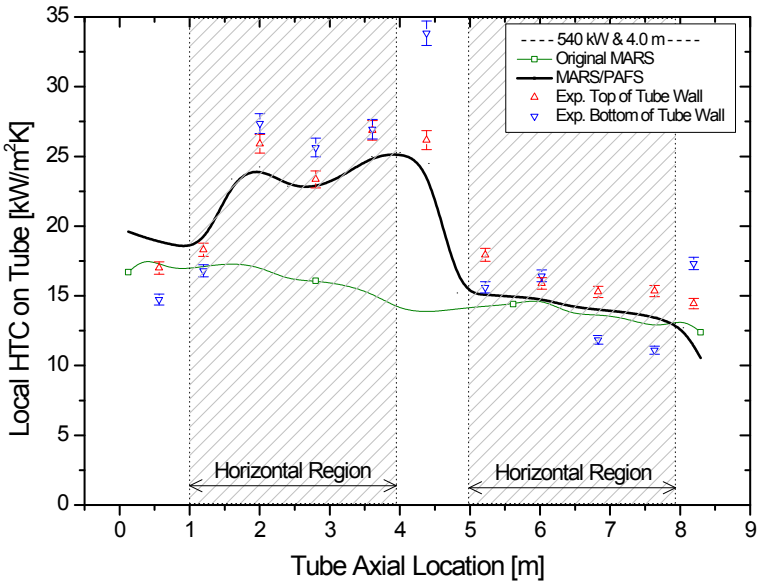

(d) Local HTCs on tube – nucleate boiling (PCCT level: 4 m)

Figure 4.2 Local HTCs of PASCAL (2/2)

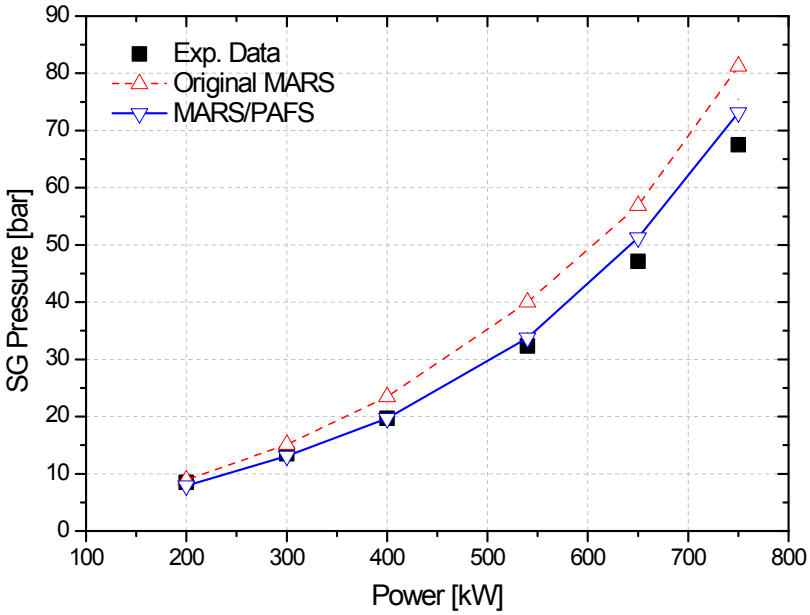

Figure 4.3 Steady-state SG pressure of PASCAL

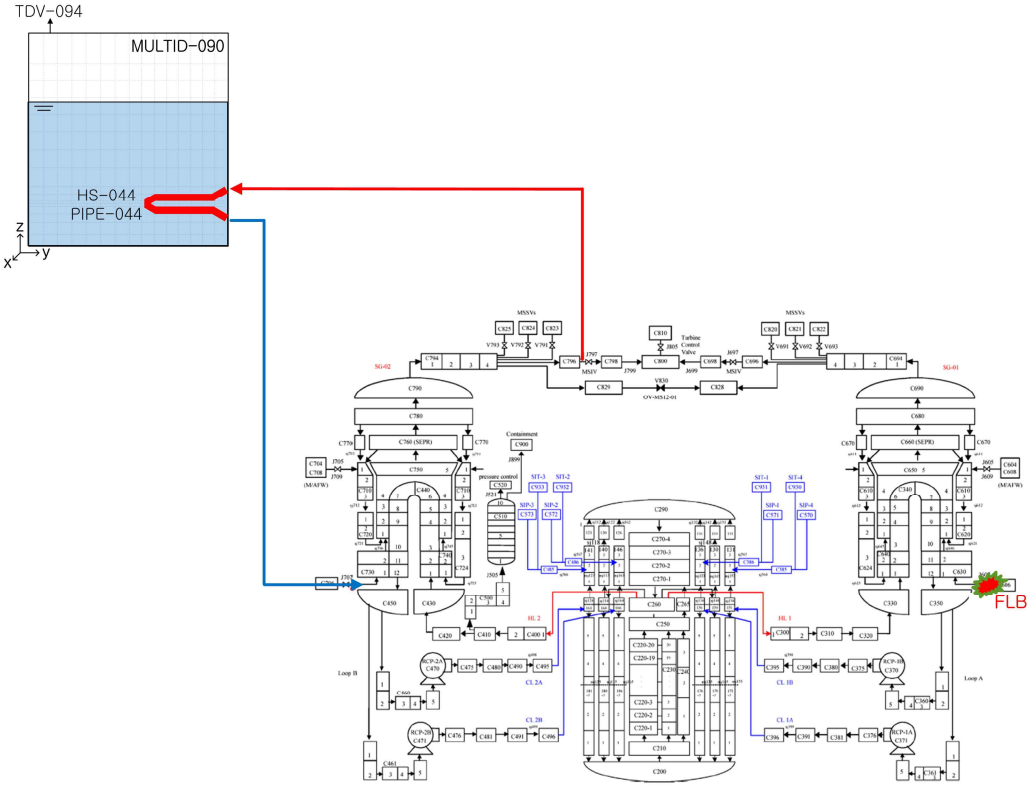

Figure 4.4 Nodalization of ATLAS-PAFS

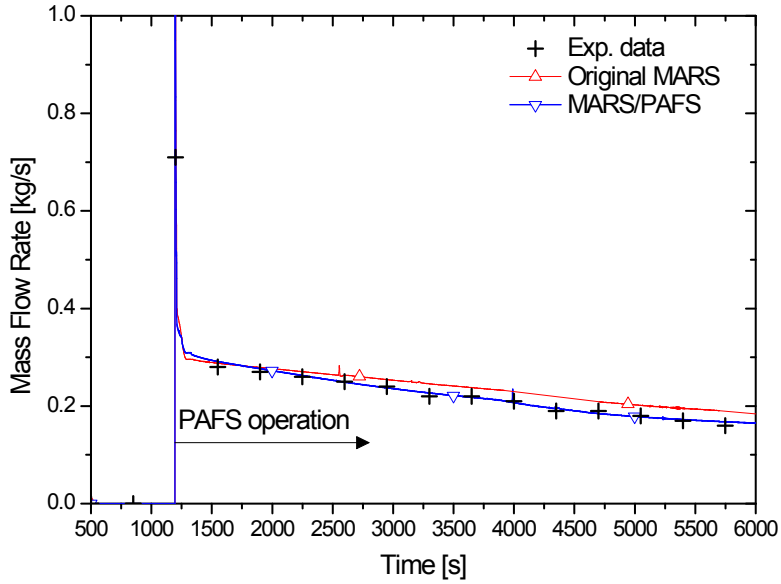

(a) PAFS flow rate

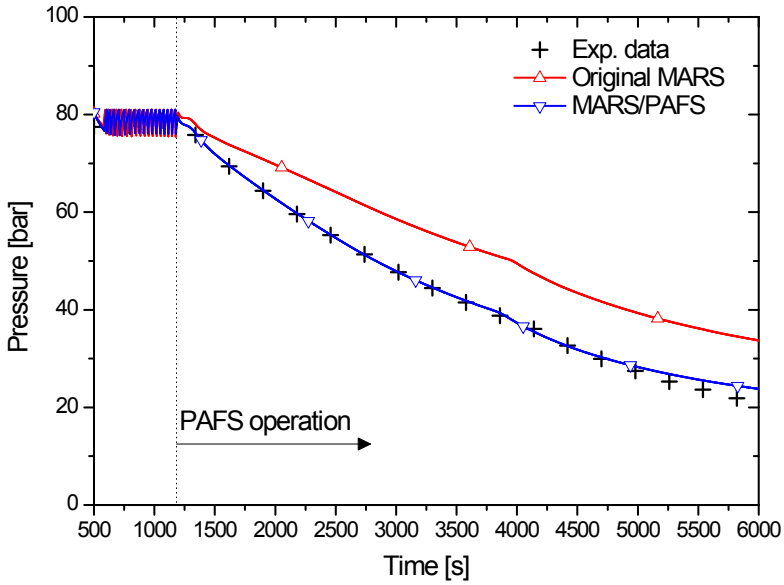

(b) SG pressure

Figure 4.5 Simulation results of ATLAS-PAFS

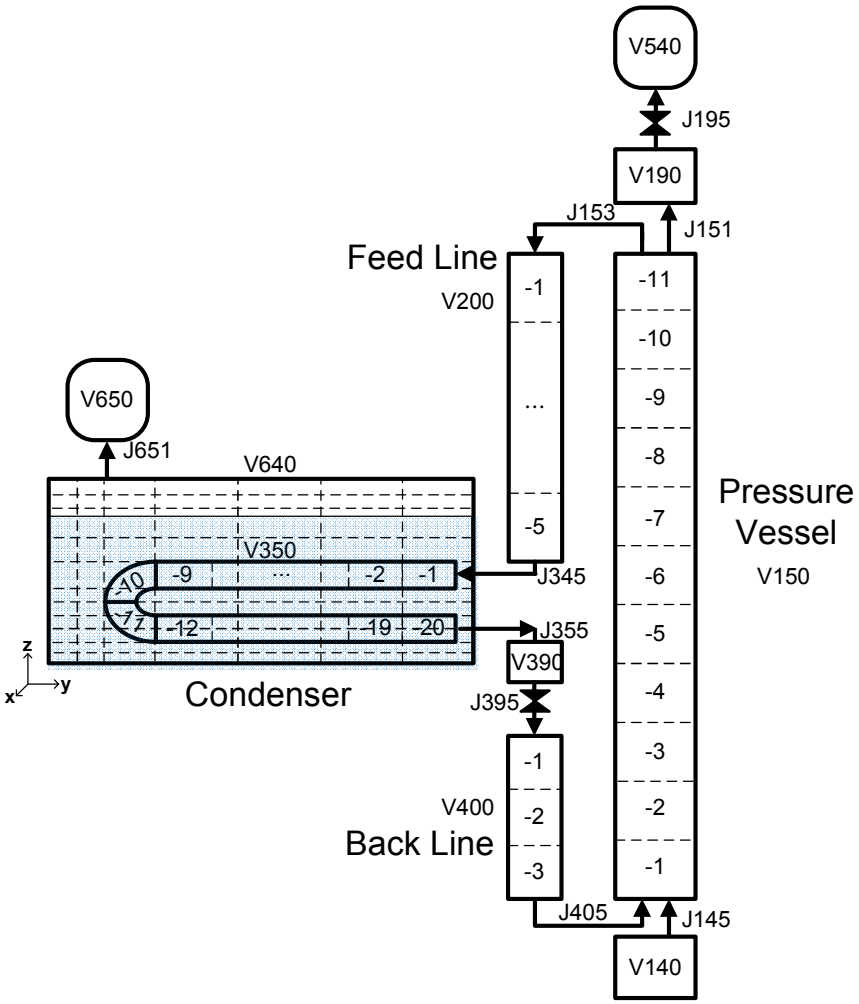

Figure 4.6 MARS nodalization of NOKO

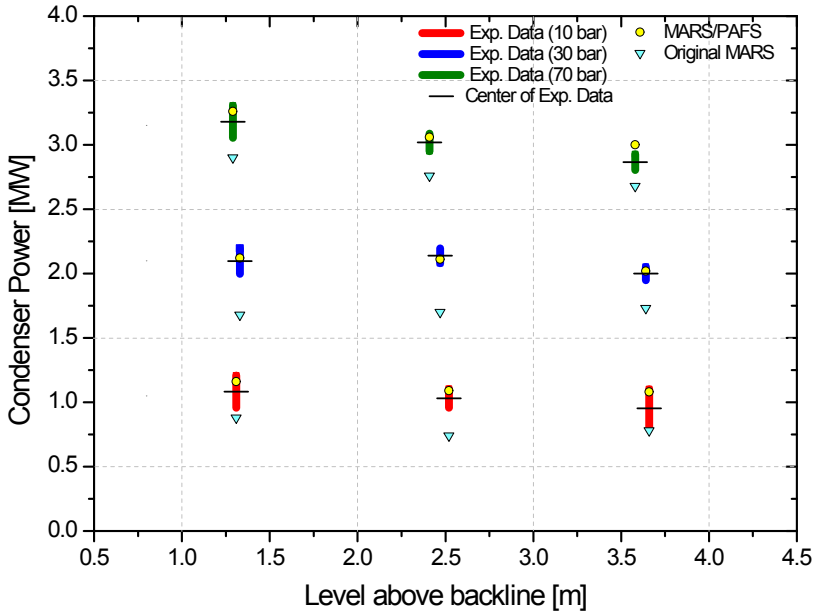

Figure 4.7 HX Heat removal performance of NOKO

Chapter 5

Conclusions

5.1 Summary

As a key equipment of passive safety systems such as PAFS, PCCS, and ECS, the horizontal U-shaped HX submerged in a large pool has been developed. In order to obtain a reliable prediction of the heat removal performance of the HX in the PAFS well, this study has developed the heat transfer model package applicable to MARS for the horizontal U-shaped HX submerged in a pool. The model package consisted of the horizontal in-tube condensation model and the natural convective nucleate boiling model on the horizontal U-shaped HX submerged in a pool. The model package was validated with various experimental data related to the passive safety systems well. The objective to develop the heat transfer model package applicable to MARS in predicting well the local HTCs at the inside/outside tube wall and the heat removal performance of the HX in the PAFS was accomplished.

For the horizontal in-tube condensation model, the original MARS code has the Shah (1979) and Chato (1962) models for the annular and stratified flow regimes, respectively. However, the original MARS code, based on those models, generally under-estimated the annular and stratified flow condensation heat

transfer in the horizontal condenser tube of the passive safety system. In order to improve the horizontal in-tube condensation model in BE codes, this study investigated the predictive capability of the previous horizontal in-tube condensation heat transfer models for annular and stratified flow within various conditions encountered in the passive safety system using the MARS code. From the assessments of nineteen annular flow- and eleven stratified flow condensation models, it was found that the annular flow condensation model by Dobson and Chato (1998) and the stratified flow condensation model by Cavallini et al. (2006) were the most applicable models to the HX of the passive safety system. By replacing the models by Shah (1979) and Chato (1962) in the original MARS code with the models by Dobson-Chato (1998) and Cavallini et al. (2006), this study improved the horizontal in-tube condensation model in MARS.

For the nucleate boiling model, this study first investigated the predictive capability of the previous nucleate boiling models for the horizontal U-shaped HX submerged in a pool using MARS. From the assessments of seven nucleate pool boiling and eight forced convective boiling models, it was found that, including the Chen (1966) model as a default model in the original MARS code, previous nucleate pool boiling and forced convective boiling models did not predict the HTCs on both upper and lower parts of the U-tube in PASCAL well enough. Thus, this study investigated the nucleate boiling heat transfer mechanism on the horizontal U-shaped HX in the PAFS and had following insights:

- The base heat transfer mode outside the HX tube is a nucleate pool boiling heat transfer. However, the upper part of U-tube is influenced by the effect of gravity-induced natural convection velocity due to the heat transfer from the lower part of U-tube additionally.

- As the PCCT water level decreases, more bubbles are generated from the lower part of U-tube and the effect of flow velocity on the upper part of U-tube increases further. Since the turbulence around the upper part of U-tube increases more due to the liquid agitation by the bubbles generated from the upper part of U-tube, the HTCs on the upper part increase more rapidly than those on the lower part.

Based on the heat transfer mechanisms, this study developed the nucleate boiling model on the horizontal U-shaped HX submerged in a pool. This model predicts the HTC on the lower and upper part of U-tube by the subcooled nucleate pool boiling correlation and the forced convective nucleate boiling correlation, respectively. From the validation results, it was found that the proposed nucleate boiling model adequately captured the phenomenological difference in the heat transfer mechanism between the upper and lower parts of the U-tube and well predicted the PASCAL and ATLAS-PAFS data for the low subcooling conditions ($\Delta T_{sub} < \sim 30$ K) within a deviation of 19 %. Additionally, this study developed the natural convection heat transfer model on the horizontal U-shaped HX submerged in a pool based on the PASCAL data to complete the modeling of the outside tube heat transfer. The proposed natural convection model similarly-predicted the HTCs for the high subcooling conditions ($\Delta T_{sub} > \sim 40$ K) within a deviation of 33.2 %. Finally, this study developed the natural convective nucleate boiling model by combining the proposed nucleate boiling model and the natural convection model.

The proposed HX heat transfer model package was validated with various steady-state and transient experimental data. The validation results revealed that the proposed model package could provide the improved prediction of the local

HTCs at the inside/outside tube wall and the heat removal performance of the HX in the passive safety system, especially PAFS. It is expected that this model package contributes to the reliable design and the safety analysis of the passive safety system.

5.2 Recommendations

Through the present study, the following further studies are suggested:

- The proposed HX heat transfer model package consists of the empirical correlations mainly. These types of correlations are easy to implement; however, they, based on the use of limited database, have shown a considerable deviation for the experimental data from different authors for different fluids and flow conditions. On the other hand, there have been many efforts to develop the mechanistic heat transfer models, i.e., the condensation model by Ahn et al. (2014) and the boiling model by Sateesh et al. (2005). Throughout the further research, if the mechanistic model describing the related heat transfer mechanisms sufficiently is developed and consequently is implemented to the proposed heat transfer model package, the applicability of the proposed model can be expanded to the heat transfer analysis of various passive safety systems.
- In developing the natural convective nucleate boiling model, this study used the PAFS-related experimental data. However, for the general applications of the proposed HX heat transfer model package to various passive safety systems, it has to be substantiated further by a wide variety

of passive safety system-related experimental data.

- The HXs of prototype passive safety systems consist of tube bundles. For the direct application of the proposed nucleate boiling model to the tube bundles, the additional term that can consider the bundle effect is required. Up to now, the bundle effect has not been investigated systematically to relate the single U-shaped tube heat transfer to the heat transfer of a U-shaped tube in a bundle, and the available experimental data is extremely limited. Throughout the further research of the bundle effect in the passive safety system, if the bundle boiling factor is deduced as suggested by Palen (1983) and consequently is applied to the proposed model, the optimum design of the passive safety system with the BE code is possible.

Nomenclature

A	Cross-sectional area [m^2], surface area [m^2]
Bo	Boiling number
C_p	Specific heat at constant pressure [J $kg^{-1}K^{-1}$]
C_{sf}	Fluid-surface combination coefficient
D	Tube diameter
D_b	Bubble departure diameter [m]
f	Fanning friction factor
f_i	Interfacial roughness factor
F	Two-phase-convection multiplier factor
F_p	Pressure function
F_{PF}	Pressure correction factor
Fr	Froude number
g	Gravitational acceleration [m s^{-2}]
G	Mass velocity [kg $m^{-2}s^{-1}$]
G_{wavy}	Wavy flow transition mass velocity [kg $m^{-2}s^{-1}$]
G_{strat}	Stratified flow transition mass velocity [kg $m^{-2}s^{-1}$]
Ga	Galileo number
h	Heat transfer coefficient [W $m^{-2}K^{-1}$]
h_c	Convective condensation heat transfer coefficient [W $m^{-2}K^{-1}$]
h_f	Film condensation heat transfer coefficient [W $m^{-2}K^{-1}$]
h_{fg}	Latent heat [J kg^{-1}]
h_{ld}	Dimensionless liquid height

H	Enthalpy [J/kg]
J_g	Dimensionless gas velocity
J_g^T	Transition dimensionless gas velocity
Ja	Jacob number
k	Thermal conductivity [W $m^{-1}K^{-1}$]
M	Molecular weight [kg $kmol^{-1}$]
Nu	Nusselt number
P	Pressure [Pa]
P_c	Critical pressure [bar]
P_r	Reduced pressure
Pr	Prandtl number
Q	Capacity [kW]
$\dot{q}$	Heat transfer rate [W]
$q"$	Heat flux [W m^{-2}]
r	Radius [m]
R_p	Surface roughness parameter [μm]
Ra	Rayleigh number
Re	Reynolds number
S	Suppression factor
St	Stanton number
T	Temperature [K]
T^+	Dimensionless liquid temperature at film surface
u	Velocity [m s^{-1}]
W	Mass flow rate [kg/s]
We	Weber number

x Vapor quality

X_{tt} Lockhart Martinelli parameter

z Axial location [m]

Greek Letters

α Void fraction

β Circumference Fraction of tube where filmwise condensation prevails

δ Liquid film thickness [m], percent deviation [%]

δ^+ Dimensionless liquid film thickness [m]

ΔP_{sat} Vapor-pressure difference corresponding to superheat temperature [Pa]

ΔT_{sat} Wall superheat [K]

ΔT_{sub} Degree of subcooling [K]

μ Viscosity (Pa s)

ϕ Two-phase multiplier

ψ Parameter defined by Shah

ψ_0 Value of ψ at zero subcooling

ρ Density [kg m^{-3}]

σ Surface tension [N/m]

τ Shear stress [Nm^{-2}]

θ Angle [rad], inclination angle [°]

Subscripts

annu	Annular flow
b	Bulk liquid
bot	Bottom of tube
cl	Centerline
cross	Cross flow
cv	Convection
exp	Experimental
eq	Equivalent
g	Gas
l	Liquid
ld	Dimensionless liquid
lf	Liquid film
lo	Liquid only
lower	Lower part of U-tube
nb	Nucleate boiling
npb	Nucleate pool boiling on a single tube
parallel	Parallel flow
sat	Saturation
strat	Stratified flow
su	Superficial vapor
sub	Subcooling
top	Top of tube
TP	Two-phase

upper	Upper part of U-tube
v	Vapor
vd	Dimensionless vapor
w	Wall
wall,in	Physical inner surface
wi	Inner wall
wo	Outer wall
*	Location on tube, can be “top” or “bot”

Superscripts

n	Order of asymptotic model

References

Ahn, T. H., Yun, B. J., Jeong, J. J., Kang, K. H., Park, Y. S., and Cheon, J., "Development of a new condensation model for the nearly-horizontal heat exchanger tube under the steam flowing conditions," *International Journal of Heat and Mass Transfer*, vol. 79, pp. 876-884, 2014.

Akers, W. W., Deans, H. A., and Crosser, O. K, "Condensation heat transfer within horizontal tubes," *Chemical Engineering Progress Symposium Series*, vol. 55, pp. 171-176, 1959.

Akers, W. W and Rosson, H. F, "Condensation inside a horizontal tube," *Chemical Engineering Progress Symposium Series*, vol. 56, pp. 145−149, 1960.

Arai, K., et al., "Performance of PCCS with horizontal U-Tube type heat exchanger," *Proceedings of NTHAS-2*, pp. 332-335, 2000.

Arai, K., Kurita, K., Yamamoto, K., and Fukuda, T., "Post-test analysis of thermal-hydraulic test using full-scale horizontal PCCS condenser," *Proceedings of ICAPP '03*, Cordoba, Spain, 2003.

Bae, B. U., Kim, S., Park, Y. S., Kang, K. H., and Yun, B. J., "Experimental investigation into the effect of the passive condensation cooling tank water level in the thermal performance of the passive auxiliary feedwater system," *Nuclear Technology*, vol. 181, pp. 479-492, 2013.

Bae, B. U., Kim, S., Park, Y. S., and Kang, K. H., “Integral effect test and code analysis on the cooling performance of the PAFS (passive auxiliary feedwater system) during an FLB (feedwater line break) accident,” *Nuclear Engineering and Design*, vol. 275, pp. 249-263, 2014.

Bang, Y. S., Chun, J. H., Chung, B. D., and Park, G. C., “Improvements of condensation heat transfer models in MARS code for laminar flow in presence of non-condensable gas,” *Nuclear Engineering and Technology*, vol. 41 (8), pp. 1015-1024, 2009.

Bennett, D. L., Davis, M. W., and Hertzler, B. C., “The suppression of saturated nucleate boiling by forced convective flow,” *AIChE Symposium Series*, vol. 76, pp. 91-103, 1980.

Bennett, L. and Chen, J. C., “Forced convective boiling in vertical tubes for saturated pure components and binary mixtures,” *AIChE Journal*, vol. 26 (3), pp. 454-461, 1980.

Bitter, R. C., “Heat transfer from a horizontal tube with transverse flow of evaporating saturated R-11,” In Heat and Mass Transfer in Refrigeration Systems and in Air Conditioning, Int. Inst. Refrigeration, F. R. G, 1972.

Bivens, D. B. and Yokozeki, A., “Heat transfer coefficient and transport properties for alternative refrigerants,” *Proceedings of International Refrigeration Conference*, pp. 299-304, 1994.

Boyko, L. D. and Kruzhilin G. N., “Heat transfer and hydraulic resistance during

condensation of steam in a horizontal tube and in a bundle of tubes," *International Journal of Heat and Mass Transfer*, vol. 10, pp. 361– 373, 1967.

Carpenter, E. F. and Colburn, A. P, "The effect of vapor velocity on condensation inside tubes," *Proceedings of the General Discussion of Heat Transfer*, The Institution of Mechanical Engineers and the American Society of Mechanical Engineers, pp. 20-26, 1951.

Cavallini, A., Censi, G., Del Col, D., Doretti, L., Longo, G. A., and Rossetto, L., "Condensation of halogenated refrigerants inside smooth tubes," *International Journal of HVAC&R Research*, vol. 8 (4), pp. 429−451, 2002.

Cavallini, A., Del Col, D., Doretti, L., Matkovic, M., Rossetto, L., Zilio, C., and Censi, G., "Condensation in horizontal smooth tubes: a new heat transfer model for heat exchanger design," *Heat Transfer Engineering*, vol. 27 (8), pp. 31−38, 2006.

Cavallini, A. and Zecchin, R., "A dimensionless correlation for heat transfer in forced convection condensation," *Proceedings Sixth International Heat Transfer Conference*, vol. 3, pp. 309−313, 1974.

Chato, J. C., "Laminar condensation inside horizontal and inclined tubes," *ASHRAE Journal*, vol. 4 (2), pp. 52−60, 1962.

Chen, J. C., "Correlation for boiling heat transfer to saturated Fluids in convective flow," *Industrial and Engineering Chemistry Process Design and Development*, vol. 5 (3), pp. 322-329, 1966.

Chen, S. L., Gerner, F. M., and Tien, C. L., “General film condensation correlations,” *Experimental Heat Transfer*, vol. 1, pp. 93-107, 1987.

Cho, Y. J., Bae, S. W., Bae, B. U., Kim, S., Kang, K. H., and Yun, B. J., “Analytical studies of the heat removal capability of a passive auxiliary feedwater system (PAFS),” *Nuclear Engineering and Design*, vol. 248, pp. 306-316, 2012.

Cho, Y. J., Kim, S., Bae, B. U., Park, Y. S., Kang, K. H., and Yun, B. J., “Assessment of condensation heat transfer model to evaluate performance of the passive auxiliary feedwater system,” *Nuclear Engineering and Technology*, vol. 45 (6), pp. 759-766, 2013.

Cho, H. K., Cho, Y. J., and Yoon, H. Y., “Heat structure coupling of CUPID and MARS for the multi-scale simulation of the passive auxiliary feedwater system,” *Nuclear Engineering and Design*, vol. 273, pp. 459-468, 2014.

Churchill, S. W. and Chu, H. H. S., “Correlating equations for laminar and turbulent free convection from a horizontal cylinder,” *International Journal of Heat and Mass Transfer*, vol. 18, pp. 1049-1055, 1975.

Colburn, A. P. and Hougen, O. A., “Design of cooler condensers from mixtures of vapours with noncondensing gases,” *Industry and Engineering Chemistry*, vol. 26, pp. 1178−1182, 1934.

Collier, J. G. and Thome, J. R., *Convective boiling and condensation (3rded.)*, McGraw-Hill, New York, 1994.

Cooper, M. G., “Heat flow rates in saturated nucleate pool boiling – a wide ranging examination using reduced properties,” *Advances in Heat Transfer*, vol. 16, pp. 157-239, 1984.

Cornwell, K., “The influence of bubbly flow on boiling from a tube in a bundle,” *Advances in Pool Boiling Heat Transfer*, Eurotherm No. 8, Paderborn, Germany, pp. 177-184, 1989.

Cornwell, K., Duffin, N. W., and Schuller, R. B., “An experimental study of the effects of fluid flow on boiling within a kettle reboiler tube bundle,” *ASME Paper 80-HT-45*, 1980.

Cornwell, K. and Houston, S. D., “Nucleate pool boiling of horizontal tubes: a convection-based correlation,” *International Journal of Heat and Mass Transfer*, vol. 37 (1), pp. 303-309, 1994.

Cornwell, K. and Scoones, D. S., “Analysis of low quality boiling on plain and low finned tube bundles,” *Proceedings of 2nd UK Heat Transfer Conference*, vol. 1, pp. 21-32, 1988.

Dittus, P. W. and Boelter, L. M. K., “Heat transfer in automobile radiators of the tubular type,” University of California Publications on Engineering, Berkeley, CA 2(13), 443, 1930.

Dobson, M. K. and Chato, J. C., “Condensation in smooth horizontal tubes,” *Journal of Heat Transfer*, vol. 120, pp. 193−213, 1998.

Forster, H. K. and Zuber, N., “Dynamics of vapor bubbles and boiling heat transfer,” *AIChE Journal*, vol. 1 (4), pp. 531-535, 1955.

Fujii, T., “Enhancement to condensing heat transfer-new developments,” *Journal of Enhanced Heat Transfer*, vol. 2 (2), pp. 127-137, 1995.

Gorenflo, D., “Pool Boiling. In: VDI Heat Atlas,” VDI-Verlag, Düsseldorf, 1993.

Gupta, A., Saini, J. S., and Varma, H. K., “Boiling heat transfer in small horizontal tube bundles at low cross-flow velocities,” *International Journal of Heat and Mass Transfer*, vol. 38 (4), pp. 599-605, 1995.

Gupta, C. P. and Prakash, R., “Engineering heat transfer,” Nem Chand and Bros., Roorkee, India, 1976.

Hwang, T. H. and Yao, S. C., “Boiling heat transfer from a horizontal cylinder at low quality crossflow,” *ASME Symposium*, vol. HTD-38, pp. 9-17, 1984.

Hwang, T. H., and Yao, S. C., “Forced convective boiling in horizontal tube bundles,” *International Journal of Heat and Mass Transfer*, vol. 29 (5), pp. 785-795, 1986.

IAEA, “Passive safety systems and natural circulation in water cooled nuclear power plants,” IAEA-TECDOC-1624, 2009.

Jaster, H. and Kosky, P. G., “Condensation in a mixed flow regime,” *International Journal of Heat and Mass Transfer*, vol. 19, pp. 95−99, 1976.

Jeong, J. J., Ha, K. S., Chung, B. D., and Lee, W. J., "Development of a multi-dimensional thermal-hydraulic system code, MARS 1.3.1.," *Annals of Nuclear Energy*, vol. 26 (18), pp. 1611-1642, 1999.

KAERI, "MARS code manual," KAERI/TR-3872/2009, 2009.

KAERI, "Report for integral effect test of the PAFS (passive auxiliary feedwater system)," APR+-PAFS-TR-12-10, 2012.

Kang, K. H., Kim, S., Bae, B. U., Cho, Y. J., Park, Y. S., and Yun, B. J., "Separate and integral effect tests for validation of cooling and operational performance of the APR+ passive auxiliary feedwater system," *Nuclear Engineering and Technology*, vol. 44 (6), pp. 597-610, 2012.

Kenning, D. B. R. and Cooper, M. G., "Saturated flow boiling of water in vertical tubes," *International Journal of Heat and Mass Transfer*, vol. 32 (3), pp. 445-458, 1989.

Kim, S., Bae, B. U., Cho, Y. J., Park, Y. S., Kang, K. H., and Yun, B. J., "An experimental study on the validation of cooling capability for the passive auxiliary feedwater system (PAFS) condensation heat exchanger," *Nuclear Engineering and Design*, vol. 260, pp. 54-63, 2013.

Kim, S., Kim, D. E., Ryu, S. U., Lee, S. T., and Euh, D. J., "Experimental investigation on the natural convection flow in pool boiling," *Nuclear Engineering and Design*, vol. 280, pp. 349-361, 2014.

Kondo, M., et al., "Confirmation of effectiveness of horizontal heat exchanger for

PCCS," *Proceedings of ICONE-14*, Miami, USA, 2006.

Kosky, P. J and Staub, F. W, "Local condensing heat transfer coefficients in the annular flow regime," *AIChE Journal*, vol. 17, pp. 1037–1043, 1971.

Krepper, E., Beyer, M., "Experimental and numerical investigations of natural circulation phenomena in passive safety systems for decay heat removal in large pools," *Nuclear Engineering and Design*, vol. 240, pp. 3170-3177, 2010.

Kutateladze, S. S., "Boiling heat transfer," *International Journal of Heat and Mass Transfer*, vol. 4, pp. 31-45, 1961.

Lee, W. J., et al., "Development of realistic thermal hydraulic system analysis code, development of nuclear thermal hydraulic verification test and evaluation technology," KAERI/RR-2235/2001, 2002.

Leong, L. S. and Cornwell, K, "Heat transfer coefficients in a reboiler tube bundle," *Chemical Engineer*, vol. 343, pp. 219-221, 1979.

Lockhart, R. W. and Martinelli, R. C., "Proposed correlation of data for isothermal two phase, two-component flow in pipes," *Chemical Engineering Progress*, vol. 45, pp. 39-48, 1947.

Mandhane, J. M., Gregory, G. A., and Aziz, K., "A flow pattern map for gas-liquid flow in horizontal pipes," *International Journal of Multiphase Flow*, vol. 1, pp. 537-553, 1974.

MKE, "Quick look report on the cooling performance of the passive auxiliary

feedwater system with the PASCAL," 9-017-A599-002-051, 2011.

Morgan, V. T., "The overall convective heat transfer from smooth circular cylinders," in T. F. Irvine and J. P. Hartnett, Eds., *Advances in Heat Transfer*, vol. 11, Academic Press, New York, 1075.

Moser, K. W., Webb, R. L., and Na, B., "A new equivalent Reynolds number model for condensation in smooth tubes," *Journal of Heat Transfer*, vol. 120, pp. 410-417, 1998.

Mostinski, I. L., "Application of the rule of corresponding states for calculation of heat transfer and critical heat flux," *Teploenergetika*, vol. 4, pp. 66-71, 1963.

Nakamura, H., et al., "Single U-tube testing and RELAP5 code analysis of PCCS with horizontal heat exchanger," *NTHAS-2*, pp. 336-343, 2000.

Nusselt, W., "Die oberflachenkondensation des wasserdampfes (the surface condensation of water vapor)," Zeit. D. Ver. Deut. Ing. Frankfurt 60, pp. 541–575, 1916.

Palen, J. W., *Heat Exchanger Design Handbook*, Hemisphere Publishing Corporation, New York, 1983.

Polley, G. T., Ralston, T., and Grant, I. D. R., "Forced crossflow boiling in an ideal in-line tube bundle," *Proc. of the 19th National Heat Transfer Conference*, ASME/AIChE, USA80-HT-46, Orlando, FL, 1980.

Reymond, O., Murray, D. B., and O'Donovan, T. S., "Natural convection heat

transfer from two horizontal cylinders," *Experimental Thermal and Fluid Science*, vol. 32, pp. 1702-1709, 2008.

Ribatski, G. and Jabardo, J. M. S., "Nucleate boiling of halocarbon refrigerants: heat transfer correlations," *International Journal of HVAC&R Research*, vol. 6 (4), pp. 349−367, 2000.

Rohsenow, W. M., "A method of correlating heat transfer data for surface boiling of liquids," *Transactions of ASME*, vol. 74, pp. 969-976, 1952.

Rosson, H. F. and Meyers J. A., "Point of values of condensing film coefficients inside a horizontal tube," *Chemical Engineering Progress Symposium Series*, vol. 61, pp. 190−199, 1965.

Sateesh, G., Das, S. K., Balakrishnan, A. R., "Analysis of pool boiling heat transfer: effect of bubbles sliding on the heating surface," *International Journal of Heat and Mass Transfer*, vol. 48, pp. 1543−1553, 2005.

Schaffrath, A., Hicken, E. F., Jaegers, H., and Prasser, H. M., "Experimental and analytical investigation of the operation mode of the emergency condenser of the SWR1000," *Nuclear Technology*, vol. 126, pp. 123-142, 1999.

Schaffrath, A. and Prasser, H. M., "Theoretical support to the NOKO experiments," FZR-224, Forschungszentrum Rossendorf, 1998.

Shah, M. M., "A general correlation for heat transfer during film condensation inside pipes," *International Journal of Heat and Mass Transfer*, vol. 22, pp. 547−

556, 1979.

Shah, M. M., “Improved general correlation for subcooled boiling heat transfer during flow across tubes and tube bundles,” *International Journal of HVAC&R Research*, vol. 11 (2), pp. 285-304, 2005.

Shah, M. M, “An improved and extended general correlation for heat transfer during condensation in plain tubes,” *International Journal of HVAC&R Research*, vol. 15, pp. 889–913, 2009.

Singh, R. L., Saini, J. S., and Varma, H. K., “Effect of cross-flow on boiling heat transfer of refrigerant-12,” *International Journal of Heat and Mass Transfer*, vol. 28 (2), pp. 512-514, 1985.

Soliman, H. M., Schuster, J. R., and Berenson, P. J., “A general heat transfer correlation for annular flow condensation,” *ASME Journal of Heat Transfer*, vol. 90, pp. 267-276, 1968.

Steiner, D. and Taborek, J., “Flow boiling heat transfer of single components in vertical tubes,” *Heat Transfer Engineering*, vol. 13 (2), pp. 43-69, 1992.

Stephan, K. and Abdelsalam, M., “Heat transfer correlations for natural convection boiling,” *International Journal of Heat and Mass Transfer*, vol. 23, pp. 73-87, 1980.

Sweeney, K. A. and Chato, J. C., “The heat transfer and pressure drop behavior of a zeotropic refrigerant mixture in a microfinned tube,” M.S. Thesis, University of Illinois at Urbana-Champaign, 1996.

Tandon, T. N., Varma, H. K., and Gupta, C. P., “Heat transfer during forced convection condensation inside horizontal tube,” *International Journal of Refrigeration*, vol. 18, pp. 210-214, 1995.

Tang, L., “Empirical study of new refrigerant flow condensation inside horizontal smooth and micro-fin tubes,” Ph.D. Thesis, University of Maryland at College Park, 1997.

Thome, J. R., El Hajal, J., and Cavallini, A., “Condensation in horizontal tubes, part 2: new heat transfer model based on flow regimes,” *International Journal of Heat and Mass Transfer*, vol. 46, pp. 3365−3387, 2003.

Thurgood, M. J., et al., “COBRA-TF: a thermal-hydraulics code for transient analysis of nuclear reactor vessel and primary coolant systems,” USNRC, NUREG/CR-3046, 1983.

Traviss, D. P., Rohsenow, W. M., and Baron, A. B., “Forced convection inside tubes: a heat transfer equation for condenser design,” *ASHRAE Transactions*, vol. 79, pp. 157–165, 1973.

USNRC, “RELAP5/MOD3 code manual,” NUREG/CR-5535, 1988.

USNRC, “RELAP5/MOD3.3 code manual,” NUREG/CR-5535/Rev P3-Vol IV, 2006.

Voloshko. A. A., “Free convection boiling of freons,” *Heat Transfer-Soviet Research*, vol. 4 (4), pp. 60-66, 1972.

Webb, R. L. and Chien, L. H., "Correlation of convective vaporization on banks of plain tubes using refrigerants," *Heat Transfer Engineering*, vol. 15 (3), pp. 57-69, 1994.

Webb, R. L. and Gupte, N. S., "A critical review of correlations for convective vaporization in tubes and tube banks," *Heat Transfer Engineering*, vol. 13 (3), pp. 58-81, 1992.

Whitaker, S., "Forced convection heat transfer correlations for flow in pipes, past flat plates, single cylinders, single spheres, and flow in packed beds and tube bundles," *AIChE Journal*, vol. 18, pp. 361-371, 1972.

Wu, T., "Horizontal in-tube condensation in the presence of a noncondensable gas," Ph.D. Thesis, Purdue University at West Lafayette, 2005.

Wu, T. and Vierow, K., "Local heat transfer measurements of steam/air mixtures in horizontal condenser tubes, *International Journal of Heat and Mass Transfer*, vol. 49, pp. 2491-2501, 2006.

Zhukauskas, A., "Heat transfer from tubes in cross flow," *Advances in Heat Transfer*, vol. 8, pp. 93-160, 1972.

Appendix A

Prediction Capability of MARS MULTID for Natural Convection Flow in Pool

In the passive safety system such as PAFS, for the prediction and modeling of the out-tube heat transfer, it is important to understand the TH phenomenon in a HX pool, especially the mixing in a pool. It affects the local water temperature and the natural convection flow velocity near the HX, and finally influences the local natural convective and nucleate boiling HTC. This section presents the main phenomena for the pool mixing and the prediction capability of MULTID in MARS for natural convection flow velocity in a pool.

According to the natural convection flow experiment (see Fig. A.1) performed in the KAERI (Kim et al., 2014), main phenomena related with the mixing in the pool are summarized as follows (see Fig. A.2): 1) When the degree of subcooling is high in the pool, a large natural convection flow occurs above the heater rod with the low natural convection flow velocity and the thermal stratification occurs below the heater. 2) When the pool temperature reaches approximately 90°C (ΔT_{sub} =10 K), the thermal stratification and the stagnant region begin to disappear and the natural convection flow velocity increases significantly due to the bubble generation.

To investigate the prediction capability of MULTID in MARS for natural convection flow in a pool, this study simulated above experiment by modeling the

pool with the MULTID component (see Fig. A.3). From the simulation results (see Figs. A.4 and A.5), it was found that MARS estimated the flow velocity reasonably at the low subcooled (or nearly saturated) condition with the bubble generation but it does not simulate the thermal-stratification and the flow velocity well at the high subcooled condition.

For the accurate prediction of the out-tube heat transfer, MARS can simulate the mixing phenomena in a pool well. Therefore, as a future work, it is recommended to improve the MARS prediction capability for the natural convection flow velocity in a pool at high subcooled condition.

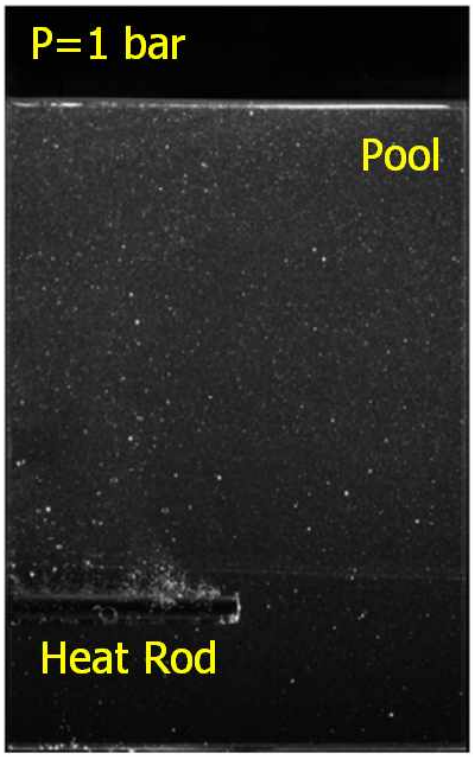

Figure A.1 Natural convection flow experiment

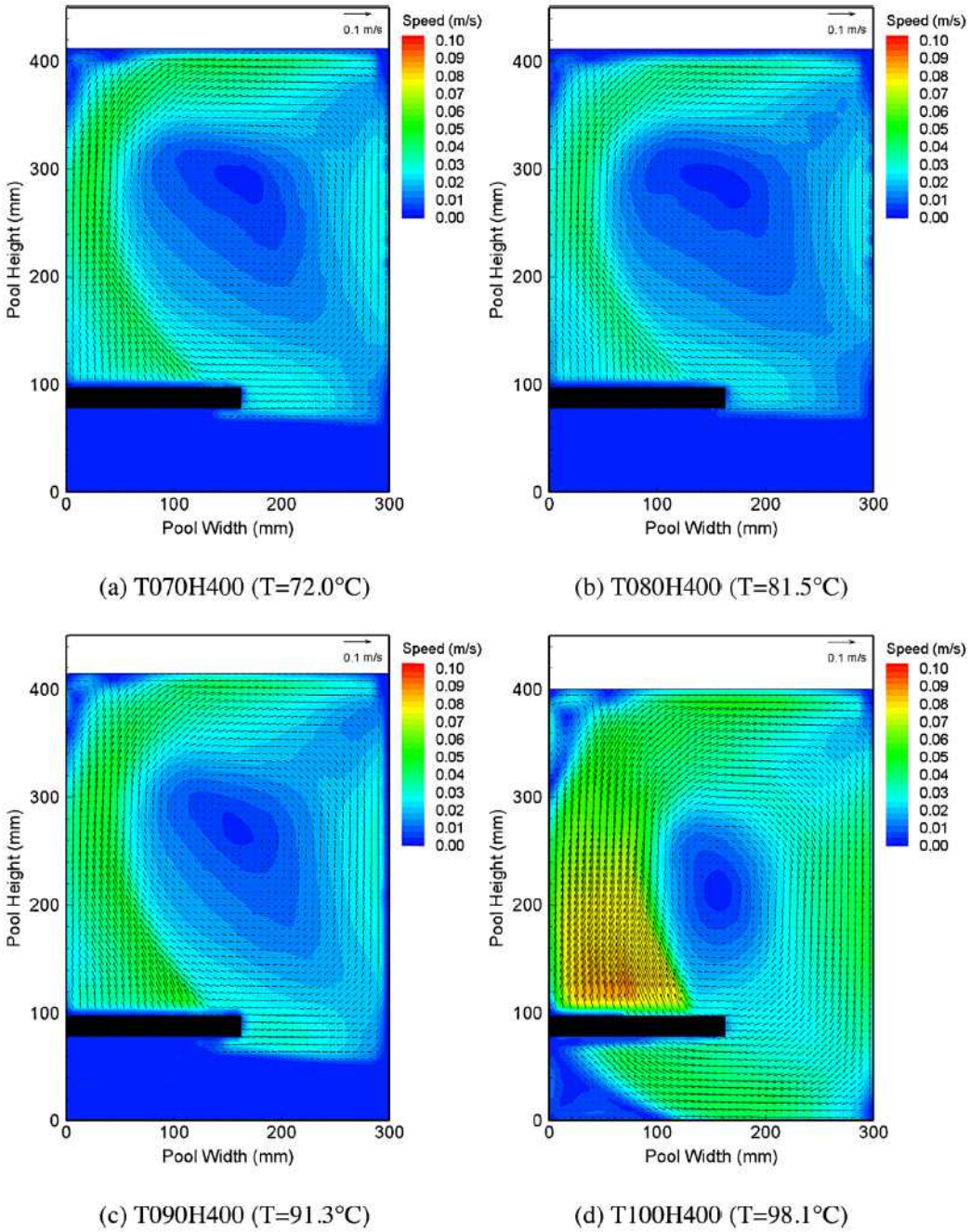

(a) T070H400 (T=72.0°C)

(b) T080H400 (T=81.5°C)

(c) T090H400 (T=91.3°C)

(d) T100H400 (T=98.1°C)

Figure A.2 Mean velocity vector field with different pool temperatures (Kim et al., 2014) – (1/2)

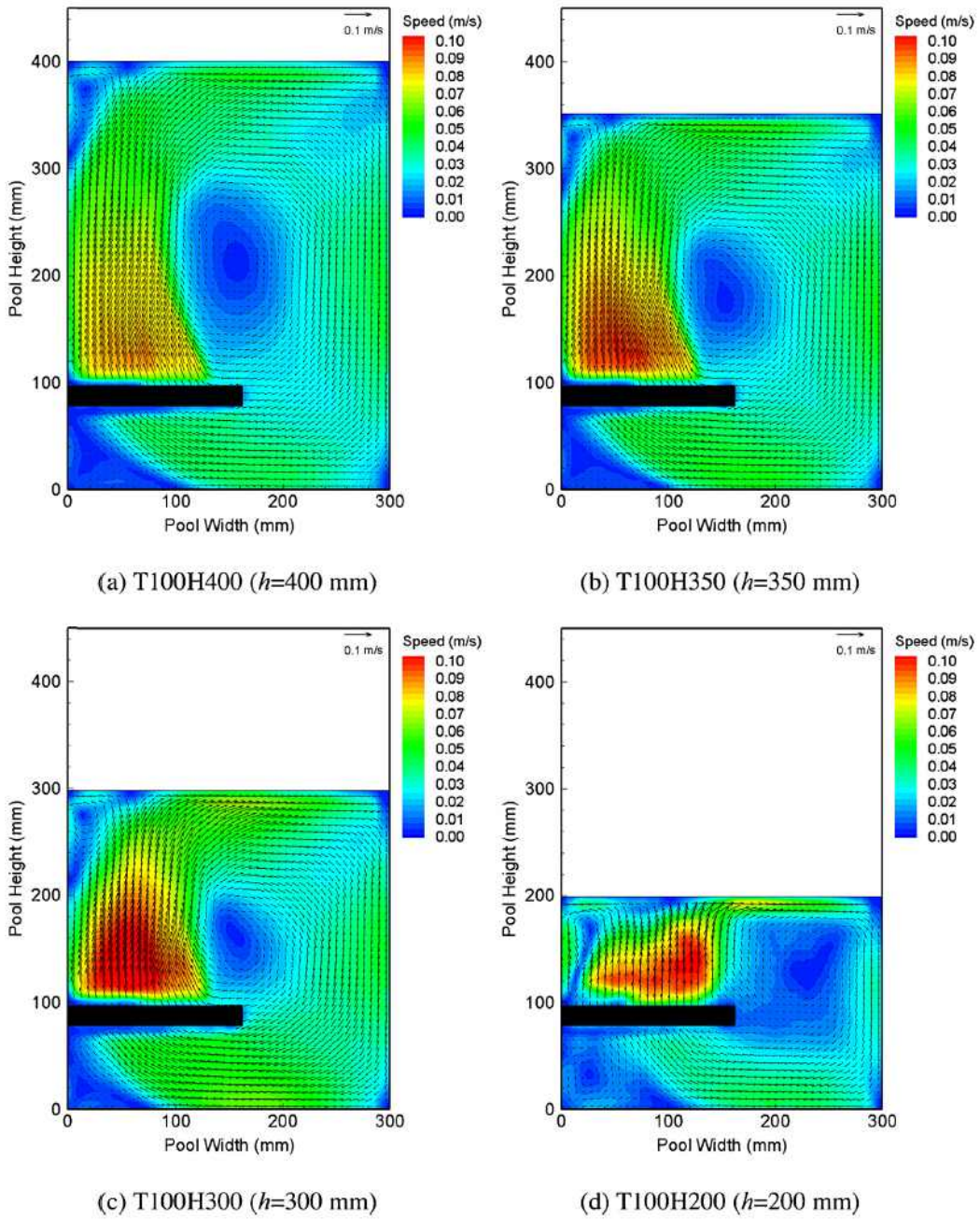

(a) T100H400 (h=400 mm)

(b) T100H350 (h=350 mm)

(c) T100H300 (h=300 mm)

(d) T100H200 (h=200 mm)

Figure A.2 Mean velocity vector field with different pool temperatures (Kim et al., 2014) – (2/2)

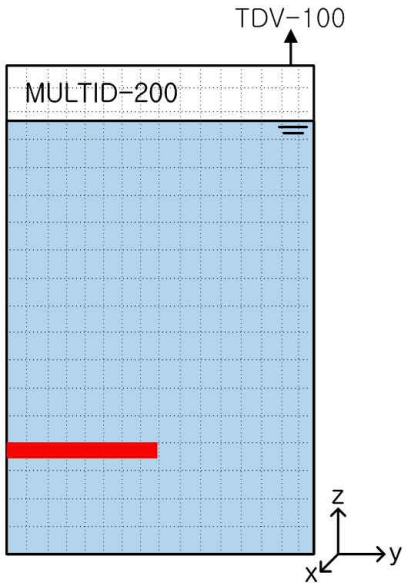

Figure A.3 MARS modeling of natural convection flow experiment

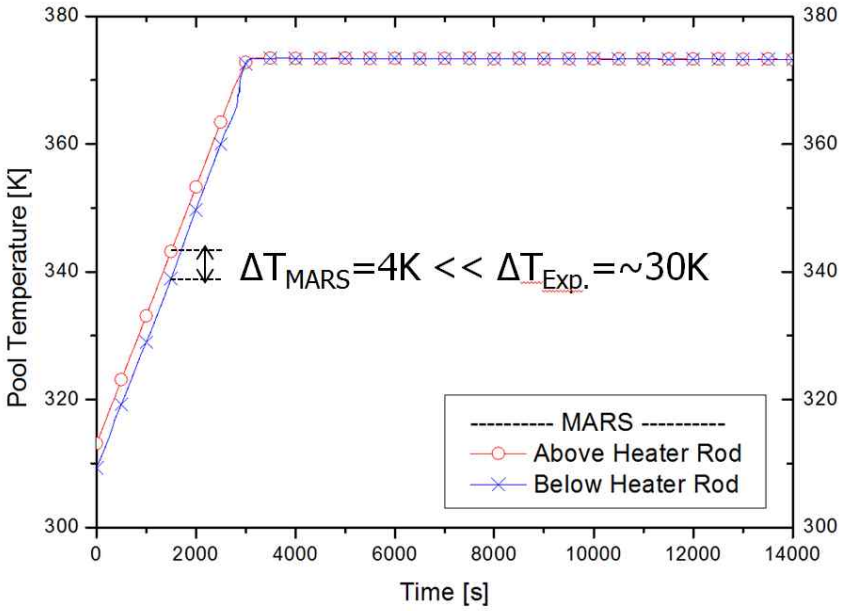

Figure A.4 Predicted pool temperature

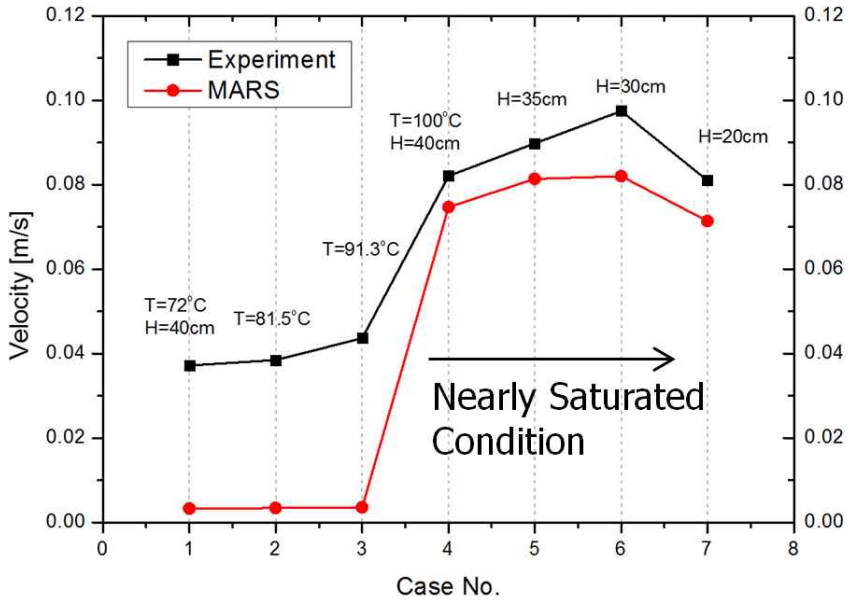

Figure A.5 Predicted natural convection velocity

Appendix B

Validation of Convection Correlation for Multi-Dimensional Flow

To predict the single-phase forced convection HTC for the multi-dimensional flow, this study proposed the convection correlation based on the asymptotic method (see Chapter 3.7.2). This section presents the validation of the proposed correlation.

The validation was performed using a commercial CFD code, FLUENT 14.0. The flow channel and meshes are generated in a three-dimensional Cartesian coordinate system using GAMBIT 2.2.30. The problem situation is as follows (see Fig. B.1). The dimensions of the test channel are: length 1 m, width 0.4 m, height 1 m. The test channel is filled with the water of 300 K as the initial condition. A horizontal cylinder (D=0.0508 m) is located in the middle of the channel. The cylinder is modeled as wall with the constant heat flux of 200 kW/m^2. In the test channel, the front and rear faces are modeled as wall. The bottom and top faces are modeled as the velocity-inlet and pressure-outlet, respectively. At the left and right faces, the periodic boundary condition is applied to consider that the physical geometry of interest and the expected pattern of the flow/thermal solution have a periodically repeating nature in this problem. This study simplified the problem situation by assuming that the bubbles are not generated from the cylinder surface. The heat transfer for the single-phase flow is considered

only in this simulation. The RNG k-epsilon model and the scalable wall functions for the near-wall treatment were used to simulate the turbulent flow. CFD simulations were performed by changing the flow direction (see Fig. 3.11).

Figure B.2 shows the representative result for streamlines around the cylinder at the flow inclination angle of 45° where the flow speed is 0.5 m/s. It is found that the water flow around the cylinder wall is simulated appropriately.

Figure B.3 shows the CFD predictions for the HTC. Specifically, the black line with square symbol indicates the HTC obtained from the simulations for the multi-dimensional flow at different flow inclination angles ranging from 0° to 90° where the flow speed is the same as 0.5 m/s. The blue line with triangle symbol indicates the HTC obtained from the simulations for the parallel flow with the velocity component parallel (θ =0°) to the cylinder according to the flow inclination angle (see Fig. 3.11). The red line with sphere symbol indicates the HTC obtained from the simulations for the cross flow with the velocity component normal (θ =90°) to the cylinder according to the flow inclination angle (see Fig. 3.11). From the CFD simulations, the heat transfer characteristics for the multi-dimensional flow can be summarized as follows: 1) At the same flow speed, the HTC increases with the flow inclination. 2) Inclined flows show the superior heat transfer behavior than the purely parallel flow with the same flow speed. 3) The effect of the normal component of the inclined flow is very strong, thus rendering the local HTC for the inclined flow (θ > ~30°) much more similar in shape to that of the purely cross flow than to that of the purely parallel flow.

To validate the proposed convection correlation (see Eq. (3.10)), the HTCs for the inclined flow should be able to be predicted by the combination of the HTC for the parallel flow and the HTC for the cross flow, based on the asymptotic

method. Figure B.4 shows the sensitivity analysis by changing the exponent, n, in Eq. (3.10) for the asymptotic method. It was found that the best correlation of data was obtained for n=2. Similarly, for the additional analysis case with the inclined flow speed of 0.25 m/s, the best correlation of data was obtained for n=2 (see Fig. B.5). Therefore, it is concluded that the proposed correlation based on the asymptotic method (n=2) is valid to predict the single-phase convection HTC for the multi-dimensional flow.

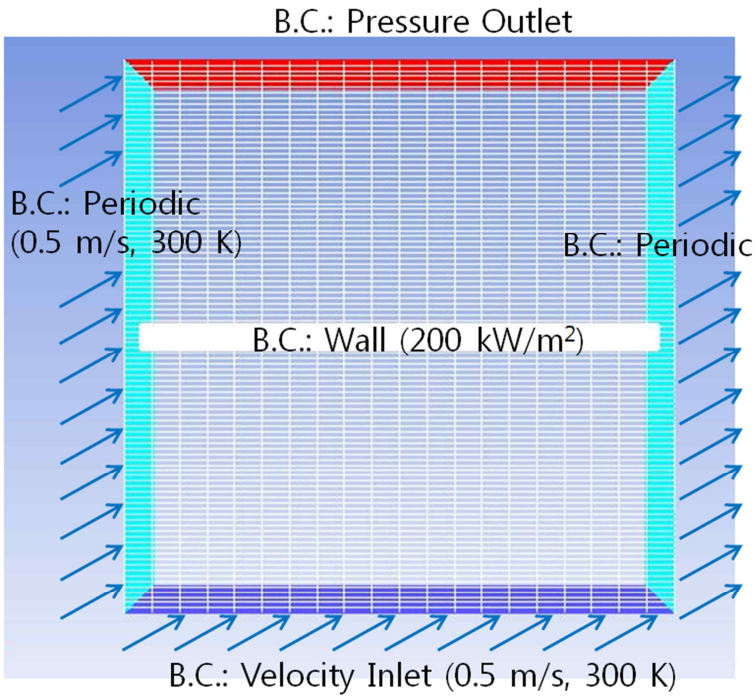

Figure B.1 Schematic diagram of CFD simulation

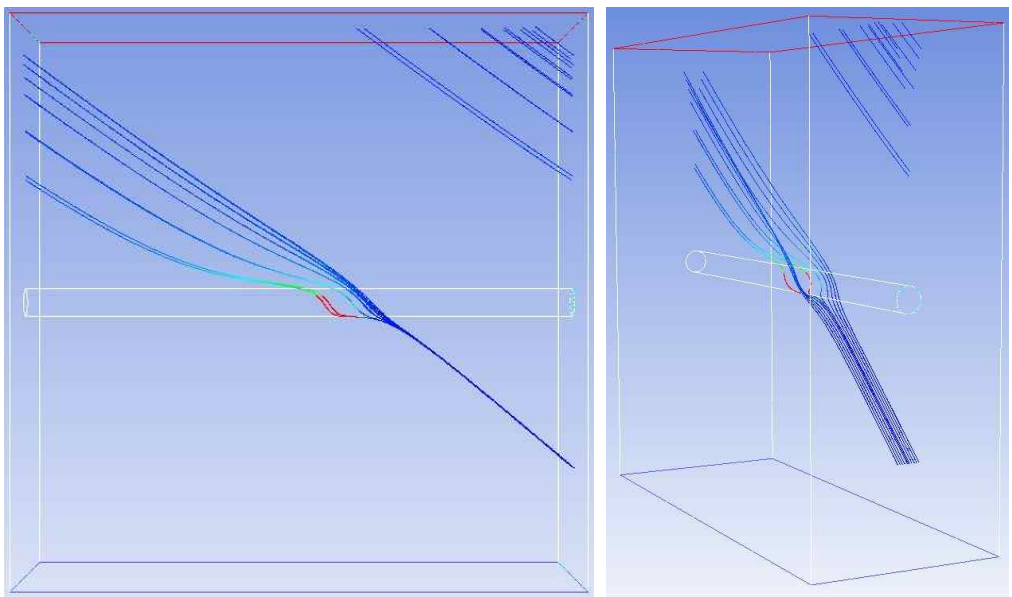

Figure B.2 Streamlines around a cylinder at inclined flow

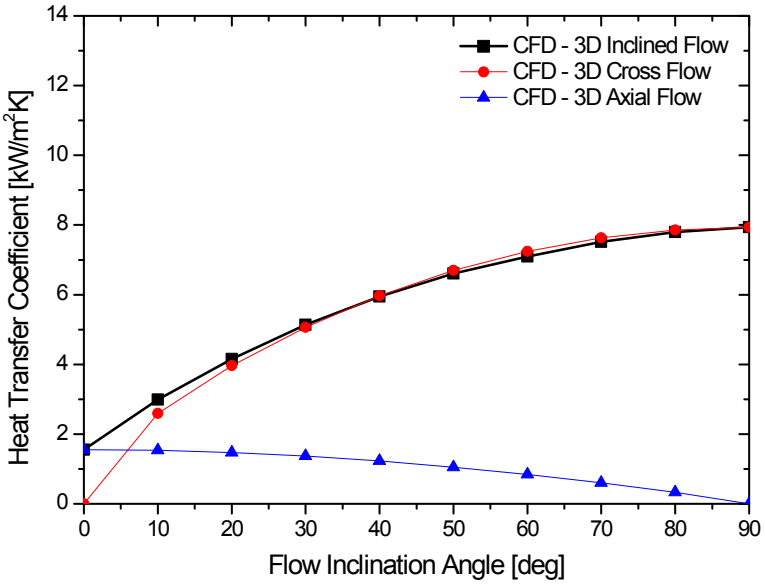

Figure B.3 CFD predictions of HTC

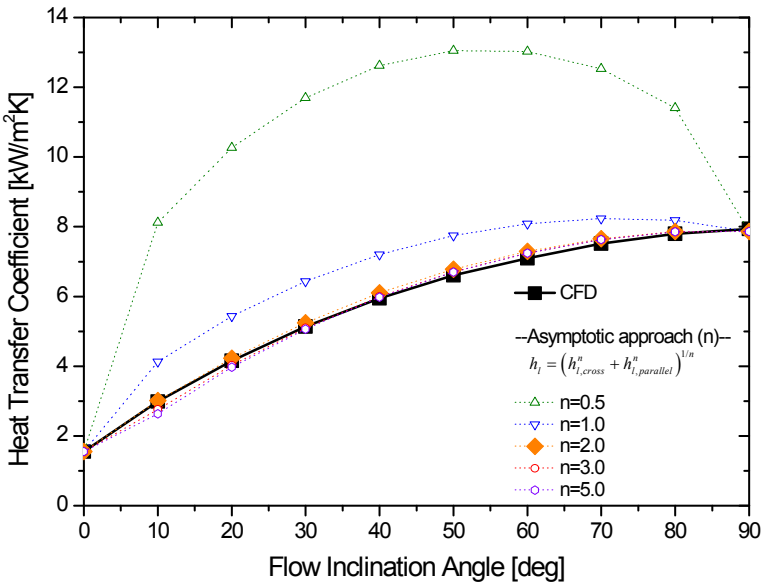

Figure B.4 Sensitivity analysis of HTC

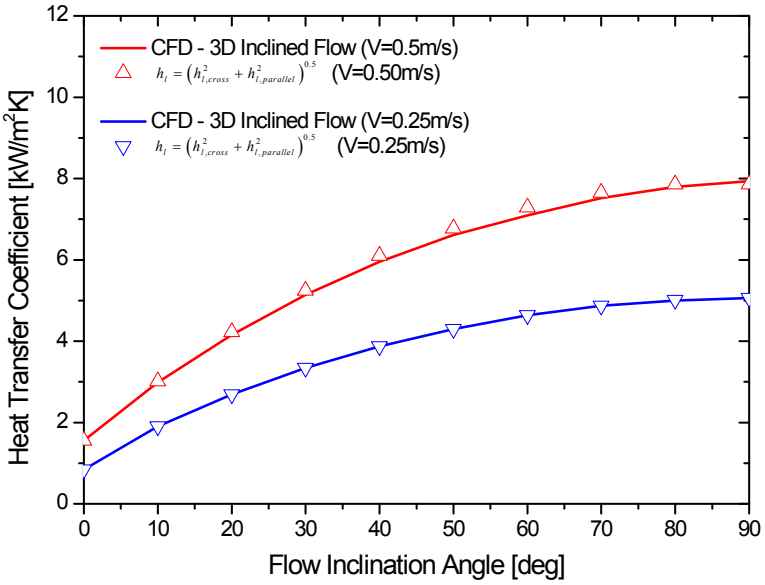

Figure B.5 Validation results of proposed correlation for multi-dimensional flow

국문 초록

PAFS, PCCS, 그리고 ECS와 같은 피동안전계통의 핵심기기로 수조 내 수평 U자형 열교환기가 개발되어 왔다. 신뢰성 있는 열교환기의 설계 및 안전해석을 위해서는 열교환기 성능을 잘 예측하는 것이 필수적이다. 본 연구에서는 최적열수력분석코드가 PAFS의 수조 내 수평 U자형 열교환기 튜브 내/외부에서의 국부 열전달계수 및 전체 열제거율을 잘 예측할 수 있도록 MARS 코드를 이용한 해석적 연구를 수행하였고, 수조 내 수평 U자형 열교환기에 대한 열전달 모델을 개발하였다.

수조 내 수평 U자형 열교환기에 대한 열전달 모델은 수평관 내부 응축 열전달 모델과 수평관 외부 자연대류 비등 열전달 모델로 구성된다. 수평관 내부 응축 열전달 모델과 관련해서는 다양한 수평관 내 증기 응축 실험데이터를 이용하여 주요 유동양식별 기존 모델들의 응축 열전달 예측 능력을 평가하였다. 평가 결과, 기존 모델들 중 환상유동에서는 Dobson-Chato (1998), 성층유동에서는 Cavallini et al. (2006)의 응축 모델이 수평관 내부에서의 증기 응축 열전달을 잘 예측함을 확인하였다. 이 모델들을 MARS에 적용함으로써 MARS의 피동안전계통 열교환기에서의 응축 열전달에 대한 예측 능력을 향상시켰다.

수평관 외부에서의 자연대류 비등 열전달 모델과 관련해서는 우선, PASCAL 실험데이터를 이용하여 기존 모델들의 비등 열전달 예측 능력을 평가하였다. 평가 결과, 기존 비등 모델들 중 수조 내 수평 U자형 열교환기의 비등 열전달 예측에 적합한 모델은 없음을 확인하였다. 여러 실험과 관련 문헌을 종합적으로 검토하여 수조 내 수평 U자형 열교환기에 대한 비등 열전달 메커니즘을 규명하였고, 수조 내 U자형 튜브에 대한 수평관 외부 비등 열전

달 모델을 개발하였다. 개발된 비등 모델을 PASCAL과 ATLAS-PAFS 실험 데이터를 이용하여 검증한 결과, 제안된 모델은 U자형 열교환기의 상부 및 하부 튜브에 대한 열전달계수를 약 ±19 % 이내에서 만족스럽게 예측함을 확인하였다. 수평관 외부에서의 자연대류 열전달 모델과 관련해서는 PASCAL 실험데이터를 이용하여 수조 내 수평 U자형 열교환기에 대한 자연대류 열전달 모델을 제시하였다. 제안된 자연대류 열전달 모델은 PASCAL 실험데이터를 약 ±33 % 이내에서 예측함을 확인하였다. 최종적으로 제안된 비등 열전달 모델과 자연대류 열전달 모델을 조합하여 수조 내 수평 U자형 열교환기에 대한 자연대류 비등 열전달 모델을 개발하였다.

제안된 열교환기 열전달 모델을 PASCAL, ATLAS-PAFS 그리고 NOKO 실험 데이터를 이용하여 검증한 결과, 개발된 열교환기 열전달 모델은 열교환기 튜브 내/외부에서의 국부 열전달계수 및 전체 열제거율을 기존 모델 대비 정확하게 예측함을 확인하였다.

본 연구에서 제안된 수조 내 수평 U자형 열교환기에 대한 열전달 모델은 최적열수력분석코드에 적용되어 PAFS를 포함하여 수조 내 수평 U자형 열교환기를 지닌 피동안전계통의 최적설계 및 안전해석에 기여할 수 있을 것이다.

주요어

수평 U자형 열교환기, 피동안전계통, PAFS, 응축 열전달 모델, 자연대류 비등 열전달 모델, MARS 코드, PASCAL

학번: 2010-30259